Stony Brook University

Alendronate and PTH Differentially Modulate Bone Quality and Reduce Adiposity in an OVX Rat Model

A Dissertation Presented

by

Andrea Trinward Kwaczala

to

The Graduate School

in Partial Fulfillment of the

Requirements

for the Degree of

Doctor of Philosophy

in

Biomedical Engineering

Stony Brook University

December 2012

Stony Brook University

The Graduate School

Andrea Trinward Kwaczala

We, the dissertation committee for the above candidate for the

Doctor of Philosophy degree, hereby recommend

acceptance of this dissertation.

Stefan Judex – Dissertation Advisor
Professor, Biomedical Engineering

Clinton Rubin - Chairperson of Defense
Department Chair and Distinguished Professor, Biomedical Engineering

Lisa Miller – Committee Member of Defense
Professor, Biomedical Engineering

Yizhi Meng – Committee Member of Defense
Assistant Professor, Materials Science and Engineering

This dissertation is accepted by the Graduate School

Charles Taber
Interim Dean of the Graduate School

Abstract of the Dissertation

Alendronate and PTH Differentially Modulate Bone Quality and Reduce Adiposity in an OVX Rat Model

by

Andrea Trinward Kwaczala

Doctor of Philosophy

in

Biomedical Engineering

Stony Brook University

2012

Post-menopausal osteoporosis is defined by a reduction in bone quantity and quality. Bone quality is an accumulation of factors including bone mass, structure, geometry, microarchitecture, tissue mineral density and chemistry. Currently, osteoporosis is treated with pharmaceuticals such as anti-catabolic bisphosphonates such as alendronate (ALN) which maintains bone mass by blocking bone resorption, or anabolic drugs such as parathyroid hormone (PTH) which increases bone mass by increasing bone formation. Due to their different modes of preserving bone, there may be differential drug-driven alterations to bone tissue quality which affect bone strength. Additionally, osteoporosis is associated with increased body mass and abdominal adiposity, factors that pose secondary risk to skeletal health; however, the effects of osteoporosis drugs on adiposity are unclear. The overall objective of this dissertation was 1.) to determine drug, dosage and duration-specific changes to bone composition and its relationship to bone mechanical properties, 2.) to determine drug-induced tissue age specific changes in bone chemistry and its relationship to micromechanical properties and 3.) to determine the interrelationship between bone quality and adiposity during drug treatment. Bone mass, morphology and microarchitecture were reduced after ovariectomy but dose-dependently improved with PTH and ALN. High dose ALN and PTH reduced tissue mineral density and tissue level mechanical properties. A finite element model revealed architecture and structural properties accounted for 91% of the change in bone stiffness, where chemistry and tissue properties did not influence bone strength. ALN and PTH had differential effects on bone metabolism which led to alterations in bone chemistry and the micro-mechanical properties of new bone surfaces. ALN had more mineralized, stiffer bone surfaces than PTH. Tissue mineralization positively correlated to changes in micro-mechanical properties. Finally, PTH and ALN significantly improved fat metabolism and altered the relationship between adiposity and bone quality. There was a strong negative relationship between trabecular architecture and marrow adiposity, where drugs altered this interaction through increases of bone coupled with decreases in fat. Overall, bone morphology and architecture are critical components of bone strength. Although small changes to bone material properties did not modulate total bone stiffness, drug-induced changes to chemistry and micromechanical properties provide insight into drug-related effects on tissue quality. Finally, osteoporosis pharmaceuticals may have secondary benefits through mitigation of fat accumulation and could be useful targets for treating diseases such as diabetic osteoporosis due to their beneficial effects on both bone and fat.

Dedication Page

This thesis work is dedicated to my father, John Greenleaf Trinward, who acted as a mentor, sounding board, motivator and above all a great friend throughout each stage of my PhD work, and throughout my life. Thank you Dad for always helping me get the hard part done, and for encouraging me to never give up on engineering, or myself. You taught me so much about imagination, how to bring ideas to life, the importance of lifelong learning, but most of all you always showed me what it means to be a good person.

I will miss you and remember your lessons every day.

Frontispiece

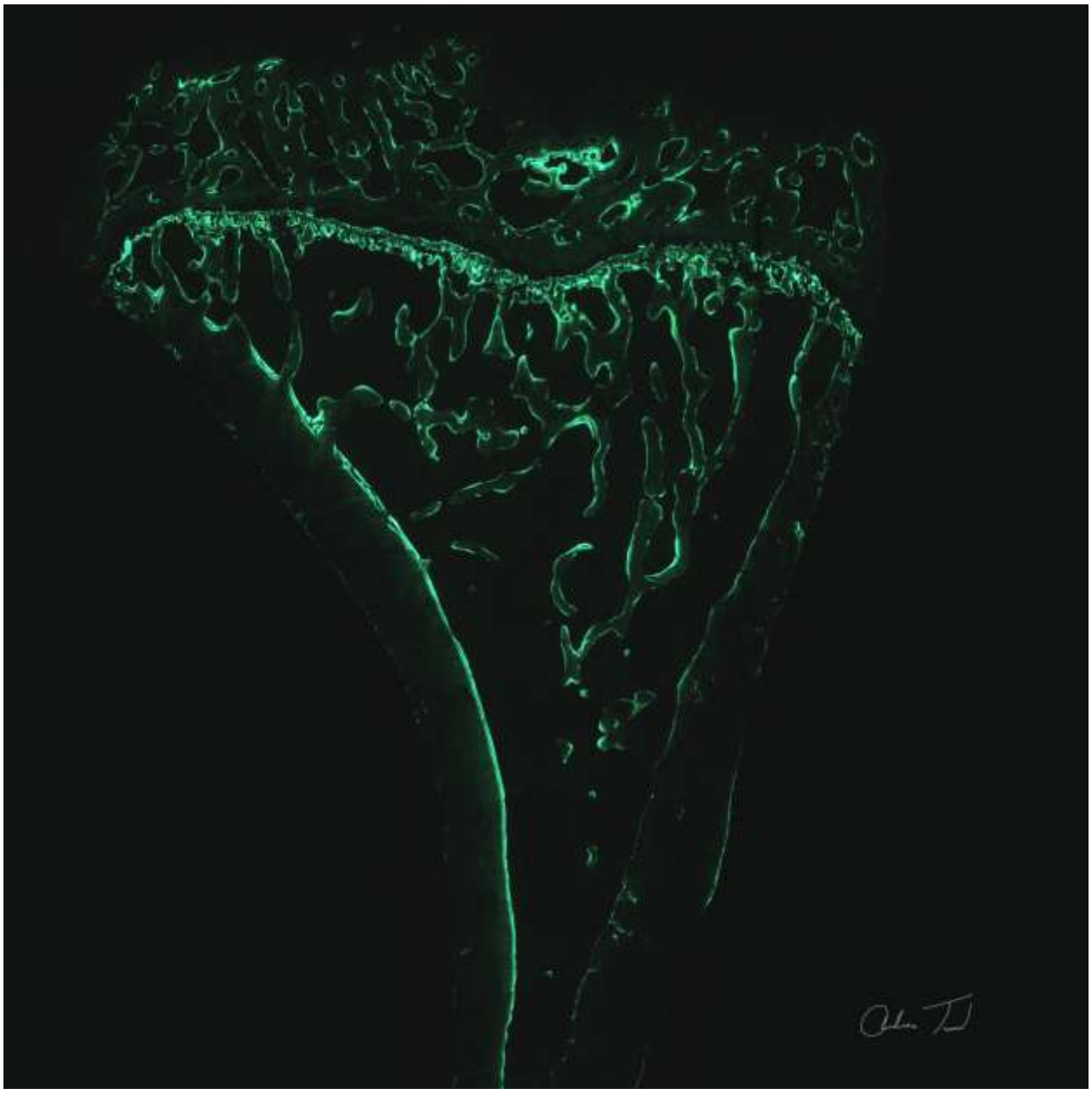

Table of Contents

List of Figures

Figure 2.8. Structural properties determined through 4 point bending of the tibial diaphysis revealed A.) Stiffness (N/mm), B.) Maximum applied load (N), C.) Elastic modulus (MPa) and D.) Maximum computed stress (MPa), for 12 mo age-matched (AC – black) controls, ovariectomized controls (OVX - white), alendronate treated (ALN –light gray) at low (L), medium (M) and high (H) doses and parathyroid hormone (PTH – dark gray) treated at low (L), medium (M) and high (H) doses with baseline animals represented (- - -).

Figure 2.9 Linear regression analysis between cortical thickness of the tibial diaphysis and structural stiffness of the tibial diaphysis determined through 4-point bending demonstrates that the increased thickness induced by H-PTH treatment (gray - triangle) did not result in a relative increased stiffness (R^2=0.02, p>0.05) when analyzed separately from the total population (black - circle) regressed (R^2=0.32, p<0.001).

Figure 3.1. A.) A representative spectral point obtained during U2B - FTIR analysis of bone showing the spectra of the cortical bone surface (blue), cortical interstitial bone (red) trabecular bone surface (pink) and trabecular interstitial bone (purple) with the characteristic carbonate, phosphate, and protein peaks defined. B.) An example of placement of the aperture within double labels obtained during FTIR analysis of bone surfaces.

Figure 3.2. Static histomorphometry determined trabecular A.) Bone area/total area (Tb.BA/TA) B.) Thickness (Tb.Th) C.) Separation (Tb.Sp) and D.) Number (Tb.N) for age-matched (AC-black), ovariectomized (OVX-white), alendronate-treated at low (L), medium (M), or high (H) doses (ALN - light gray) and PTH-treated at low (L), medium (M), or high (H) doses (PTH - dark gray) with 6 mo old baseline animals (- - -).

Figure 3.3. Dynamic histomorphometry of the trabecular bone within the tibial metaphysis sectioned longitudinally determined trabecular A.) mineralizing surface/bone surface (Tb. Mineralizing Surface/BS) B.) mineral apposition rate (Tb.MAR) and C.) bone formation rate/bone surface (Tb.BFR/BS) for age-matched (AC-black), ovariectomized (OVX-white), alendronate-treated at low (L), medium (M), or high (H) doses (ALN - light gray) and PTH-treated at low (L), medium (M), or high (H) doses (PTH - dark gray) with 6 mo old baseline animals (- - -).

Figure 3.4. Dynamic histomorphometry of the cortical bone of the tibial metaphysis sectioned longitudinally determined Endosteal A.) mineralizing surface/bone surface (Ec. Mineralizing Surface/BS) B.) mineral apposition rate (Ec.MAR) and C.) bone formation rate/bone surface (Ec.BFR/BS) for age-matched (AC-black), ovariectomized (OVX-white), alendronate-treated at low (L), medium (M), or high (H) doses (ALN - light gray) and PTH-treated at low (L), medium (M), or high (H) doses (PTH - dark gray) with 6 mo old baseline animals (- - -).

Figure 3.5. FTIR analysis on the bone surfaces of the tibial metaphysis revealed Tissue A.) Mineralization (900-1200/1600-1700) B.) Crystallinity (1034-1036/1024-1026) C.) Collagen cross-linking (1659-1661/1689-1691) and D.) Carbonate Incorporation (1414-1424/900-1200) E.) Protein content (1600-1700) and F.) Phosphate content (900-1200) for age-matched (AC-black), ovariectomized (OVX-white), alendronate-treated for high dose alendronate (H-ALN - light gray) and high dose PTH-treated (H-PTH - dark gray) on the cortical surface, cortical interstial region, trabecular surface and trabecular interstitial region, statistically compared regional differences within a treatment group.

Figure 3.6. FTIR analysis revealed tissue mineralization (900-1200/1600-1700) at the A.) Cortical bone surface (far left), cortical interstitial space (middle left), trabecular bone surface (middle right) and trabecular interstitial space (far right) for age-matched (AC-black), ovariectomized (OVX-white), H-alendronate-treated (H-ALN - light gray) and H-PTH-treated rats (H-PTH - dark gray) statistically compared across treatment groups and bone regions.

Figure 3.7. FTIR analysis of bone surfaces (gray) and interstitial bone (black) revealed tissue mineralization (900-1200/1600-1700). Statistical differences within a group were determined with a paired-wise Student t-test comparing bone surface properties (gray) to interstitial properties (black).

Figure 3.8. Nanoindentation of the tibial metaphysis to determine elastic moduli (E) of A.) Cortical bone surfaces B.) Cortical interstitial bone, C.) Trabecular bone surfaces and D.) Trabecular interstitial bone for age-matched (AC-black), ovariectomized (OVX-white), alendronate-treated at low (L), medium (M), or high (H) doses (ALN - light gray) and PTH-treated at low (L), medium (M), or high (H) doses (PTH - dark gray).

Figure 3.9. Nanoindentation of the tibial metaphysis to determine tissue hardness of A.) Cortical bone surfaces B.) Cortical Interstitial bone, C.) Trabecular bone surfaces and D.) Trabecular interstitial bone for age-matched (AC-black), ovariectomized (OVX-white), alendronate-treated at low (L), medium (M), or high (H) doses (ALN - light gray) and PTH-treated at low (L), medium (M), or high (H) doses (PTH - dark gray).

Figure 3.10. Nanoindentation of bone surfaces (gray) and interstitial bone (black) revealed A.) Elastic moduli and B.) Tissue hardness for age matched controls (AC), OVX controls (OVX), high alendronate treated (H-ALN) and high PTH treated (H-PTH) rats.

Figure 4.1. Representative images from *in vivo* μCT: A.) A scout view of the region of interest scanned (between white lines) B.) The applied script showing the segmented image from a single gray scale slice C.) A segmented 3D image with subcutaneous fat (gray) and visceral fat (pink) separated.

Figure 4.2. Longitudinal change in body mass for age-matched controls (AC- black solid) ovariectomy controls (OVX - dashed gray), OVX + alendronate-treated at low (L - solid black), medium (M – dashed dark gray), or high (H - dotted light gray) doses or OVX + PTH-treated at low (L - solid black), medium (M - dashed dark gray), or high (H - dotted light gray) doses.

Figure 4.3. *In vivo* microCT of the L4 to the L1 vertebrae scanned at 6, 8 and 12 months of age revealed longitudinal changes in Vertebral A.) bone volume (Vt.BV) and B.) apparent mineral density (Vt.App.MD) for age-matched controls (AC- black solid) ovariectomy controls (OVX - dashed gray), OVX + alendronate-treated at low (L - solid black), medium (M – dashed dark gray), or high (H - dotted light gray) doses or OVX + PTH-treated at low (L - solid black), medium (M - dashed dark gray), or high (H - dotted light gray) doses.

Figure 4.4. Trabecular microarchitecture of the vertebral body from desktop μCT determined Trabecular A.) Bone volume fraction (Tb.BV/TV) B.) Thickness (Tb.Th) C.) Number (Tb.N) D.) Separation (Tb.Sp) E.) Connectivity density (Tb.Conn.D) F.) Apparent mineral density (Tb.AppMD) and G.) Tissue mineral density (Tb.TMD) for age-matched (AC-black), ovariectomized (OVX-white), alendronate-treated at low (L), medium (M), or high (H) doses (ALN - light gray) and PTH-treated at low (L), medium (M), or high (H) doses (PTH - dark gray) with baseline animals represented (- - -) and OVX baseline represented (…).

Figure 4.5. In vivo longitudinal μCT scans evaluated abdominal fat volume. Representative images at A.) 6 months old, B.) 8 months old and C.) 12 months old which show the abdominal fat separated into subcutaneous (gray) and visceral (red) fat, with adipose tissue increasing with age.

Figure 4.6. *In vivo* microCT of the abdomen scanned at 6, 8 and 12 months of age revealed longitudinal changes in A.) Visceral adipose volume (Vis.Adipose V) and B.) Subcutaneous adipose volume (Sub.AdiposeV) for age-matched controls (AC- black solid) ovariectomy controls (OVX - dashed gray), OVX + alendronate-treated at low (L - solid black), medium (M – dashed dark gray), or high (H - dotted light gray) doses or OVX + PTH-treated at low (L - solid black), medium (M - dashed dark gray), or high (H - dotted light gray) doses.

Figure 4.7. A.) Extracted gonadal fat pad mass of all animals correlated to body weight. B.) Fat pad mass of 12 month animals correlated to their 12 month total fat volume (*in vivo* μCT).

Figure 4.8. Body Mass (BM - diamond), total adipose tissue/body weight (TAT/BW - circle) and visceral adipose tissue/body weight (VAT/BW - triangle) correlated to A.) bone volume, B.) and apparent mineral density (App.MD).

Figure 4.9. Bone area of the tibial metaphysis determined histologically at 12 months through Osteomeasure for age-matched (AC-black), ovariectomized (OVX-white), alendronate-treated at low (L), medium (M), or high (H) doses (ALN - light gray) and PTH-treated at low (L), medium (M), or high (H) doses (PTH - dark gray) with baseline animals represented (- - -) and OVX baseline represented (…).

Figure 4.10. A.) Adipocyte number for 5 fields of view within the tibial metaphysis for age-matched (AC-black), ovariectomized (OVX-white), alendronate-treated at low (L), medium (M), or high (H) doses (ALN - light) and PTH-treated at low (L), medium (M), or high (H) doses (PTH - dark gray) with baseline animals represented (- - -) and OVX baseline represented (…). B.) Representative images sectioned at 8 μm, stained with touloudine blue O and Giemsa for AC (top) and OVX (bottom).

Figure 4.11. Bone marrow adipocyte number correlated to bone marrow trabecular area determined through histological analysis of the tibial metaphysis for all 12 month old animals (black – dashed), AC and OVX animals (black-square), PTH treated animals (light gray – triangle) and ALN treated animals (dark gray –triangle).

List of Tables

List of Abbreviations

ANOVA – analysis of variance

ANCOVA – analysis of covariance

BFR/BS – bone formation rate per bone surface

App.MD or BMD – apparent bone mineral density

BS – bone surface

BS/BV – bone surface to volume ratio

BV – bone volume

BV/TV – bone volume fraction

Conn.D – connectivity density

Ct.Ar – cortical area

Ct.Th – cortical thickness

Ct.TMD – cortical tissue mineral density

E – elastic modulus

IGF-1 – insulin-like growth factor-1

J or pMOI – polar moment of inertia

MAR – mineral apposition rate

microCT or μCT – micro-computed tomography

MS/BS – mineralizing surface per bone surface

MSC – mesenchymal stem cell

N – Newton

ν – Poisson's ratio

OVX -- ovariectomized

PBS – phosphate buffered saline

PTH – parathyroid hormone

RT-PCR – real time reverse transcriptase polymerase chain reaction

RNA – ribonucleic acid

Tb.Sp – trabecular separation

Tb.N – trabecular number

Tb.Th – trabecular thickness

Tb.TMD – trabecular tissue mineral density

TV – tissue volume

Acknowledgments

This research was kindly funded by the NIH research grant AR052778 and NIAMS.

I would like to thank my thesis committee for agreeing to serve as members of my team. Thank you Stefan, Clint, Lisa and Yizhi, for your wisdom, words of encouragement and for pushing me to be the best biomedical engineer that I could be.

A special thank you to Stefan for taking me on as a student and making me a member of your team. This opportunity has taught me so much about myself as a student, as a scientist and as a person and I have you to thank for giving me a nurturing place to grow.

Thank you to Steve Tommasini for acting as a mentor and role model throughout my PhD work. As the post doc in the lab you were always my first line of defense and worked tirelessly to help me find answers to all of my tough questions. We made a great team and worked so well together. I hope we have many opportunities to work together in the future.

Thank you to Sarah Manske for teaching me a thing or two about FE modeling and training me in PCR. More importantly, thanks for being a terrific friend and support system through my rough days. You were always a kind listener and offered up positive feedback to help me get back on track.

Thank you Danielle Green, your friendship and constant companionship during my time at Stony Brook. You helped me in ways you don't even know. You were the best sounding board and gave excellent advice. You helped motivate me to get things done and I am a better scientist because of your support.

Thank you to the members of the Judex and Rubin labs for your help with sacrifices, data analysis and thesis defense preparations. I learned the most from you and am so grateful for your challenging questions and motivation throughout this process. A special thanks to Alyssa Tuthill.

A very special thank you each and every one of my family members, especially my parents, for your love and encouragement. You motivated me to get to where I am today. Even as our family goes through a hardship, you have helped me rise to the top and finish the job I set out to do. I could not be here without the lessons you taught me over my lifetime. It is in difficult times that you get to see who people really are and what they are made of, and I am so proud to be a member of this family.

Finally, thank you to my new husband for supporting me in this challenging process and for loving me even on the days when the data got difficult to interpret. Your intellectual and emotional support to my thesis work are worth recognizing. Thank you for your friendship over the last eight years. I can't wait to spend the rest of our lives around the dinner table discussing our work with one another!

Publications

This is a list of peer-reviewed publications, book chapters and conference proceedings that were produced during the course of the dissertation.

PEER REVIEWED JOURNAL PUBLICATIONS

Steven Tommasini, **Andrea Trinward**, Alvin Acerbo, Lisa Miller, Stefan Judex, Changes in intracortical microporosities induced by pharmaceutical treatment of osteoporosis as detected by high resolution micro-CT. **Bone**, March *2012.*

Preparing for submission to **Osteoporosis International**: **Andrea Kwaczala**, Steven Tommasini, Sarah Manske, Stefan Judex. Bone and Fat are perturbed in an osteoporotic rat model but normalized with parathyroid hormone and alendronate treatment.

Preparing submission to **Journal of Biomechanics**: **Andrea Kwaczala**, Steven Tommasini, Sarah Manske, Lisa Miller, Stefan Judex. Dose-dependent improvements in microarchitecture with alendronate and PTH enhance bone strength despite reductions in tissue material properties.

Preparing submission to **Journal of Bone and Mineral Research**: **Andrea Kwaczala**, Alvin Acerbo, Steven Tommasini, Lisa Miller, Stefan Judex. Drug Induced alterations in bone metabolism result in alendronate and PTH dose-dependent changes in bone surface properties measured through nanoindentation and FTIR.

Preparing for submission to the **Journal of Bone and Mineral Research** for August 2012: Alvin Acerbo, **Andrea Kwaczala**, Steven Tommasini, Stefan Judex, Lisa Miller. The effects of estrogen withdrawal and fluoride treatment on bone chemical properties and the relationship to its nanomechanical properties.

CONFERENCE PROCEEDINGS AND PRESENTATIONS

Young Investigator's Award and Plenary Poster Winner: Trinward A, Tommasini SM, SM Manske Acerbo A, Miller LM, Judex S. Alendronate and PTH Dose-Dependent Improvements in Microarchitecture Lead to Improved Bone Strength despite Reductions in Tissue Material Properties. Minneapolis, MN. American Society of Bone and Mineral Research 2012.

Tommasini SM, **Trinward A,** SM Manske Acerbo A, Miller LM, Judex S Identification of Biochemical, Mechanical, and Structural Factors that Define Bone Quality. Minneapolis, MN. American Society of Bone and Mineral Research 2012.

Trinward A, Tommasini SM, Acerbo A, Miller LM, Judex S. Modulation of bone's mechanical properties by its architecture, chemical composition and age. San Diego, CA. American Society of Bone and Mineral Research 2011.

Plenary Poster Winner: SM Tommasini, **Trinward A**, S Judex. Changes in Osteocyte Lacunar Network Induced by Estrogen Withdrawal and Pharmaceutical Treatment of Osteoporosis as Detected by Synchrotron Micro-CT. San Diego, CA. American Society of Bone and Mineral Research 2011.

Trinward A, Tommasini SM, Acerbo A, Miller LM, Judex S. Modulation of bone's mechanical properties by its architecture, chemical composition and age. Toronto, Can. American Society of Bone and Mineral Research 2010.

Tommasini SM, **Trinward A,** Acerbo A, Miller LM, Judex S. Intermittent PTH Treatment Increases Intracortical Osteocyte Density and Decreases Fat Mass in Ovariectomized Rats. Toronto, Can. American Society of Bone and Mineral Research 2010.

Tommasini S M, **Trinward A**, Acerbo A, Dunsmuir J H, Miller, L M, Judex S. PTH Treatment Increases Intracortical Microporosities as Detected by Synchrotron Radiation-Based NanoCT. Orthopedic Research Society 2010.

CONFERENCE PROCEEDINGS AND PRESENTATIONS (Continued)

Acerbo AS, Tommasini SM, **Trinward A**, Judex S, L.M. Miller. Rapid Determination of Bone Chemical Composition and Distribution En Block using Synchrotron-Based Fourier Transform Infrared Imaging**.** American Society of Bone and Mineral Research 2009.

Trinward A, Tommasini SM, Lublinsky S, Miller LM, Judex S. Alendronate and Parathyroid Hormone Interventions Normalize the Bone-Fat Relationship in OVX Rat Model. Pittsburgh, PA. Biomedical Engineering Society, 2009

Tommasini SM, **Trinward A**, Lublinsky S, Miller LM, Judex S.Benefits to Bone Quality by Short and Long-Term Osteoporosis Treatments are Site-Specific American Society of Bone and Mineral Research 2009.

Chapter 1

INTRODUCTION

1.1 Introduction to Skeletal Biology

Bone constituents:

The skeletal system is an organ that allows locomotion, provides structural support and protection to internal organs and acts as a calcium reservoir [2]. Bone is a tissue matrix rich in cells that are sensitive to chemical, mechanical and hormonal signals [2]. These cells can be characterized into four types: osteocytes, osteoblasts, osteoclasts and bone lining cells. The extracellular matrix is made of 20% water, 35% organic material (proteins and cells) and 45% inorganic mineral (mineral). The organic phase is composed mostly of a protein called Type I collagen which gives bone its flexibility and tensile strength. The inorganic phase is composed of a mineral called hydroxyapetite which hardens the matrix by incorporation of mineral into the collagen fibrils which increases bone's compressive strength [3].

Bone is composed of two types of tissue called cortical and trabecular bone. Cortical bone is densely packed tissue that provides the majority of bone's mechanical strength. The cortical bone is 5-10% porous; pores are made up of Haversian and Volkmann's canals, a network of small channels of blood vessels that carry nutrients through blood flow to the densely packed tissue. Cortical bone accounts for 80% of the skeletal mass [4].

Trabecular bone is found within cortical shells of most bones. It is made up of a series of interconnected plates and rods that network together to form a tissue that has the appearance of a sponge with a high porosity between 75-95% [5]. The empty space is filled with a gelatinous

medium called bone marrow which is rich with bone cells, progenitor cells such as mesenchymal stem cells, hematapoetic stem cells, blood and nutrients [6].

Skeletal homeostasis and bone remodeling:

Bone is a dynamic tissue that has active cellular mechanisms causing constant turnover. Bone cells degrade the bone matrix and replace it with new tissue in a pair of coupled processes called bone remodeling [7]. Remodeling occurs throughout the skeletal life for a variety of reasons: in order to release calcium into the blood stream for systemic distribution, to adapt to changes in mechanical demand, or to repair itself after incidences of microdamage in order to maintain skeletal integrity [8]. The old bone is removed by the osteoclasts and replaced with new bone matrix which is secreted by the osteoblasts. Bone is remodeled along marrow exposed surfaces in small basins called resorption packets or resorption pits [9].

The bone resorption process is triggered by a number of cytokines and growth factors in response to its chemical, mechanical and hormonal environment. Bone marrow contains the cells responsible for the bone remodeling process [10] which is in surface contact with 70-85% of trabecular bone. This makes trabecular bone more susceptible to bone turnover due to the constant interaction of remodeling cells on trabecular surfaces. Twenty five percent of trabecular bone is remodeled every year, while only 3% of cortical bone is remodeled [6]. In diseased states, such as osteoporosis, trabecular bone is susceptible to large reductions in bone mass and bone density [11].

Osteoclasts are multinucleated cells responsible for bone resorption. They differentiate from the hematopoietic stem cell lineage. Osteoclastogenesis is initiated through a series of cytokines including colony stimulating factor and interleukin-1, 3, 6 and 11 [6, 12].

Intracellular signaling leads to the differentiation of bone marrow hematopoietic stem cells into osteoclasts [13]. Osteoclasts are recruited to bone surfaces where they create a seal with their ruffled cell edge [2]. The cells demineralize the exposed bone by excreting acids and enzymes that degrade extracellular matrix and form resorption pits along exposed bone surfaces [2]. Unexposed cortical bone is removed by a basic multicellular unit (BMU) called a cutting cone that tunnels into the dense tissue originating from a Haversian canal or the marrow exposed surface, called the endosteum [14]. Bone remodeling is a coupled process; during resorption, osteoclasts actively secrete cytokines that signal for osteoblast recruitment in order to initiate new bone formation at the remodeling site [15, 16].

Osteoblasts are mononucleated cells responsible for bone formation. They differentiate from the mesenchymal stem cell lineage or from bone lining cells residing on bone surfaces [10]. Osteoblastogenesis, or osteoblast differentiation, occurs in response to the secretion of a variety of hormones and cytokines including estrogen and insulin-like growth factor-1 [17, 18]. Osteoblasts are also stimulated by the same cytokines that stimulate osteoclastogenesis, including interleukin-6 and 11, which demonstrates the coupled activation of the remodeling process [6]. Osteoblasts lay down new bone by secreting matrix called osteoid along the bone surface. This material is composed predominantly of collagen [19]. The new bone is poorly mineralized but quickly becomes incorporated with hydroxyapetite crystals to mineralize the collagen matrix to normalize the material properties to match surrounding tissue [20]. Occasionally an osteoblast gets embedded into the extracellular matrix as new bone is being laid down. When this occurs, the osteoblast becomes a part of a network of bone cells within the extracellular matrix called osteocytes.

Osteocytes are bone cells responsible for cellular signaling and bone communication. Intracellular signaling occurs between osteocytes and from osteocyte to other bone cells through long cellular processes called canaliculi that create gap junctions across the bone matrix [21]. Cell-to-cell signaling is conducted through the gap junctions via secretion of secondary messengers that are transmitted as hormones and paracrine factors which activate signaling pathways [22]. Osteocytes are said to be highly sensitive to mechanical stimulation, they are critical initiators of both resorption and formation in response to changes in their mechanical strain environments. In low strain environments, osteocytes undergo apoptosis which attracts osteoclasts to initiate bone resorption to remove excess bone mass [23]. During incidences of high strain, osteocytes recruit osteoblasts to increase bone mass in order to relieve the strain placed on the cells from the increased mechanical loads [21]. Osteocytes can communicate directly with bone lining cells to stimulate bone lining cell differentiation into osteoblasts when new bone formation is required [24].

Bone lining cells are attached to the surfaces of bone tissue. They are flattened, inactive osteoblasts that remain quiescent until cellular communication initiates their differentiation [10]. Bone lining cells are thought to be sensitive to mechanical stimulation and can differentiate into osteoblasts during cyclic mechanical loading, including fluid shear flow across their surfaces [22]. They are also activated by osteoclast-released chemicals during resorption [24]. When activated, differentiated bone lining cells will form new bone directly at their site of attachment [14]. They have cell surface receptors for both estrogen and parathyroid hormone, indicating their sensitivity to not just mechanical and chemical signaling but to hormonal signaling as well [25]. Due to their high sensitivity to estrogen, it is believed that bone lining cells are a key

player, and potential pharmacologic target to treat bone diseases where estrogen deficiency is a major cause of bone loss, such as post-menopausal osteoporosis.

Measurements of bone quality:

Bone quality is an ambiguous term that is used to describe changes in the parameters which differentially alter bone strength. Initially, the severity of osteoporosis and the effectiveness of drug treatments were determined solely by bone mineral density measurements. However, clinically measured bone density is not be a good predictor of fracture occurrence [26], because it is strongly influenced by bone quantity but does not provide information regarding quality. For instance, patients with low bone mass that is highly mineralized can get similar density readings as patients with high bone mass which is poorly mineralized. Therefore it is apparent that higher resolution measures of bone properties are necessary to accurately measure osteoporosis and monitor treatment efficacy.

Bone quality can be characterized by geometry and structural properties, microarchitectural properties and its tissue level material properties. Bone structure and geometry include the shape and overall bone tissue volume, length of the femoral neck and cortical thickness and bone volume fraction, all of which are closely correlated to bone mass.

The tissue microarchitecture is a high resolution characterization of the trabecular bone which is said to be closely linked to fracture resistance and strength [27]. Trabecular architecture is summarized by the number of trabeculae, their connectivity and thickness as well as their alignment. The structural modeling index defines the trabecular alignment as either perpendicular to loading (plate-like) or parallel to the direction of loading (rod-like) on a scale of 0 to 3, zero being perfectly plate-like and 3 being perfectly rod-like [28]. In osteoporotic bone

loss, the trabecular structure transitions to more rod-like with a higher structural modeling index, closer to 3 [29].

Bone quality is also defined by tissue level material properties. Tissue density and mineralization and matrix organization: such as the number of cross-linking of collagen fiber size, orientation, and maturation of the mineral crystals [11]. Tissue level mechanical properties have been shown to correlate to changes in chemical properties [30].

Bone structure, geometry and trabecular microarchitecture and tissue mineralization can be measured through micro-computed tomography. The indices of bone quality obtained by micro-computed tomography have been shown to be excellent predictors of bone strength [31], [32]. Additionally, tissue mineral density and mineral distribution can be determined through microradiography, and scanning electron microscopy. The chemical composition can be measured through Fourier transform infrared microspectroscopy as well as Raman spectroscopy. Dynamic histomorphometry has commonly been used to determine the metabolic activity of bone which can affect its overall strength [33, 34].

Mechanical properties of bone:

In the laboratory, mechanical testing is conducted on human bone biopsies, cadaver bones or specimens harvested from animal studies. Mechanical testing is done in order to determine bone material properties such as maximal applied load and inherent tissue elasticity. Bone strength is dependent on bone mass, architecture and tissue material properties, so measurements of elasticity require normalization to determine inherent properties of the material [35]. The overall goal of pharmaceuticals is to maintain or improve bone strength by modulating the properties which enables the bone to bear loads.

Mechanical properties illustrate how a material responds under a given load. Bone mechanics can be defined by a number of factors including applied force, deformation or displacement, stiffness, stress, strain and Young's modulus. To experimentally determine the mechanical properties of bone, a force or applied load, deforms a material while displacements are measured. During this process an applied force relative to the amount of displacement it causes creates a force-displacement curve. This curve is characteristic to individual bones, and although follows a similar shape during loading, each bone specimen will differ depending on the structural and material properties of the bone.

The curve consists of a toe-in region, a linear region (stiffness), a yield point (yield load) followed by a region of necking and plastic deformation finished with maximum load and mechanical failure. From the linear portion of the fore-displacement curve the stiffness of the material can be computed, which is a measure of how pliable or rigid the material is under a given load, in bone it is considered a measure of how brittle the material is. Based on the known geometry of the bone, typically its moment of inertia (I or J) and the distance to the center of mass, the forces and displacements can be converted into a stresses and strains to create a stress-strain curve.

Stresses (σ) are the forces acting throughout a deformable body and are measured as force per unit area, a measure of pressure. It is simply defined as the force normalized by the geometry of the material. Strain is the displacement of a material in reference to its original length or location; it is a unitless measurement, usually expressed as a decimal or a percentage. It is referred to as the elongation or shortening of a material and has a relationship to the stress applied to the material. The relationship between stress and strain creates a distinct curve that

inherent material properties are extracted from. Young's modulus is the measure of the elasticity of a material which is determined from the linear region of the stress-strain curve [36].

The invasive and destructive nature of mechanical testing makes it difficult to measure bone strength clinically. Historically, patients are evaluated for risk of fracture by their number of incidence of fracture in conjunction with a Dual X-Ray Absorptiometry (DXA) T-score. This score compares the patient's bone mineral density to the population mean. If the patient, in his demographic falls one standard deviation below the average T-score they are considered osteopenic. If the patient falls 2.5 standard deviations below the population mean, they are considered osteoporotic. Taken into conjunction the age and incidence of fracture in the individual, the doctor will recommend whether their patient is a candidate for pharmaceutical therapy. For instance, a 50 year old woman with a previously reported fracture and a T-score below -1, would likely be prescribed with a drug, the same patient with no fracture would be monitored regularly to determine changes in BMD with aging [37]. The drastic reduction in circulating estrogen after the onset of menopause can cause severe degradation to bone mass which is termed post-menopausal osteoporosis.

1.2 Post-menopausal Osteoporosis

Biology and incidence:

Estrogen is a sex steroid present in the body. It is produced predominantly in the ovaries by developing egg follicles beginning at the onset of menstruation until menopause [38]. During menopause, women experience a significant decrease in circulating levels of estrogen. This can result in decreased bone volume and mineral density causing an increased risk of skeletal fracture, called post-menopausal osteoporosis [26, 39-41]. Post menopausal osteoporosis is

caused by a mismatch in bone remodeling rates, where resorption is faster than formation leading to a net loss in bone mass [6].

Estrogen is a key regulator of bone metabolism due to its inhibitory effects on bone resorption as well as its activation of bone formation. Estrogen stimulates bone formation through the activation of osteoblasts via estrogen receptors and cell signaling to bone lining cells [38]. Estrogen replacement therapy has been shown to increase the differentiation of pre-osteoblasts and increase osteoblast proliferation in estrogen-deficient rats [42]. It can also stimulate osteoclast apoptosis, and reduce resorption rates [7]. Reduction in circulating estrogen leads to reductions in bone mass and density, and severe degradation of trabecular microarchitecture and mechanical properties [43]. This includes a decrease in trabecular number and thickness as well as increase in the spacing between struts and reduced connectivity density [11].

Reduced circulating estrogen also alters body composition causing weight gain, fat accumulation and reduced lean body mass [44-49]. Estrogen loss has negative consequences on fat metabolism including increased leptin and cholesterol concentrations [50-52]. Estrogen replacement therapy has been shown to reverse the effects of bone loss [49], while decreasing the effects of menopause-related obesity, visceral fat accumulation and leptin hormone levels [50, 53]. Although fat and metabolic effects of estrogen-withdrawal are important factors of menopause, prevention of skeletal degradation is still the main focus of most therapies used to treat post-menopausal osteoporosis.

Over 1.5 million osteoporotic related fractures occur each year, most commonly in the hips, spine and wrists [54]. Thirty percent of women over the age of 75, and fifty percent of women over the age of 85 have experienced a spinal fracture [54]. The direct costs in the U.S.

are up to $18 billion dollars a year [55]. Post-menopausal osteoporosis is commonly treated with several pharmaceuticals used to maintain bone mass which are broken into two classes 1.) anabolic drugs which increase bone formation or 2.) anti-catabolic drugs which reduce resorption.

1.3 of Post-menopausal Osteoporosis

Alendronate:

Alendronate (ALN), clinically known as FOSOMAX, is a bisphosphonate used to treat osteoporosis. Bisphosphonates are a class of drugs most commonly used to treat metabolic bone diseases including Paget's disease, osteogenesis imperfecta, hypercalcemia, osteopenia and osteoporosis [56]. Alendronate is anti-catabolic that works as a specific inhibitor of osteoclast-mediated bone-resorption by binding to bone's hydroxyapetite [57].

The structure of a bisphosphonate is composed of two phosphonates and two side chains called R^1 and R^2 that are joined by carbon. The phosphonates are chelating agents that bond strongly to metal ions such as calcium, and magnesium. This creates a high affinity for the drug to bind to the hydroxyapetite crystals found on the bone surface; the affinity of binding is increased more to bone sites where active remodeling is in progress [57]. After the drug is bound to bone it interacts with osteoclasts during remodeling. When an osteoclast attaches to the tissue surface it secretes enzymes that digest the bone. The R2 side chain residing in the bone is released and enters the osteoclast causing it to lose its resorptive properties which triggers osteoclastic apoptosis, preventing further resorption [7, 56].

By blocking bone resorption alendronate increases bone mineral density. A ten year clinical study in women with post-menopausal osteoporosis demonstrated that alendronate taken

at 10 mg for 10 years increased bone mineral density in the lumbar spine by 13.7% and in the proximal femur by 6.7% [58]. It has also been shown to improve the microarchitecture of bone compared to placebo treatment in post-menopausal women. After alendronate was taken for three years, bone volume fraction was 17% greater, trabecular thickness was 13.4% higher and trabecular spacing was significantly less in treated women compared to untreated women [40]. It is clinically proven to reduce the incidence of hip fractures [59], vertebral fractures [59, 60] and non-vertebral fractures in post menopausal women [59, 61].

Anti-catabolic drugs suppress natural bone turnover so there is an increase in tissue mineralization that may be detrimental to tissue health. Long term alendronate use has been shown to increase microdamage by accumulation of microcracks in dogs [62-64]. Microdamage has been associated with increased risk of fracture and is prevalent in post-menopausal women [65]. Because the drug remains in the skeletal system long after treatment ends, it is important to consider treatment duration and potential over-suppression [56]. FDA has added a femur fracture warning to all bisphosphonate prescriptions because of an increased rate of atypical spontaneous midshaft fractures. This may be due to tissue level changes in material properties of the bone matrix, which could lead to tissue damage accumulation or overmineralization since bone remodeling is suppressed during treatment.

Parathyroid hormone:

Parathyroid hormone (PTH) is naturally secreted by the parathyroid gland. It is an anabolic hormone which increases bone mass by stimulating bone formation. It is an 84-amino acid sequence and is responsible for regulating blood calcium concentrations [66, 67]. A synthetic analog of PTH called hPTH(1-34) has been shown to have similar anabolic effects to naturally

secreted PTH. PTH increases the production of cytokines and growth factors such as IGF-1 and TGF-B which act directly on osteoblastic cells to increase bone formation [68]. PTH can stimulate the commitment of mesenchymal stem cells in the bone marrow niche towards osteoblastic cell lineage [69],[70]. PTH receptors are more abundant on bone cells that are not adjacent to osteoid, indicating its key role in osteoblast recruitment to sites of active remodeling including increasing recruitment of preosteoblasts from marrow stromal cells [71]. PTH enhances osteoblast productivity, osteoblastic cell differentiation and maturity of bone lining cells and prevents osteoblast apoptosis [72-74].

Teriparatide is the only FDA approved version of synthesized parathyroid hormone. It is used in patients with severe cases of osteoporosis who are unable to take other medications [75], due to high costs, the need for daily injections and because long-term side effects are largely unknown [11]. In animal studies, there have been incidences of bone cancer called osteosarcoma that may develop during long term PTH treatment [76].

Women treated with Teriparatide at 20-µg or 40-µg were 35 or 40% less likely to have one or more non-vertebral fractures as compared to placebo controls. Post-menopausal related loss in bone mineral density was significantly reduced with PTH therapy compared to placebo controls where 40-µg dosage had the greatest effect at preventing bone density losses [41]. Another study showed a three year effect of PTH with estrogen replacement in post-menopausal women continuously increased bone mineral density to values 13% greater in the vertebral body and 2.7% greater in the hip than placebo controls [77]. The largest increases in bone mineral density were seen in the first year of treatment [78]. PTH administration creates bone with similar structural properties of healthy tissue; Teriparatide increased the amount of trabecular bone with improved trabecular architecture and induced a 22% increase in cortical bone [28].

Others have shown similar positive effects of PTH administration on bone mass and density in post-menopausal women [79, 80].

1.4 The Metabolic Consequences of Estrogen Withdrawal

***Body compositional changes with menopause**:*

It is well documented that there is a positive association between body weight and bone mass or bone mineral density, demonstrating the beneficial effects of increased mass has on skeletal health. Higher mechanical demand on the skeleton from increased body mass leads to remodeling that favors formation and increased skeletal mass to absorb the higher mechanical loads [81, 82]. There is conflicting data regarding body composition and high fat mass and its role on bone quality. Some found a positive relationship between total fat content and bone mineral density in pre-menopausal women, which was independent of body mass or lean tissue mass [85-89]. Others report no relationship between fat mass and bone mass when fat mass was normalized by body mass [83, 84]. Finally, new studies demonstrate the negative effects of fat mass on skeletal health. Visceral fat mass has been shown to have a negative relationship to bone mineral density, and post-menopausal obesity is associated with worsened metabolic health and reduced bone mineral density and increased risk of fracture [85-92].

Obese post-menopausal women have higher bone mass and bone mineral density with decreased risk of developing hip fractures compared to healthy weight individuals [52, 91, 93, 94]. Inversely, underweight individuals tend to have smaller skeletal systems and are at a higher risk of developing severe osteoporosis due to underloading of the skeleton [95, 96]. This negative effect of reduced body mass is worsened after menopause when people undergo rapid weight loss which results in severe bone loss [97, 98].In fact, obesity and its associated fat

accumulation, particularly the accumulation of visceral adipose tissue may have negative effects on bone quality.

Patients with type 1 and type 2 diabetes have lower bone mineral density with a higher fracture risk than their healthy weight counterparts [99]. It has also been shown that post menopausal obese women have lower rates of bone formation and suppressed collagen formation than healthy weight women, indicating a potential change to tissue material properties, and perhaps bone quality [100]. This suggests that the bone-fat relationship is complex and skeletal health relies on more than just mechanical load bearing of the skeleton. Menopause can cause drastic increases to visceral fat content, increase tissue fat accumulation and significantly alter fat metabolism leading to metabolic health problems [45, 46, 101]. It also causes increased tissue fat accumulation within the bone marrow, muscle and the liver [102, 103].

Osteoporotic patients become increasingly susceptible to lipotoxicity with aging [104]. Fat cells called adipocytes collect excess circulating fat called free fatty acids in order to prevent lipotoxicity [105]. Sequestered free fatty acids get converted into triglycerides which accumulate into adipose depots for long term storage [106, 107]. Triglycerides are a key energy source involved in metabolism and transportation of dietary fat [108]. When energy is needed, the liver hydrolyzes triglycerides into free fatty acids and glycerol which are then carried out of the liver via the blood and transported to mitochondria for energy production [109]. High levels of triglycerides have been linked to atherosclerosis, heart disease, stroke and obesity [110]. Adipocytes and its progenitors are sensitive to circulating free fatty acid levels and insulin levels, as well as hormonal regulators such as estrogen, leptin and insulin like growth factor-1 [111].

Hormonal regulation of bone and fat:

Estrogen is a beneficial factor in bone health. It acts directly on mesenchymal stem cells and bone lining cells to activate bone formation and can also prevent osteoclast mediated resorption, both which positively regulate bone mass [7, 42]. Adipocytes produce estrogen, demonstrating a protective mechanism of fat accumulation against bone loss [15, 112]. Additionally, estrogen replacement has been shown to reverse the effects of food- and ovariectomy-induced obesity [50].

Another hormonal regulator of bone is the hormone leptin which is synthesized by adipocytes. Circulating levels of leptin are directly proportional to the total amount of fat in the body [113, 114]. Leptin regulates appetite, energy intake and expenditure [115]. It is produced by both white and brown adipocytes, within the ovaries, skeletal muscle, bone marrow, the pituitary gland and in the liver [113]. Leptin has positive effects on bone health and is an important regulator of bone metabolism. Leptin promotes bone marrow stromal cell differentiation into osteoblasts [116], and inhibits osteoclast formation [117]. Leptin increases with age and substantially increases in obese women [118]. Leptin concentrations increased in healthy weight women after the onset of menopause but obese women had higher initial levels of leptin that increase further after menopause [119]. Other studies show leptin levels were decreased in post-menopausal women and demonstrate that estrogen is necessary to modulate leptin concentrations [120].

Insulin-like growth factor 1 (IGF-1) is an endocrine hormone responsible for regulation of growth and development [121]. Synthesized primarily in the liver, it is an important hormone for the regulation of bone mass through its stimulatory effects on bone formation [122]. In adults, IGF-1 is anabolic to bone; it increases the activation of healthy osteoblasts through

binding to IGF-1 receptors on the osteoblast surface which directly stimulates osteoblast productivity [123-125]. It does not have an effect on mesenchymal stem cell differentiation [126]. Studies have shown that it plays an important role in bone integrity by increasing mineralization and trabecular bone volume [127]. There is a decline in IGF-1 levels during aging which contributes to decrease in bone mineral density occuring throughout adulthood [128]. Bone mineral density is correlated to serum levels of IGF-1 in post-menopausal women [126]. IGF-1 stimulation in a mouse model increased bone formation rates and increased trabecular and cortical bone volumes. This was caused by increased production of osteoid by osteoblasts independent of differentiation of new osteoblasts [115].

1.5 Molecular Regulation of Bone and Fat

The bone-fat progenitor:

Osteoblasts and adipocytes are inherently linked through their common progenitor, the mesenchymal stem cells, which reside within the bone marrow [129], [130]. PTH can differentiate periosteal osteoblast progenitor cells towards osteoblastic lineages [42]. Recent clinical evidence demonstrates that post-menopausal osteoporotic bone loss is accompanied by increased marrow adiposity [131]. Early differentiation of the mesenchymal stem cells has been associated with a few key transcriptional pathways, PPAR-y (adipogenic) Wnt-9 and (osteoblastic) and activation of transcriptional factors such as RUNX2 (osteoblastic).

Peroxisome proliferator-activated receptor-gamma (PPAR-y) is involved in adipogenesis by regulating the commitment of mesenchymal stem cell to a preadipocyte differentiation and adipocyte formation [132]. PPAR-y is known as the master regulator of adipogenesis; it is necessary for the terminal differentiation of cells into adipocytes. PPAR-y deficient mice have

reduced marrow adiposity, increased osteoblastogenesis and lower bone formation [133]. PPAR-y has been shown to suppress osteoblastogenesis while promoting osteoclastogenesis [133, 134]. There is cross-talk between the PPAR-y and Wnt signaling pathways leading to an inverse relationship between adipogenic and osteogenic differentiation [135].

Wnt signaling is necessary for both osteoblastic differentiation as well as bone formation. Wnt signaling is highly involved in growth and development and plays an important role in early differentiation of osteoblasts and regulation of bone mass [136-138]. The canonical pathway activates mesenchymal stem cell differentiation into preosteoblasts through activation of the β-catenin pathway and activation of transcription factors such as Runx2 [139]. Activation of the Wnt pathway regulates commitment of mesenchymal stem cells to osteoblastic lineages, it increases osteoblastic progenitor populations, ensures terminal differentiation of preosteoblasts and is also involved in increasing bone mineralization [140]. Wnt signaling modulates osteoblastagenesis through activation of the transcription factor Runx2. Runx2 is a major transcription factor for osteoblast differentiation and bone formation [138, 141] It also activates signaling pathways which are linked to PTH stimulation [142]. Runx2 is a regulator of collagen formation through osteopontin upregulation [143].

The bone-fat pathway driving MSC differentiation has recently become a topic of interest, yet the effects of osteoporotic drugs on this relationship are greatly unstudied. Fat mass and adiposity are important predictors of bone health, and may negatively impact bone quality. Maintenance of bone quality, and not quantity, will soon be the standard of care during pharmacological treatments for osteoporosis. During this transition it is critical to identify the role of drug treatments on skeletal health and fat accumulation and to monitor how this relationship is altered.

1.6 Objective and Hypotheses

The overall objective of this dissertation was to identify how ovariectomized Sprague Dawley rats treated with alendronate and parathyroid hormone would induce drug and dosage-specific improvements to bone mass, architecture and chemical composition and how these changes modified bone mechanical properties as well as to determine the role of fat metabolism and adiposity on bone quality.

This objective was addressed with the following hypotheses and research questions.

Hypothesis 1: There are drug and dosage-specific improvements to bone microarchitecture, geometry and tissue material properties which positively correlate to improvements in structural mechanical properties.

Research Questions:

(1) Are microarchitectural parameters, measured through μCT, reduced in OVX treated rats, and dose-dependently recovered with ALN and PTH treatment?

(2) Are tissue material properties of cortical bone measured through FTIR and nanoindentation altered by OVX, ALN or PTH treatment?

(3) Are structural bone properties, measured through finite element modeling reduced with OVX and dose-dependently improved with ALN and PTH treatment?

(4) Do alterations to bone architecture and material properties influence structural properties?

Specific Aim 1: To determine ovariectomy and drug, dosage and duration-specific alterations to vertebral and femoral bone architecture and geometries. Beginning at 6 months of age, OVX Sprague Dawley rats were treated with three doses of alendronate or parathyroid hormone for six months. Post sacrifice, the femoral metaphysis and diaphysis and the tibial diaphysis were extracted and measured with high resolution desktop micro-computed tomography to determine bone mass, structural microarchitecture and tissue mineral density. Tissue material properties of the femoral diaphysis were determined through nanoindentation and Fourier transform infrared microspectroscopy. Structural mechanical properties were determined through finite element modeling of the femoral metaphysis, which incorporated tissue material properties from nanoindentation. Structural properties were correlated to mechanical properties.

Hypothesis 2: Drug and dosage-specific changes to the chemistry of trabecular and cortical bone composition varies in new bone formation compared to interstitial bone. Changes in chemistry positively correlate to changes in tissue mechanical properties.

Research Questions

(1) Are there differential and dose-dependent changes to bone metabolism with PTH and ALN treatment?

(2) Do cortical and trabecular surface properties differ from intracortical properties after ALN and PTH treatment?

(3) How do changes in the chemistry of new and old bone influence the mechanical behavior of the material?

Specific Aim 2: To determine ovariectomy and drug and dosage-specific alterations on bone metabolism and subsequently the chemical composition and mechanical properties of bone

surfaces as they compare to interstitial bone. Beginning at 6 months of age, OVX Sprague Dawley rats were treated with three doses of alendronate or parathyroid hormone for 6 months. Animals were injected with calcein 10/9 days and 4/3 days prior to sacrifice. Tibial metaphyseal bone was embedded, sectioned, imaged with a fluorescence microscope, and analyzed using Osteomeasure to determine changes to bone metabolism. The remaining bone block was analyzed with FTIR equipped with fluorescence microscopy and nanoindentation to determine changes in tissue material properties of bone surfaces. The contribution of chemical composition to mechanical properties was determined through correlative analysis.

Hypothesis 3. The strong-negative relationship between bone quantity and measures of fat metabolism and adiposity are modulated differentially by ALN and PTH.

Research Questions:

(1) How does body composition influence bone mineral density, and how does OVX and drug treatment influence this relationship?

(2) What measures of fat metabolism correlate to bone quality?

(3) Does the interaction between bone and fat become stronger with higher resolution analysis of the bone marrow environment?

Specific Aim 3: To determine ovariectomy and drug-specific effects on abdominal body composition, bone quantity and adiposity. Beginning at 6 months of age, OVX Sprague Dawley rats were treated with various doses of alendronate and parathyroid hormone for 2 months or 6 months. To measure the genotypic response, after short term treatment (2 months), bone marrow was extracted and analyzed using RT-PCR primers for PPAR-γ, RUNX2, Wnt9b and RANK-L;

this was done to determine early genetic differentiation of marrow stromal cells prior to a phenotypic change. To measure the phenotypic response, vertebral bone volume and mineral density, abdominal fat volume and lean tissue volume were measured longitudinally at 6, 8 and 12 months through in vivo micro-computed tomography. Post-sacrifice, after 2 months, or 6 months of treatment, bone microarchitecture was determined of the L-4 vertebral body through desktop μCT. Blood serum, fat pads and livers were extracted, weighed and measured for triglycerides and free fatty acids. Leptin, IGF-1 and alkaline phosphatase concentrations was determined from the blood serum. Marrow adiposity and bone quantity were determined through histological analysis of the tibial metaphysis. Bone marrow precipitate and livers were analyzed for triglycerides, free fatty acid concentrations. Measures of bone quantity were correlated to measures of metabolism and adiposity.

Chapter 2

DOSE-DEPENDENT IMPROVEMENTS IN MICROARCHITECTURE WITH ALENDRONATE AND PTH ENHANCE BONE STRENGTH DESPITE REDUCTIONS IN TISSUE MATERIAL PROPERTIES

2.1 Abstract

Osteoporosis is associated with a loss of bone mass and deterioration in tissue quality. Drugs such as alendronate (ALN) and parathyroid hormone (PTH) differentially counteract bone loss, which may lead to drug-specific changes in bone architecture and material properties, factors that modulate bone's mechanical properties. To determine how drug-induced changes in bone structure and tissue properties relate to mechanical properties, OVX rats were subjected to 6mo of high (H), medium (M) or low (L) doses of ALN and PTH. Morphologic (μCT), chemical (FTIR), and mechanical properties (nanoindentation, finite element modeling, 4pt bending) of cortical and trabecular bone in the femoral metaphysis and tibial diaphysis were determined. Six month old Sprague Dawley rats (n=10/group) were assigned to age-matched controls (AC), OVX controls, OVX treated with specified doses of hPTH or ALN. At 12mo of age, OVX rats had 81% less trabecular bone than AC. There were dose-dependent improvements to architecture: L-PTH had similar BV/TV as OVX, while M- and H-PTH had 2x, and 7x more BV/TV and L-, M- and H-ALN had 1x, 2x and 4x more BV/TV than OVX. Compared to AC, H-PTH and H-ALN maintained or improved both trabecular and cortical architecture, but decreased cortical tissue mineral density by 6% and 3%. Nanoindentation of the cortical bone showed that H-PTH and H-ALN had a 9% and 14% smaller elastic modulus and a 10% and 11% lower tissue hardness than AC. Incorporation of tissue morphology and elastic moduli into a finite element model estimated that when compared to AC, OVX had 12% lower stiffness while H-PTH and H-ALN were 46%

and 18% stiffer. Similar patterns across groups were observed in the tibial diaphysis. When combined via multiple linear regressions, Ct.Th, Tb.BV/TV, and Tb.Th. explained 91% of the variability in stiffness. The inclusion of chemical and/or tissue mechanical properties did not enhance this association. These data demonstrate that despite deteriorated tissue properties in ALN and PTH treated rats, maintenance of bone architecture resulted in a structure with superior mechanical stiffness. While this reiterates the importance of preserving bone structure during osteoporosis, the drug-induced reductions in tissue material properties may indicate material detriment, especially with long term use.

2.2 Introduction

Post menopausal osteoporosis is associated with a decrease in bone quantity and quality, increasing the risk for skeletal fracture [144] It is a result of a mismatch in the bone remodeling processes where bone resorption occurs at a faster rate than formation [145]. This leads to a net loss in bone mass, with a degradation of both the bone structure and its material properties. Osteoporotic bone loss is characterized by cortical thinning and degradation to the trabecular compartment [146]. Trabecular bone loss is characterized by a reduction and thinning in trabeculae, increased trabecular separation [147] and a transition in trabecular elements from plate-like to rod-like structures, which all contribute to changes in overall bone strength [148].

Osteoporosis drug treatments are classified in two categories that work differentially to prevent tissue degradation: either by increasing formation (anabolic i.e. PTH) or decreasing resorption (anti-catabolic i.e. bisphosphonate). Parathyroid hormone is an anabolic drug that effectively mitigates bone loss by stimulating bone formation to rates faster than resorption, leading to a net gain in bone mass. Teriparatide is a shorter peptide analog of PTH, clinically

proven to increase bone mass and bone density in post-menopausal women [80-83]. PTH stimulates new bone formation that has similar structural properties of healthy tissue; it can improve trabecular architecture and increase cortical bone thickness [28, 39]. The anabolic action of PTH is highly effective at increasing bone mass, but the rapid rate of bone formation may affect the maturity and mineralization of surface properties [149] which can lead to irregular mineral density distribution of the bone matrix [152]. Ultimately, lowered tissue mineralization can reduce tissue material properties [150] and may negatively influence total bone strength.

Alendronate is an anti-catabolic drug that works as a specific inhibitor of osteoclast-mediated bone-resorption [57], and has been clinically proven to maintain bone mass, and increase bone density when taken at 10 mg for 10 years [58]. It maintains bone microarchitecture during estrogen withdrawal [40], and reduces the incidence of hip, vertebral and non-vertebral fractures in post menopausal women [60-62]. But anti-catabolic drugs suppress natural bone turnover, increases tissue mineralization, tissue hardness and stiffness [151]. Alendronate-induced changes in tissue material properties can lead to tissue brittleness, and accumulation of microcracks [62, 152] which both have been shown to increase fracture susceptibility in post-menopausal women [65].

Since bone loss and therefore fractures typically occur in regions rich in trabecular bone, characterization of trabecular microarchitecture is critical for defining drug-specific changes to bone quality and its impact of structural properties. Finite element modeling has proven to be a useful tool in estimating bone strength both in laboratory models [153] and clinically [154]. However, the current models commonly disregard drug-induced modification to tissue level material properties [155], which may influence total bone strength.

In this study, we aim to determine the effects of estrogen withdrawal and drug treatment on tissue level material properties (nanoindentation, FTIR), characterize the bone microarchitecture (μCT), utilize tissue material properties to estimate bone strength (finite element modeling analysis) and measure structural mechanical properties (4 point bending). Measures of bone chemistry, micro-mechanical tissue properties and morphological properties will be independently regressed against measures of bone stiffness and strength as well as combined via multivariate analysis. We hypothesize that ovariectomy will induce reductions to bone structure and tissue level properties and alendronate and PTH will dose-dependently improve bone structure but will differentially modulate tissue material properties all of which will influence bone structural mechanical properties.

2.3 Materials and Methods

Experimental Design

All procedures were reviewed and approved by the Institutional Animal Care and Use Committee of Stony Brook University. All rats were individually housed in standard cages and allowed free access to standard rodent chow and tap water and were weighed twice weekly to monitor changes in body mass. Adult five-months-old female Sprague-Dawley rats were ovariectomized and mass-matched into normal age matched controls (AC), ovariectomized controls (OVX), and ovariectomized rats treated with either alendronate (ALN) or parathyroid hormone (PTH) at three different doses.

At 6 months of age, 10 normal and 10 OVX rats were sacrificed as baseline controls, drug treatment began. Alendronate was injected subcutaneously twice per week; high-dose rats received 2mg/kg (H-ALN), medium-dose rats received 100μg/kg (M-ALN), and low-dose rats

received 10µg/kg) (L-ALN). Parathyroid hormone was injected subcutaneously five times per week: high at 75µg/kg (H-PTH), medium at 15 µg/kg (M-PTH), and low at 0.3 µg/kg (L-PTH). Drugs were administered at the dosages listed, per injection. Treatment doses were determined based on previous literature for the clinically relevant dose extrapolated to the rat model (medium), the maximum tolerable dose without known evidence of cytotoxicity (high) and a dose low enough to prevent some OVX induced bone loss (low).

All animals, except AC controls, were ovariectomized at 5 months of age. Baseline animals were sacrificed at 6 months of age. Drug treatments began a 6 months of age and continued for 6 months, and animals were sacrificed at 12 months of age.

Micro-computed Tomography

Post sacrifice, the left femora were extracted, cleaned of soft tissue, preserved in ethanol and stored at -20 C. The tibial diaphysis was extracted, cleaned of soft tissue, preserved in phosphate buffered saline and stored at -20°C. The metaphyseal region of the femur and the diaphysis of the femur and tibia were individually scanned at 18 µm resolution (300 ms integration time, 45 kV, 177 µA) by desktop micro-computed tomography (µCT40, Scanco, Medical AG, Basserdorf, Switzerland). A 3D Gaussian filter was applied to the images and a global threshold separated bone from background (sigma=0.3, sigma support=1, lower threshold=290). The femoral metaphyseal scans were separated into cortical and trabecular bone compartments using a previously established automated script [156]. The trabecular bone compartment was characterized by bone volume fraction (BV/TV), trabecular thickness (Tb.Th.) trabecular number (Tb.N.), trabecular separation (Tb.Sp), structural modeling index (SMI) and trabecular tissue mineral density (Tb.TMD). The femoral and tibial diaphyses were analyzed for cortical

properties: cortical bone volume (Ct.BV), cortical thickness (Ct.Th.), polar moment of inertia (pMOI) and tissue mineral density (Ct.TMD).

Fourier Transform Infrared Microspectroscopy (FTIR)

The femoral diaphysis was microscopically analyzed using synchrotron-based Fourier transform infrared microspectroscopy (FTIR) to measure chemical composition across the cortical surface. The left femoral diaphysis was cut using a diamond blade saw, cleaned of soft tissue and dehydrated in a series of ethanol solutions (70%, 80%, 90%, 100%, 3-4 days each). Bones were embedded in epoxy resin with the proximal end exposed. The indenting surface was polished using abrasive silicon carbide papers of decreasing particle size (600, 800 and 1200 μm) and were polished with a series of diamond suspension polishing solutions (3 μm, 1 μm, 0.25 μm and 0.05 μm).

The highly polished surface of the bone blocks were analyzed with FTIR at Brookhaven National Labs at the U10B beamline. A spectrophotometer, with an IR microscope and MCT detector was used in a frequency range of 4,000 to 650 cm for spectral mapping. Spectra were collected at 128 scans per point, with 4x4 binning in reflectance mode. Data was collected and processed using Opus software. Background scans were collected periodically on a highly reflective gold window to reduce instrumentation noise.

Reflective data were transformed into absorbance data using a Kramer's Kronig transformation algorithm [157]. Absorbance data was analyzed using Cytospec software to determine mineralization (phosphate/protein ratio (900-1200/1600-1700), collagen cross-linking (1659-1661/1689-1691), crystallinity (1034-1036/1024-1026), carbonate substitution (1414-1424/900-1200), protein content (1600-1700) and phosphate content (900-1200, **Figure 2.1**).

Nanoindentation

After non-invasive FTIR analysis, bone blocks were subjected to nanoindentation to determine the tissue level mechanical properties of the femoral diaphysis. The bottom of epoxy samples were mounted to metal disks with cyanoacrylate glue and sonicated to thoroughly clean the bone surface of residue.

Highly polished surfaces of cortical bone were indented using a nanoindenter system (Triboindenter; Hysitron, Minneapolis, MN) with a Berkovich indenter tip. Bones were indented using a trapezoidal load function at a constant loading rate of 100 μN/s for ten seconds followed by a constant 10000 μN load for 10 second hold, followed by a constant unloading rate of -100 μN/s for ten seconds. The elastic response was calculated from the 20-90% portion of the unloading curve using calculations previously described [155].

Each bone was indented 48 times at points that spanned across the entire diaphyseal cortex. Indent locations were visually selected to avoid contact with large pores or cracked surfaces at a distance no less than 100 μm from another. Outliers for each sample were individually removed if they fell more than 2 standard deviations away from the sample mean. The average indentation tissue elastic modulus (N/mm) and tissue hardness for all 48 indents were averaged to a single data point, group averages and standard deviations were calculated. The elastic moduli for individual groups were applied to a finite element model.

Diaphyseal Mechanical Testing

On the day of mechanical testing, tibiae were removed from the freezer and allowed to thaw to room temperature. Bones were individually subjected to 4-point bending in the anterior-posterior direction (MTS, Eden Prairie, MN). Samples were loaded to failure at a constant load rate of

0.01mm/s. Force-displacement curves were generated during the mechanical test and were individually computed to stress-strain curves using geometric measures of inertia (I_{yy}) and center of mass (c), previously calculated through high resolution μCT of the tibial diaphysis. Strain values were computed using the following equation for bone mechanically tested in four-point bending[158] :

$$\boldsymbol{\varepsilon = \frac{6cd}{a(3L-4a)}}$$

Where:
ε = strain (unitless)
c= distance from the center of mass
d=measured displacement
a= distance from upper jig contact point to lower jig contact point
L= distance between lower jig contact points

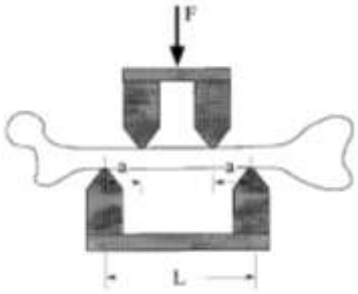

Stiffness was calculated from the linear region of the force displacement curve. Maximum force was defined as the largest applied loading force. Apparent modulus was calculated from the linear region of the stress-strain curve and maximum stress was defined as the largest computed stress.

Stress values were computed using the following equation:

$$\boldsymbol{\sigma = \frac{Fac}{2I}}$$

Where:
σ =Stress (GPa)
F= applied force
a= distance from upper jig contact point to lower jig contact point
c= distance from the center of mass
I= moment of inertia (determined through μCT)

Finite Element Modeling

To characterize the mechanical response to an applied load, the femoral metaphyseal bone regions, were submitted to a finite element model (Scanco, Medical AG, Basserdorf, Switzerland). 3D images that were generated from micro-CT analysis were separated into

cortical and trabecular bone compartments and converted into structural elements and nodes at a one-to-one basis at 18 μm resolution. All disconnected elements were removed from the sample and the remaining object was subjected to a frictionless uniaxial compression simulation (Ulrich, 1999) applied through the proximal and distal surfaces to correspond to longitudinal loading in the z-direction. Linear elastic properties were assigned to the sample as defined by treatment group averages as determined through nanoindentation (GPa), with a Poisson's ratio for bone (ν) of 0.3 for all samples [159]. An iterative FE-solver (Van Rietbergen, 1995) with a force and displacement tolerance of $1x10^{-4}$ determined structural apparent stiffness. Maximum applied loads in cortical and trabecular compartments, % load carried by trabecular bone, structural stiffness and Young's modulus were estimated.

Statistical Analysis

All values were presented as means +/- standard deviations. Statistical significance between groups was determined using a One-Way ANOVA followed by a Tukey post-hoc test, or a Dunnett post hoc test where noted. The differences between groups were reported with their associated p-values. Measures of bone quality were individually regressed against bone strength using linear regression analysis, the R^2 value and associated p values were reported. A multivariate analysis was used to determine the combinatorial contribution of structural and tissue material properties to bone strength.

2.4 Results

Structural morphology of the femoral diaphysis:

Diaphyseal bone from femoral diaphysis, analyzed through desktop microCT, revealed evidence of ovariectomy induced bone loss. At 12 months of age, after 7 months of ovariectomy (OVX), OVX controls had 3.3% thinner cortical bone with 1.8% lower tissue mineral density in OVX compared to age-matched controls (AC) although these reductions were not yet significant ($p>0.05$). H-ALN and H-PTH treated rats had cortical bone volumes that were 14 and 21% higher and cortical thicknesses 12 and 20% thicker than AC controls ($p<0.001$), this was accompanied by an increase in polar moment of inertia compared to their lower doses ($p<0.01$). Yet, H-ALN and H-PTH had tissue mineral densities that were 3.4 and 6.1% lower than AC controls ($p<0.001$, **Figure 2.2**). Similar changes occurred after OVX and high-dose treatments in the tibial diaphysis (**Table 2.1**).

Tissue mechanical properties of the femoral diaphysis:

Changes to femoral cortical bone tissue mineral density induced by PTH and ALN were accompanied by reductions in tissue-level mechanical properties measured through nanoindentation. OVX had 2.4% lower elastic modulus and 4.2% lower tissue hardness compared to AC but the difference was not significant ($p>0.05$). Compared to AC controls, L- and H-ALN treated rats had 13.9 and 14.2% lower elastic modulus ($p<0.01$); PTH treated rats also had lower elastic moduli with 11.1 (L-PTH), 11.2 (M-PTH) and 9.9% (H-PTH) lower elastic modulus than AC controls ($p<0.05$, Dunnettt). L-ALN, L-PTH and M-PTH treated rats had 17.7% (L-ALN), 16.7% (L-PTH) and 15.8% (M-PTH) lower tissue hardness than AC controls ($p<0.01$, Dunnett, **Figure 2.3**).

Tissue chemical properties of the femoral diaphysis:

FTIR analysis of the femoral diaphysis revealed few changes in femoral cortical bone chemistry after OVX or with drug treatment. There were no significant changes to tissue mineralization or protein content. There was a small but significant increase in crystallinity in L-PTH treated animals which were 6% higher than OVX controls ($p<0.05$). Additionally, M-PTH had 10% higher collagen cross-linking than AC controls ($p<0.05$). M-ALN had 6% higher carbonate incorporation than OVX controls ($p<0.001$) L-ALN treated animals had 7.8% lower phosphate content than OVX controls ($p<0.05$), which were also 6.8% lower than H-ALN treated animals ($p<0.05$, **Figure 2.4**).

Trabecular architecture of the femoral metaphysis:

The metaphyseal bone of the distal femur, analyzed by desktop μCT, was separated into cortical and trabecular bone compartments (**Figure 2.5**). Data showed that OVX degraded the trabecular micro-architecture compared to AC controls, but PTH and ALN treatments dose-dependently improved trabecular micro-architecture. OVX controls had 6.1x lower bone volume fraction (BV/TV) than AC controls ($p<0.001$). M-ALN and M-PTH treated rats had 3.1x and 2.8x greater BV/TV than OVX controls ($p<0.05$). H-ALN and H-PTH treated rats had 7.6x and 9.9x greater BV/TV than OVX controls ($p<0.001$). Additionally, H-PTH treated rats had 54% higher BV/TV than AC controls ($p<0.001$).

The improvement to BV/TV by drug treatment was due to dose-dependent increases in trabecular number (Tb.N) and trabecular thickness (Tb.Th). OVX controls had 47% lower Tb.N than AC controls ($p<0.01$). L-, M- and H- ALN treated rats had higher Tb.N by 52, 59 and 57%

compared to OVX controls ($p<0.001$). M- and H-PTH treated rats had 48 and 65% higher Tb.N than OVX controls ($p<0.01$, Figure 4b). Tb.Th was unchanged in OVX controls compared to AC controls ($p>0.05$), but H-ALN treated rats had 39% higher Tb.Th than OVX controls ($p<0.01$) and M- and H-PTH treated rats had 36 and 59% thicker trabeculae than OVX controls ($p<0.01$).

Structural modeling index (SMI) increased by 30% after OVX, but H-ALN restored SMI to a value 42% lower than OVX controls ($p<0.001$). M-PTH had 41% lower SMI than OVX controls ($p<0.0$) H-PTH reduced the SMI by 83% compared to OVX controls ($p<0.001$), which was also 75% lower than AC controls ($p<0.001$, **Figure 2.6**). There was no change in trabecular tissue mineral density across all groups.

Structural mechanical properties of the femoral metaphysis:

Tissue material properties of the femoral diaphysis, determined through nanoindentation, were input into a finite element model of the femoral metaphysis which simulated a z-direction compression loading. OVX had an estimated 8.6% lower stiffness compared to AC controls but the difference was not yet significant ($p>0.05$). Despite the reduction in tissue material properties in ALN and PTH treated animals; there were dose-dependent improvements to structural mechanical properties. Trends showed L-, M- and H-ALN had 1.3, 8.3 and 26.5% higher stiffness than OVX controls, where only H-ALN was significant ($p<0.01$). M- and H-PTH had 6.1 ad 46.7% higher stiffness than OVX controls, where only H-PTH was significant ($p<0.01$). Additionally, H-ALN and H-PTH had 16.5 and 35.1% higher stiffness than AC controls ($p<0.01$). The apparent modulus, a calculation of the inherent material properties, showed that H-

PTH treated rats had an apparent modulus 20% higher than L-PTH ($p<0.01$) and 16% higher than M-PTH ($p<0.05$), which was also 26% higher than AC controls ($p<0.001$).
In AC controls, 33% of the mechanical load was carried by trabecular bone, but after OVX, only 8% of the total load was carried by trabecular bone ($p<0.001$). L-, M- and H-ALN treated rats reversed the shift in trabecular load contribution so that 15, 21 and 35% of the load was carried by trabecular bone while L-, M- and H-PTH treated rats carried 7, 18, and 42% of the load through their trabeculae (**Figure 2.7**).

Cortical and trabecular architecture and morphology correlated positively to structural mechanical properties, for instance: 71% of the change in bone stiffness was explained by trabecular thickness ($p<0.001$). Linear regression of individual parameters indicated a consistent positive relationship by both bone mass and architecture to total bone stiffness (**Table 2.3**). Chemistry and tissue mineral density did not correlate to changes in micro-mechanical properties when analyzed for each individual animal (**Table 2.4-upper values**). Correlations were improved moderately when group averages were used to correlate chemical properties and TMD to micromechanical properties (**Table 2.4-lower values**). When combined via multiple linear regressions, parameters of bone microarchitecture: Ct.Th, Tb.BV/TV and Tb.Th explained 91% of the variability in stiffness ($p<0.001$) while chemical or tissue mechanical properties did not enhance this association.

Structural mechanical properties of the tibial diaphysis:

The tibial diaphysis was subjected to 4-point bending to determine structural bone mechanical properties. Results supported the findings from the finite element model where OVX had moderate reductions in mechanical properties including 27.8% lower maximum load, 10.5%

lower stiffness with no difference in apparent modulus compared to AC controls ($p>0.05$). L-, M-, and H-ALN had 14.4, 18.9 and 41.0% higher stiffness than OVX controls, where only H-ALN was significant ($p<0.05$). L-, M- and H-PTH had 10.5, 15.4 and 31.0% higher stiffness than OVX controls but none of these differences were significant ($p<0.05$). Similarly, H-ALN and H-PTH had 46.8 and 59.3% higher maximal applied load than OVX controls ($p<0.01$, **Figure2.8**). Diaphyseal bone stiffness positively correlated to cortical thickness ($R^2=0.16$, $p<0.001$), when H-PTH treated rats were evaluated separately from the population, this correlation was strengthened, demonstrating a potential deficit to tissue quality and a reduction in the material strength. Despite the anabolic effect of H-PTH treatment which significantly increased bone volume and cortical thickness, it was not accompanied by proportional increases to bone stiffness (**Figure 2.9**) suggesting that the material deposited had reduced mechanical capability. This data also demonstrates a discrepancy between the mechanical properties estimated through the finite element model and measured through 4 point bending. In the finite element model H-PTH treated rats had increased elastic moduli, but when the tibial diaphysis was experimentally tested, H-ALN treated rats had 55% higher elastic moduli than OVX controls ($p<0.05$), where H-PTH rats had only a 13% higher elastic moduli than OVX controls which was not significant ($p>0.05$).

Individually, bone volume ($R^2=0.09$, $p<0.01$), polar moment of inertia ($R^2=0.24$, $p<0.001$), cross sectional area ($R^2=0.09$, $p<0.01$), and cortical thickness ($R^2=0.03$, $p>0.05$) correlated to apparent modulus and when combined via multivariate analysis, these parameters accounted for 33% of the modulation in modulus where tissue mineral density did not contribute to bone mechanics (**Table 2.5**).

2.5 Discussion

The degradation of microarchitectural parameters due to OVX was dose-dependently improved with ALN and PTH treatment. ALN and PTH decreased the micro-material properties of bone which correlated to decreases in tissue mineral density. When material properties were applied to a finite element model, OVX showed a reduction in bone stiffness while high doses of ALN and PTH increased bone stiffness, despite reductions in tissue level properties.

Bone quality is a culmination of its micro architecture, geometry, and tissue material properties which all contribute to its structural mechanical properties [35]. High resolution computed tomography (CT) provided structural properties and tissue mineral density, in both cortical and trabecular compartments. Bone microarchitectural parameters are strong predictors of bone strength [31, 32]; our data demonstrated the relationship between architecture and structural mechanics.

Through the use of an ovariectomized rat model with varying doses of both alendronate and parathyroid hormone we were able to create a model with large variability in measures of bone microarchitecture and tissue mineral density. Dose-dependent improvements to morphology were drug-specific, where ALN had the largest effect on trabecular number while PTH increased trabecular thickness. These data confirms others findings where bone microarchitecture is degraded with OVX and recovered with alendronate and PTH treatments [160]. Our study uniquely developed a diverse population of micro-architectural parameters through dose-dependent drug improvements which led to strong correlative analysis to evaluate the contributors of bone strength through multivariate analysis. Our results indicated that bone architecture, but not micro-mechanical properties or chemistry play a significant role in predicting bone's total stiffness and ability to withstand mechanical loads. Our study also

revealed that relatively high doses of alendronate and PTH can be detrimental to tissue micro-mechanical properties, which has also been reported in humans [151] and OVX is also detrimental to micromechanical properties in rats [161].

The lack of change in chemical data could be due to lower remodeling in the cortical bone. Some evidence of drug-specific, dose-dependent changes was seen when looking at the phosphate content specifically. Here, we found that L-ALN treated rats had significantly less phosphate content than H-ALN treated rats. This demonstrates the need to analyze changes to protein and phosphate content independently. The small changes that occur in the cortical bone could be occurring in both parameters simultaneously resulting in no net change in FTIR measured mineralization levels. Additionally, since remodeling is not occurring throughout the cortical tissue, future work should focus on regions of high turnover such as the trabecular bone where large differences in remodeling rates may have more significant effects on bone chemistry [162].

This study's multi regression analysis demonstrated that 91% of the variance in bone stiffness was due to changes in morphological properties, where micro-mechanical and chemical properties did not significantly modify bone stiffness. Ultimately, we highlighted the importance of preserving bone mass after estrogen withdrawal. The reductions in overall bone strength caused by cortical thinning and trabecular bone degradation in the untreated osteoporotic rats demonstrated the need to utilize treatments maintain and preserve tissue architecture. Minor reductions in tissue material properties may provide evidence of material deficits caused by drug therapy which may reduce bone strength, particularly during long term drug use. Reductions in material level mechanical properties may explain the increased occurrence of atypical subtrochanteric fractures after long term bisphosphonate use, as these drug-induced alterations to

material properties are similar to changes observed in patients with osteoporotic related fractures [163].

Although finite element modeling estimated an improvement in overall bone stiffness with high doses of ALN and PTH treatments compared to controls, despite reductions to tissue material properties, the model was limited to uni-directional compression loading. The reduction in material properties may have greater consequences for fracture toughness [164], or impact crack propagation mechanics [165]. Future work should be conducted to determine the consequences of these drug-induced reductions to tissue modulus during alternative loading regimes.

Additionally the apparent modulus estimation by the standard finite element model revealed that H-PTH treated rats had higher bone elastic modulus, and therefore had higher maximal stress, due to its relative increase in bone morphology. But when tested experimentally via 4 point bending of the tibial diaphysis, this was not confirmed. In fact, the H-PTH group had deficient inherent material properties compared to the rest of the study samples (**Figure 2.9**). This demonstrated that despite the anabolic action of PTH on bone mass through increased cortical thickening, the inherent material properties were not mechanically competent. However, it should not be assumed that changes measured through FEA in the femoral metaphysis will mimic changes in the tibial cortical bone, where much smaller changes in morphology and tissue deposition occur. These data suggest that the model could be improved to demonstrate the relative impact of tissue material properties on structural mechanics. Here, we demonstrate that the trabecular bone architecture plays a significant role in bone strength, and preservation of this compartment is critical for preventing fracture risk which is in agreement with previously reported studies [166, 167].

Multivariate analysis demonstrated that morphology, and not chemistry or tissue material properties are critical determinants of bone structural mechanics. It has been shown that bone's chemical makeup influences its micro-mechanical properties [168]. A better understanding of changes to surface material properties at active remodeling sites could provide information on the drug-induced alterations to the mineralization process and its consequences of tissue quality.

2.6 Figures

Figure 2.1. A representative spectral map obtained during FTIR analysis of bone showing the characteristic carbonate, phosphate, and protein peaks [1].

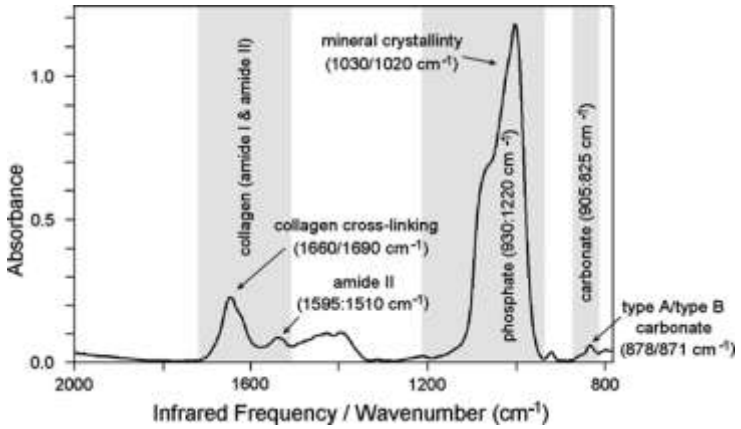

Figure 2.2. MicroCT analysis of the femoral diaphysis determined A.) Bone volume (BV) B.) Cortical thickness (Ct.Th.) C.) Polar moment of Inertia (J) and D.) Tissue mineral density (TMD) for age-matched (AC-black), ovariectomized (OVX-white), alendronate-treated at low (L), medium (M), or high (H) doses (ALN - light gray) and PTH-treated at low (L), medium (M), or high (H) doses (PTH - dark gray) with baseline animals represented (- - -).

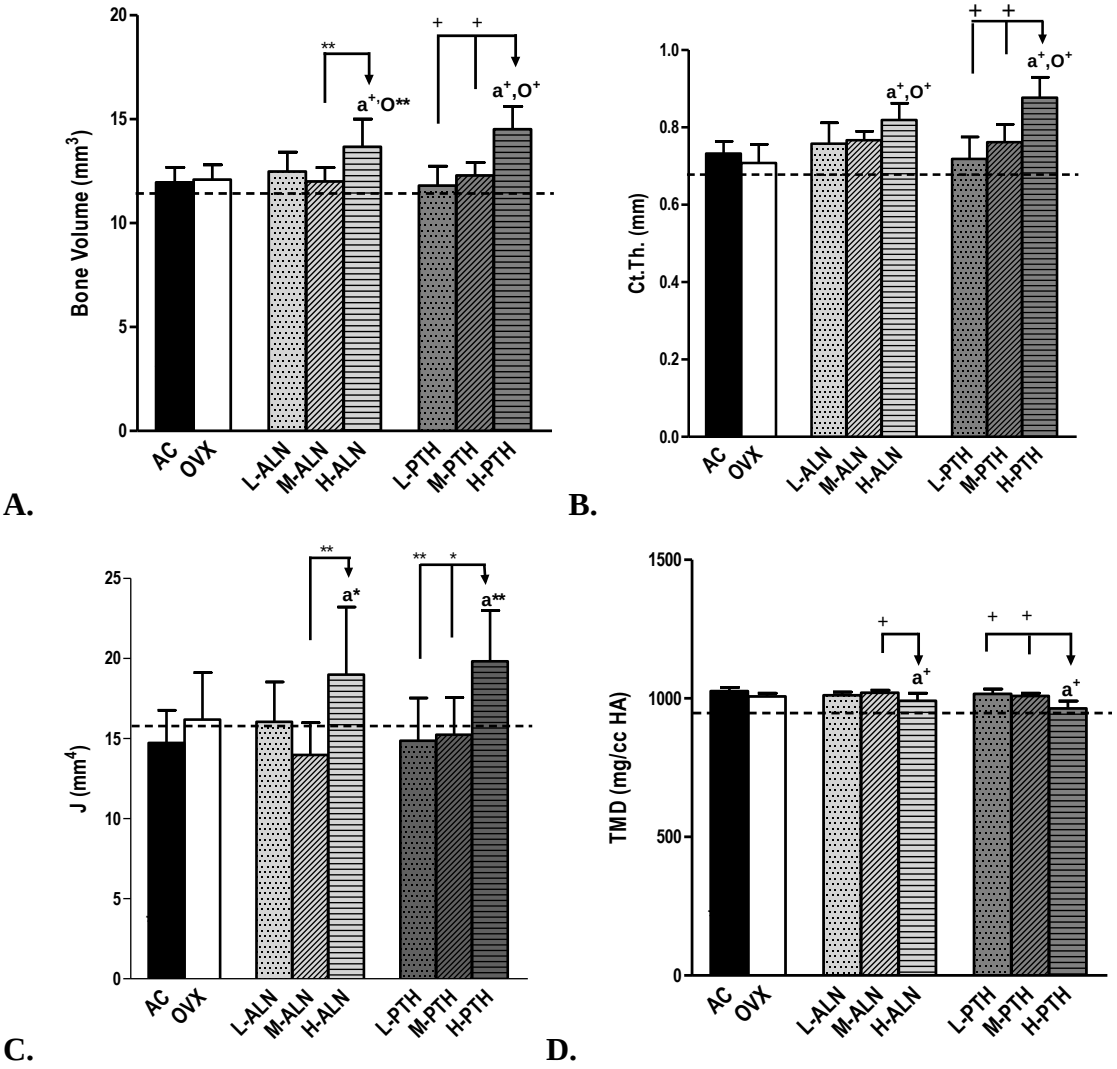

Figure 2.3. Nanoindentation analysis of the femoral diaphysis determined tissue level A.) Elastic modulus and B.) Hardness for age-matched (AC-black), ovariectomized (OVX-white), alendronate at low (L), medium (M), or high (H) doses (ALN - light gray) and PTH at low (L), medium (M), or high (H) doses (PTH - dark gray) with baseline animals represented (- - -).

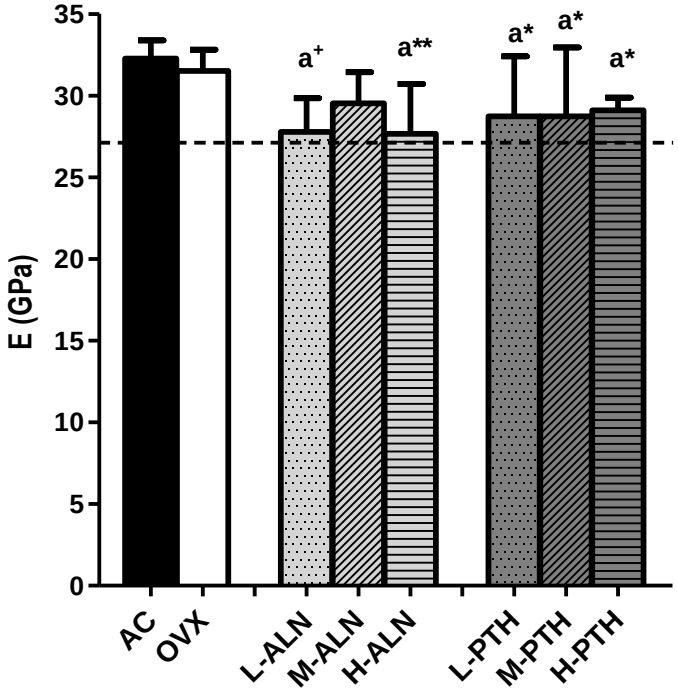

A.

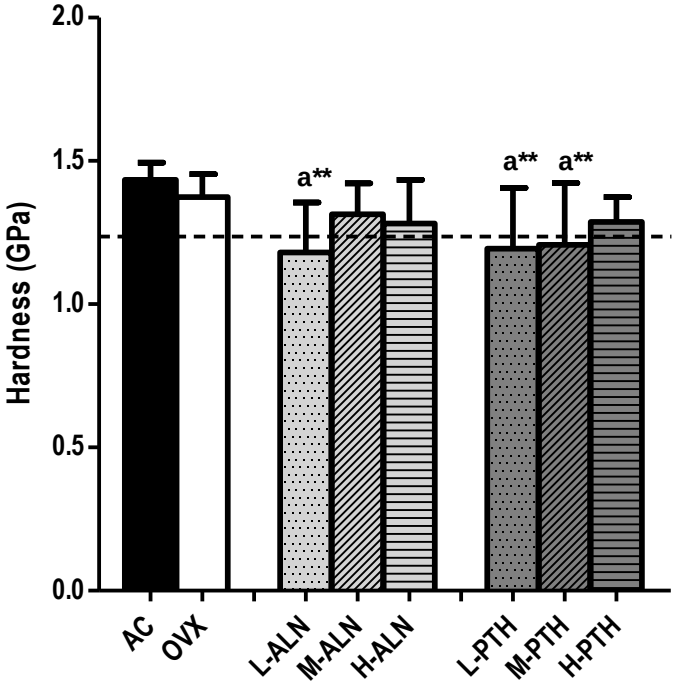

B.

Figure 2.4. Fourier transform infrared microspectroscopy of the femoral diaphysis of 12 month old animals determined tissue level A.) Mineralization, B.) Crystallinity, C.) Collagen cross-linking, D.) Carbonate incorporation, E.) Protein content and F.) Phosphate content for age-matched (AC-black), ovariectomized (OVX-white), alendronate at low (L), medium (M), or high (H) doses (ALN - light gray) and PTH at low (L), medium (M), or high (H) doses (PTH - dark gray).

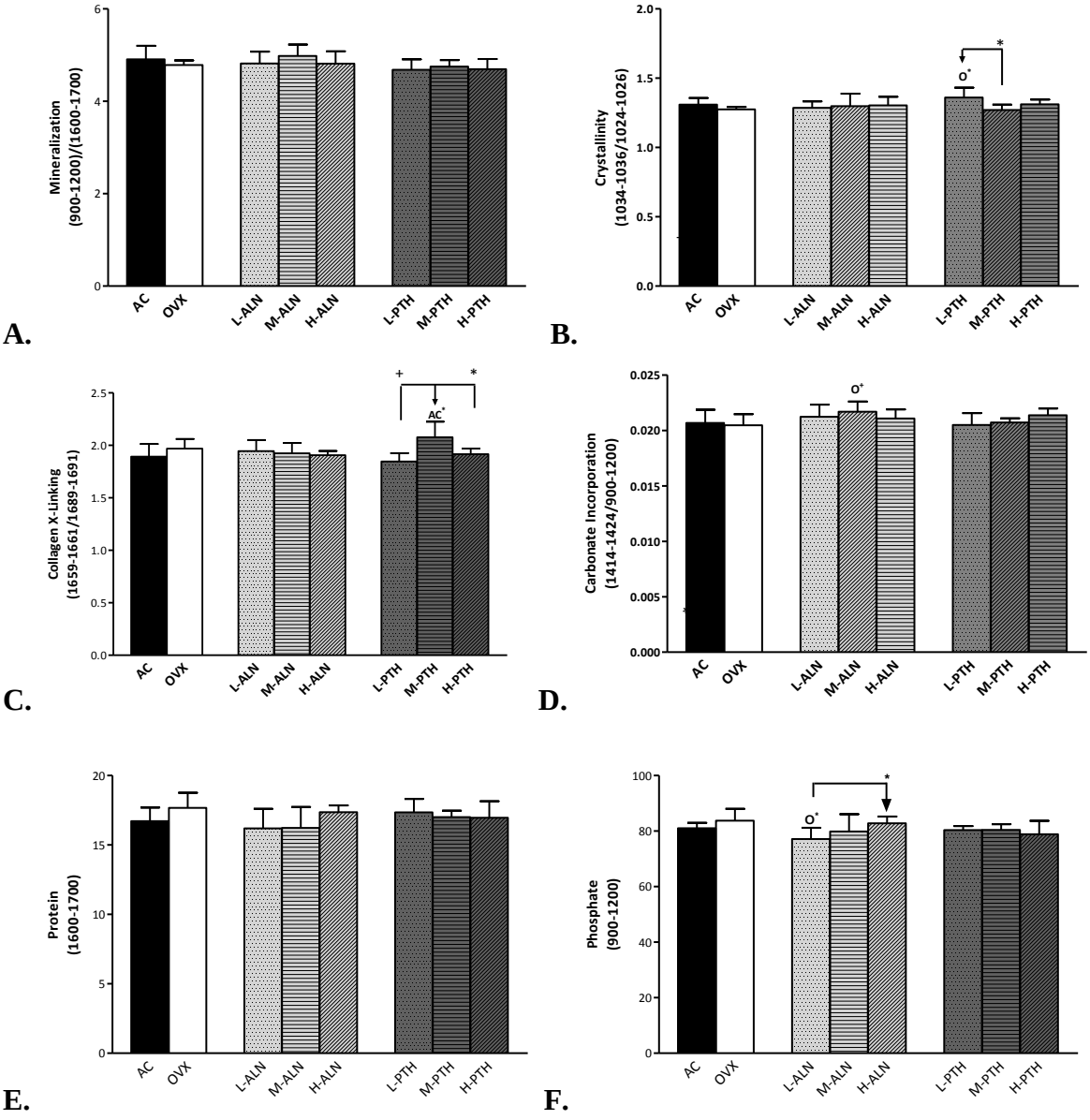

Figure 2.5. Representative images obtained from µCT analysis of the femoral metaphysis separated into cortical and trabecular bone compartments of 12 month old animals A.) age-matched controls (AC) B.) ovariectomized controls (OVX) C.) OVX+L-ALN treated D.) OVX+M-ALN treated E.) OVX+H-ALN treated, F.) OVX+L-PTH treated, G.) OVX+M-PTH treated, H.) OVX+H+PTH treated rats.

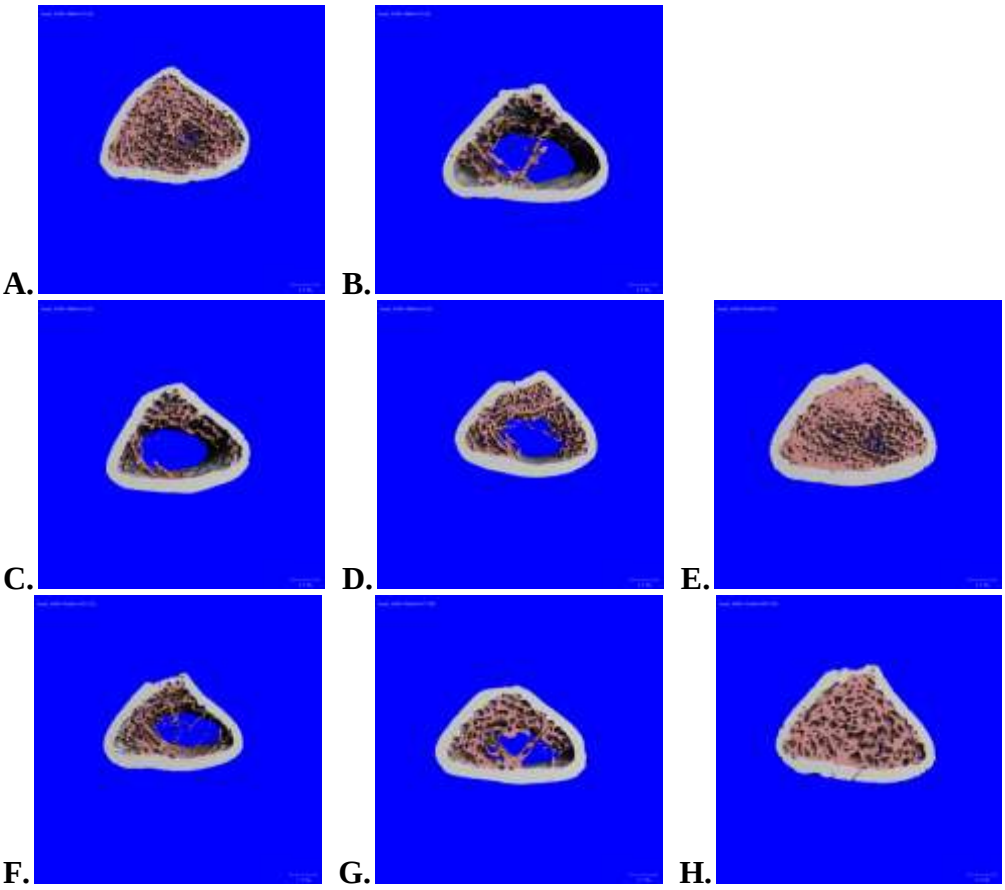

Figure 2.6. MicroCT analysis of the femoral metaphysis determined trabecular A.) Bone volume fraction (BV/TV) B.) Thickness (Tb.Th) C.) Number (Tb.N) D.) Separation (Tb.Sp) E.) Connectivity density (Tb.Conn.D) F.) Structural modeling index (SMI) G.) Apparent mineral density and H.) Tissue mineral density for age-matched (AC-black), ovariectomized (OVX-white), alendronate-treated at low (L), medium (M), or high (H) doses (ALN - light gray) and PTH-treated at low (L), medium (M), or high (H) doses (PTH - dark gray) with baseline animals represented (- - -) and OVX baseline represented (…).

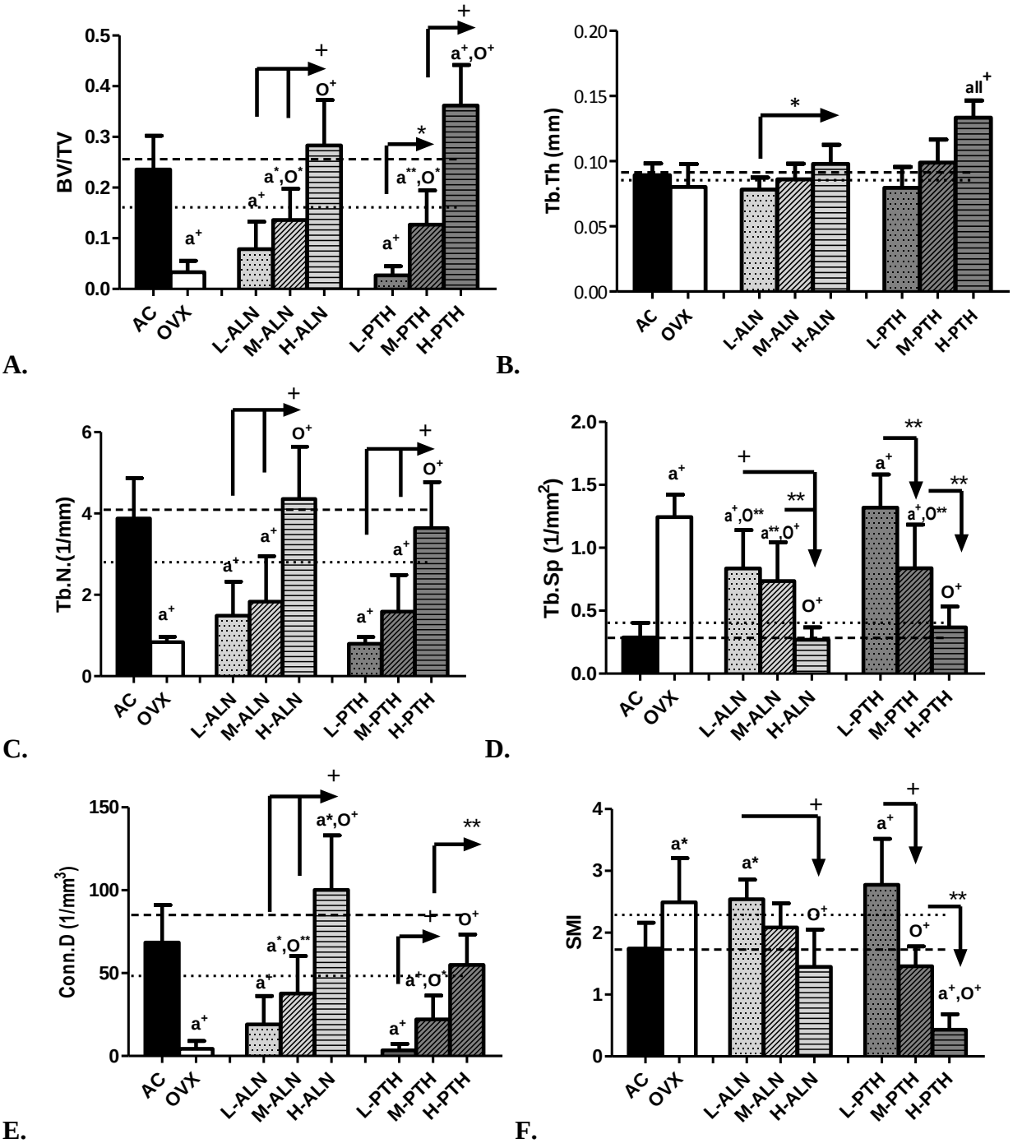

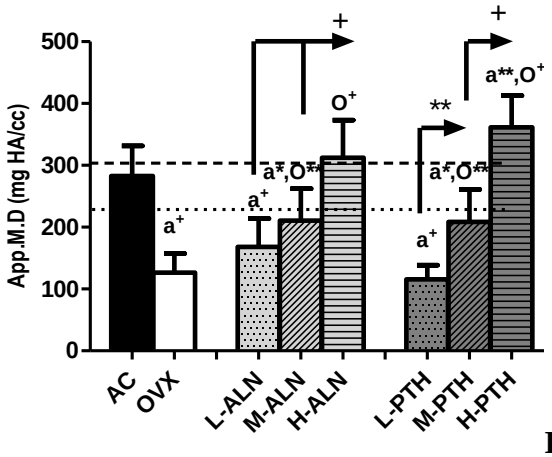
App.M.D (mg HA/cc)
500
400
300
200
100
0
AC
OVX
L-ALN
M-ALN
H-ALN
L-PTH
M-PTH
H-PTH
a+
a*,O+
O+
**
a**,O+
+

G.

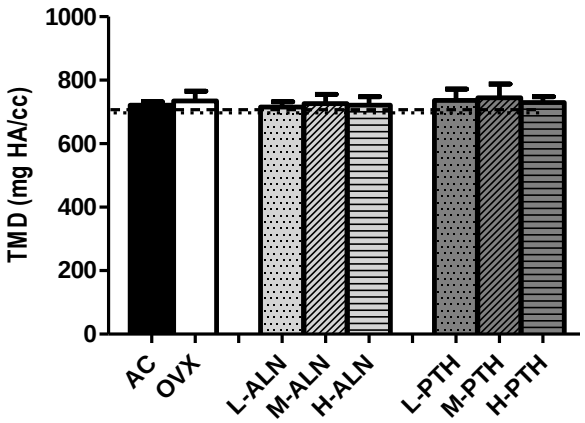
TMD (mg HA/cc)
1000
800
600
400
200
0
AC
OVX
L-ALN
M-ALN
H-ALN
L-PTH
M-PTH
H-PTH

H.

Figure 2.7. A finite element model for a 1N compressive load applied in the z-direction on the metaphyseal femur of 12 month old animals determined A.) Structural stiffness of the whole bone, B.) Structural apparent modulus C.) % load carried by trabecular bone D.) Maximal force in the cortical bone and E.) Maximal force in the trabecular bone for age-matched (AC-black), ovariectomized (OVX-white), alendronate at low (L), medium (M), or high (H) doses (ALN - light gray) and PTH at low (L), medium (M), or high (H) doses (PTH - dark gray).

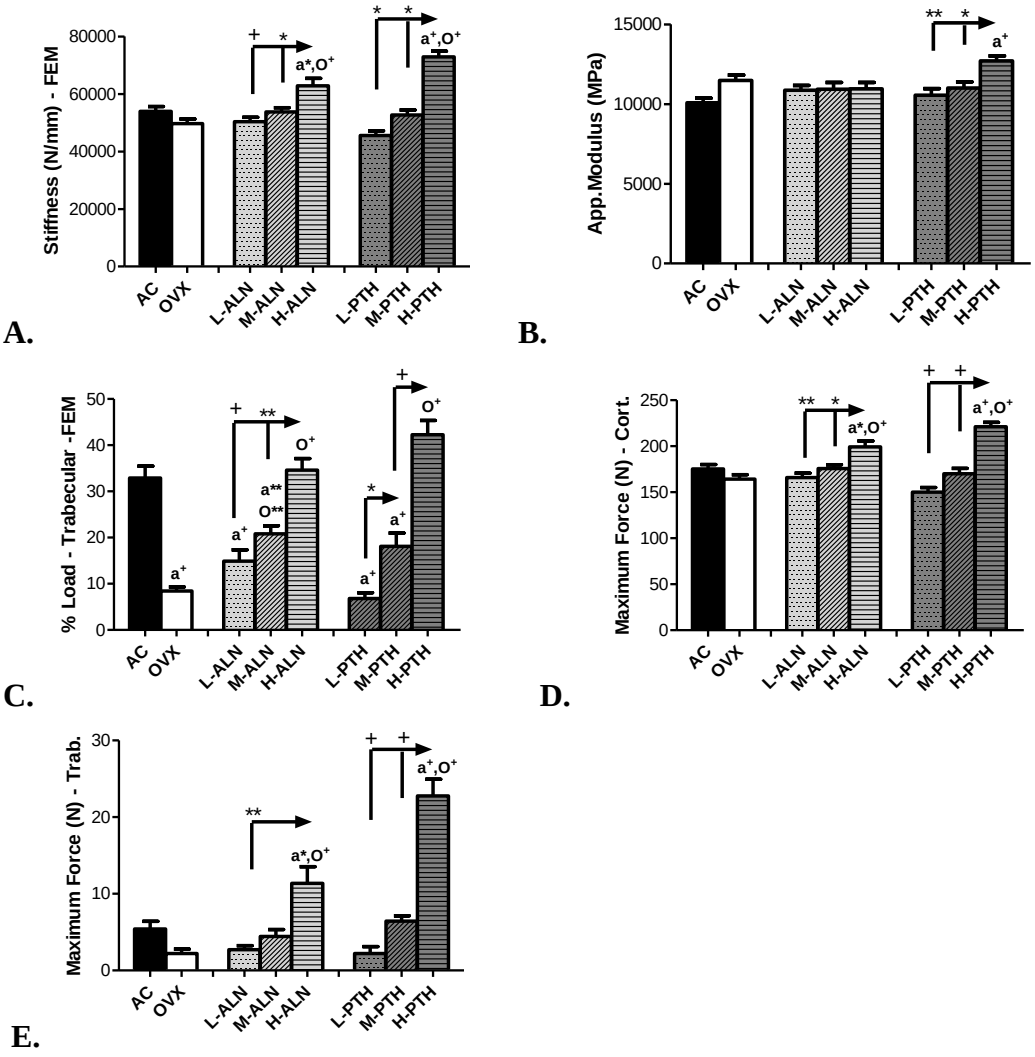

Figure 2.8. Structural properties determined through 4 point bending of the tibial diaphysis revealed A.) Stiffness (N/mm), B.) Maximum applied load (N), C.) Elastic modulus (MPa) and D.) Maximum computed stress (MPa), for 12 mo age-matched (AC – black) controls, ovariectomized controls (OVX - white), alendronate treated (ALN –light gray) at low (L), medium (M) and high (H) doses and parathyroid hormone (PTH – dark gray) treated at low (L), medium (M) and high (H) doses with baseline animals represented (- - -).

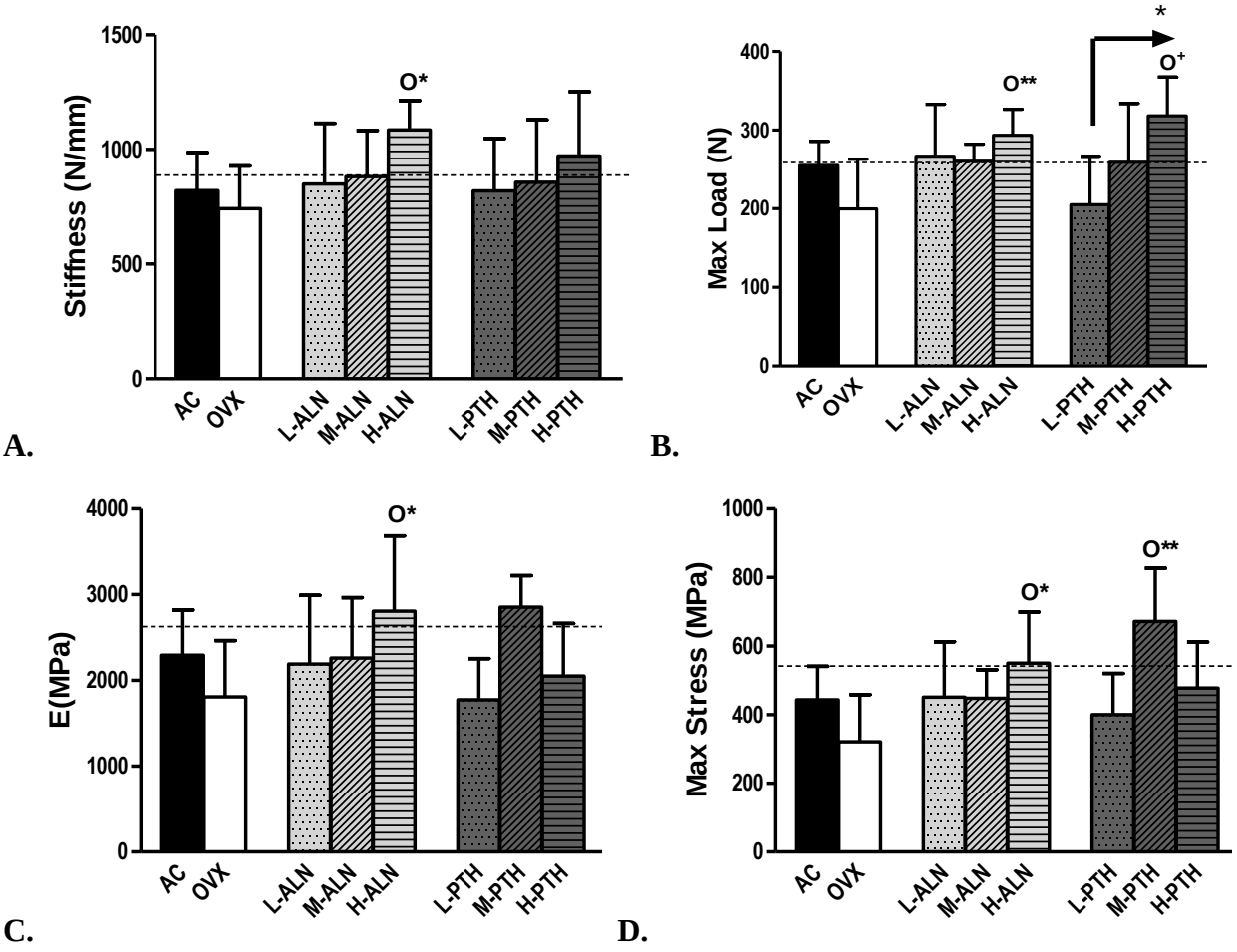

Figure 2.9 Linear regression analysis between cortical thickness of the tibial diaphysis and structural stiffness of the tibial diaphysis determined through 4-point bending demonstrates that the increased thickness induced by H-PTH treatment (gray - triangle) did not result in a relative increased stiffness (R^2=0.02, p>0.05) when analyzed separately from the total population (black - circle) regressed (R^2=0.32, p<0.001).

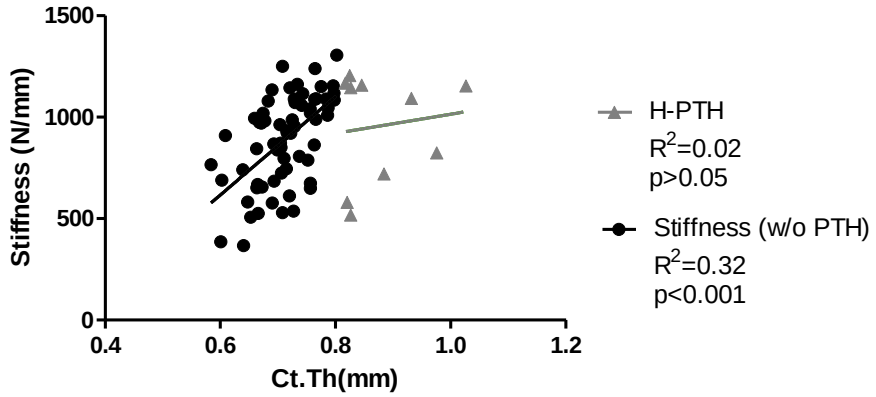

2.7 Tables

Table 2.1. Tibial and femoral bone architecture at 12 months of age after 6 months of drug treatment

		AC	OVX	L-ALN	M-ALN	H-ALN	L-PTH	M-PTH	H-PTH
Tibial Diaphysis	**BV** [mm^3]	**12.11±0.43** HP	**12.79±0.71** HP	**12.97±1.07**	**12.53±0.77**	**13.41±1.23**	**13.14±0.64** HP	**12.82±0.65** HP	**15.39±0.64** AC O LP MP
	Ct.Th [mm]	**0.71±0.03** HP	**0.71±0.03** HP	**0.70±0.06**	**0.73±0.03**	**0.74±0.04**	**0.71±0.05** HP	**0.80±0.08**	**0.87±0.10** AC O LP
	J [mm^4]	**5.52±0.62** HP	**6.64±1.09**	**6.64±1.37**	**5.82±0.61**	**7.23±2.11**	**6.69±0.08**	**5.71±0.77** HP	**8.32±1.06** AC MP
	TMD [mg HA/cc]	**981±32** HA HP	**965±36** HP	**990±22** HA	**974±20**	**954±20**	**991±29** HP	**998±9** HP	**944±19** AC LP MP
Femoral Diaphysis	**BV** [mm^3]	**11.96±0.72** HA HP	**12.10±0.71** HA HP	**12.49±0.93**	**12.00±068** HA	**13.67±1.33** AC O MA	**11.80±0.94** HP	**12.30±0.62** HP	**14.52±1.10** AC O LP MP
	Ct.Th [mm]	**0.73±0.03** HA HP	**0.71±0.05** HA HP	**0.76±0.05**	**0.77±0.02**	**0.82±0.04** AC O	**0.72±0.06** HP	**0.86±0.05** HP	**0.88±0.05** AC O LP MP
	J [mm^4]	**14.73±2.04** HA HP	**16.19±2.92**	**16.05±2.48**	**13.99±2.01** HA	**18.99±4.23** AC MA	**14.87±2.67** HP	**15.25±2.31** HP	**19.82±3.17** AC LP MP
	TMD [mg HA/cc]	**1026±14** HA HP	**1007±12**	**1012±11**	**1020±9** HA	**991±27** AC MA	**1016±17** HP	**1008±10** HP	**964±27** AC LP MP
Femoral Metaphysis	**BV** [mm^3]	**6.62±2.26** O LA MA LP MP	**0.77±0.47** AC HA HP	**1.90±1.48** AC HA	**3.25±1.53** AC HA	**7.57±2.58** O LA MA	**0.67±0.42** AC HP	**2.79±1.94** AC HP	**9.23±2.92** AC LP MP
	BV/TV	**0.24±0.07** O LA MA LP MP	**0.03±0.02** AC MA HA MP HP	**0.08±0.05** AC HA	**0.14±0.06** AC O HA	**0.28±0.09** O LA MA	**0.03±0.02** AC MP HP	**0.13±0.07** AC O LP HP	**0.36±0.08** AC O LP MP
	Conn.D [$1/mm^3$]	**68.49±22.61** O LA MA LP MP	**4.36±4.65** AC MA HA MP HP	**19.02±17.18** AC HA	**37.66±22.64** AC O HA	**100.14±32.88** O LA MA	**3.38±3.90** AC HP	**22.05±14.43** AC O LP HP	**54.88±18.44** O LP MP
	Tb.N [1/mm]	**3.88±0.99** O LA MA LP MP	**0.84±0.13** AC HA HP	**1.49±0.84** AC HA	**1.83±1.11** AC HA	**4.36±1.28** O LA MA	**0.80±0.16** AC HP	**1.59±0.90** AC HP	**3.64±1.13** O LP MP
	Tb.Th [mm]	**0.089±0.01** HP	**0.080±0.02** HP	**0.078±0.01** HA	**0.086±0.01**	**0.098±0.01** LA	**0.080±0.02** HP	**0.099±0.02** HP	**0.133±0.01** AC O LP MP
	Tb.Sp [1/mm]	**0.288±0.12** O LA MA LP MP	**1.244±0.18** AC MA HA MP HP	**0.836±0.30** AC HA	**0.735±0.31** AC O HA	**0.270±0.10** O LA MA	**1.320±0.26** AC MP HP	**0.837±0.35** AC O LP HP	**0.368±0.16** O LP MP
	SMI	**1.75±0.42** O LA LP HP	**2.49±0.71** AC HA HP	**2.54±0.32** AC HA	**2.08±0.39**	**1.45±0.60** O LA	**2.77±0.75** AC MP HP	**1.46±0.32** O LP HP	**0.43±0.25** AC O LP MP
	App.MD [mg HA/cc]	**283±49** O LA MA LP MP	**127±31** AC MA HA MP HP	**168±46** AC HA	**211±51** AC O HA	**312±61** O LA MA	**116±23** AC MP HP	**209±52** AC O LP HP	**361±51** AC O LP MP
	TMD [mg HA/cc]	**722±10**	**734±31**	**716±16**	**726±29**	**721±26**	**736±36**	**745±44**	**730±18**

Data are mean ± standard deviations. Difference in letters denominate significant differences to given groups: AC – age matched controls, O – OVX controls, LA(low)/MA(medium)/HA(high) – Alendronate, LP(low)/MP(medium)/HP(high) – PTH. (ANOVA and Tukey)

Table 2.2. Mechanical properties of the tibial diaphysis (4 point bending) femoral diaphysis (nanoindentation) and femoral metaphysis (finite element modeling) at 12 months of age, after 6 months of treatment

		AC	OVX	L-ALN	M-ALN	H-ALN	L-PTH	M-PTH	H-PTH
Tibial Diaphysis (4-pt Bending)	**Stiffness [N/mm]**	**820±167**	**742±186** HA	**849±265**	**882±202**	**1086±128** O	**820±228**	**856±273**	**972±280**
	Yield Load [N]	**161±32**	**150±50**	**186±47**	**183±38**	**195±36**	**157±45**	**164±44**	**214±54**
	Maximum Load [N]	**255±31**	**200±63** HA HP	**267±66**	**260±22**	**293±33** O	**205±62** HP	**259±75**	**318±49** O LP
	E [GPa]	**2.30±0.5**	**1.81±0.7** HA	**2.19±0.8**	**2.26±0.7**	**2.81±0.9** O	**1.78±0.5**	**2.86±0.4**	**2.05±0.6**
	Yield σ [MPa]	**275±115**	**245±123**	**315±93**	**307±95**	**358±69**	**308±89**	**404±106**	**338±129**
	Max. σ [MPa]	**444±98**	**321±137** HA MP	**451±161**	**448±83**	**550±149** O	**400±120**	**672±155** O	**478±135**
Femoral Diaphysis (nanoindentation)	**E [GPa]**	**32.26±1.11** LA HA LP MP HP	**31.50±1.31**	**27.77±2.07** AC	**29.53±1.91**	**27.66±3.06** AC	**28.73±3.67** AC	**28.73±4.21** AC	**28.09±0.79** AC
	Hardness [GPa]	**1.43±0.06** LA LP MP	**1.37±0.08**	**1.18±0.17** AC	**1.31±0.11**	**1.28±0.15**	**1.19±0.21** AC	**1.21±0.22** AC	**1.29±0.09** AC
Femoral Metaphysis (finite element model)	**CSA [mm^2]**	**18.0±1.73** O LP	**14.5±1.04** AC HA HP	**15.6±2.14** HA	**16.6±1.80**	**19.3±2.32** O LA	**14.5±1.36** AC HP	**16.2±2.39** HP	**19.3±2.01** O LP MP
	Stiffness [N/mm]	**53.97±5.60** HA HP	**49.69±5.05** HA HP	**50.34±4.65** HA	**53.80±4.57** HA	**62.86±7.69** AC O LA MA	**45.54±5.25** HP	**52.73±5.42** HP	**72.91±6.34** AC O LP MP
	Max Force Trab [N]	**10.09±0.96** HA HP	**10.09±0.96** HA HP	**10.09±0.96** HA	**10.09±0.96**	**10.09±0.96** AC O LA	**10.09±0.96** HP	**10.09±0.96** HP	**10.09±0.96** AC O LP MP
	Max Force Cort [N]	**10.09±0.96** HA HP	**10.09±0.96** HA HP	**10.09±0.96** HA	**10.09±0.96** HA	**10.09±0.96** AC O LA MA	**10.09±0.96** HP	**10.09±0.96** HP	**10.09±0.96** AC O LP MP
	E [GPa]	**10.09±0.96** HP	**11.48±1.06**	**10.87±0.88**	**10.93±1.09**	**10.96±1.10**	**10.56±1.30** HP	**11.00±1.24** HP	**12.71±0.98** AC LP MP
	% Load Trab Bone	**32.9%** HA HP	**8.4%** HA HP	**14.9%** HA	**20.8%**	**34.6%** AC O LA	**6.8%** HP	**18.1%** HP	**42.3%** AC O MP LP

Data are mean ± standard deviations. Difference in letters denominate significant differences to given groups: AC – age matched controls, O – OVX controls, LA(low)/MA(medium)/HA(high) – Alendronate, LP(low)/MP(medium)/HP(high) – PTH. (ANOVA and Tukey)

Table 2.3. Linear regression analysis of trabecular bone architecture of the femoral metaphysis (microCT) to its structural mechanical properties (finite element modeling)

	BV/TV	Tb.Th [mm]	Tb.N [1/mm]	Tb.Sp [1/mm]	Conn.D [1/mm4]	SMI
Stiffness [N/mm]	R^2=0.55 p<0.001	R^2=0.71 p<0.001	R^2=0.44 p<0.001	R^2=0.42 p<0.001	R^2=0.34 p<0.001	R^2=0.45 p<0.001
App. Modulus [GPa]	R^2=0.03 p>0.05	R^2=0.12 p<0.01	R^2=0.00 p>0.05	R^2=0.00 p>0.05	R^2=0.34 p>0.05	R^2=0.45 p>0.05
% Load Trab. Bone	R^2=0.88 p<0.001	R^2=0.38 p<0.001	R^2=0.81 p<0.001	R^2=0.75 p<0.001	R^2=0.69 p<0.001	R^2=0.47 p<0.001
Max Trab. Load [N]	R^2=0.68 p<0.001	R^2=0.67 p<0.001	R^2=0.35 p<0.001	R^2=0.28 p<0.001	R^2=0.24 p<0.001	R^2=0.56 p<0.001

Table 2.4. Correlations between chemistry (FTIR) and tissue mechanical properties (nanoindentation) of the femoral diaphysis

	Mineralization (900-1200)/(1600-1700)	Crystallinity (1034-1036)/(1024-1026)	Collagen Cross Linking (1659-1661)/(1689-1691)	Carbonate Substitution (1414-1424)/(900-1200)	Protein (1600-1700)	Phosphate (900-1200)	TMD [mg HA/CC]
Elasticity [GPa]	R^2=0.03 R^2=0.03	R^2=0.02 R^2=0.00	R^2=0.01 R^2=0.11	R^2=0.01 R^2=0.26*	R^2=0.00 R^2=0.08*	R^2=0.02 R^2=0.24*	R^2=0.03 R^2=0.04
Hardness [GPa]	R^2=0.02 R^2=0.18*	R^2=0.01 R^2=0.01	R^2=0.00 R^2=0.02	R^2=0.00 R^2=0.06	R^2=0.00 R^2=0.05	R^2=0.03 R^2=0.36*	R^2=0.03 R^2=0.10
TMD [mg HA/cc]	R^2=0.12* R^2=0.30*	R^2=0.04 R^2=0.00	R^2=0.01 R^2=0.00	R^2=0.00 R^2=0.09*	R^2=0.04 R^2=0.08*	R^2=0.00 R^2=0.01	N/A

*Denotes significantly non-zero slope of the regression line.

Table 2.5. Correlations between structural (microCT) and mechanical (4 pt bending) properties of the tibial diaphysis

	Bone Volume [mm^3]	**BV/TV**	**Ct.Th [mm]**	**pMOI [mm^4]**	**TMD [mg HA/cc]**	**App.MD [mg HA/cc]**
Stiffness [N/mm]	R^2=0.04 p>0.05	R^2=0.00 p>0.05	R^2=0.20 p<0.001	R^2=0.00 p>0.05	R^2=0.02 p>0.05	R^2=0.03 p>0.05
Yield Load [N]	R^2=0.11 p<0.01	R^2=0.02 p>0.05	R^2=0.26 p<0.001	R^2=0.02 p>0.05	R^2=0.02 p>0.05	R^2=0.04 p>0.05
Max Load [N]	R^2=0.09 p<0.01	R^2=0.01 p>0.05	R^2=0.28 p<0.001	R^2=0.00 p>0.05	R^2=0.00 p>0.05	R^2=0.00 p>0.05
App Modulus [MPa]	R^2=0.08 p<0.01	R^2=0.00 p>0.05	R^2=0.03 p>0.05	R^2=0.24 p<0.001	R^2=0.03 p>0.05	R^2=0.03 p>0.05
Yield Stress [MPa]	R^2=0.01 p>0.05	R^2=0.01 p>0.05	R^2=0.10 p<0.01	R^2=0.08 p<0.01	R^2=0.00 p>0.05	R^2=0.00 p>0.05
Max Stress [MPa]	R^2=0.03 p>0.05	R^2=0.01 p>0.05	R^2=0.06 p<0.05	R^2=0.14 p<0.001	R^2=0.00 p>0.05	R^2=0.00 p>0.05

Chapter 3

ALENDRONATE AND PTH DIFFERENTIALLY MODULATE BONE METABOLISM RESULTING IN DOSE-DEPENDENT CHANGES TO BONE SURFACE PROPERTIES MEASURED THROUGH NANOINDENTATION AND FTIR

3.1 Abstract

Bone quality is an important concern, particularly during osteoporosis drug treatment. Drugs such as alendronate (ALN) and parathyroid hormone (PTH) have been clinically successful at mitigating the effects of bone loss. The modes at which ALN and PTH maintain bone mass are different, where the anti-catabolic drug ALN blocks bone resorption while the anabolic drug PTH increases bone formation. To determine whether ALN and PTH differentially modulate tissue material properties, we subjected OVX rats to 6 months of varying doses of ALN and PTH. Morphologic (histological), chemical (FTIR), and tissue mechanical properties (nanoindentation) of cortical and trabecular bone in the tibial metaphysis were determined. The material properties of bone surfaces were compared to the properties of interstitial bone. Six month old Sprague Dawley rats (n=10/group) were assigned to age-matched controls (AC), OVX controls, OVX treated with high (H), medium (M) or low (L) doses of hPTH (75, 15, 0.3μg/kg/day), or ALN (100, 10 or 1μg/kg/2x week). At 12 months, after 7 months of OVX, OVX controls had 65% lower trabecular number (Tb.N) and 174% greater separation than AC controls ($p<0.05$) in the tibial metaphysis. H-PTH-treated rats had 108% thicker trabeculae than OVX controls ($p<0.001$), while ALN-treated animals had 1.4x (L) 1.8x (M) and 2.5x (H) higher Tb.N than OVX controls. At 12 months of age, OVX controls had a 112% more mineralizing

surfaces than AC controls ($p<0.05$). PTH-treated rats had 171% (L), 280% (M) and 261% (H) greater mineralizing surfaces than AC controls ($p<0.001$). ALN-treated rats had 27% (L), 59% (M) and 81% (H) lower mineralizing trabecular surfaces than OVX controls ($p<0.01$). There were no differences in crystallinity, collagen cross-linking or carbonate substitution between AC, OVX, H-ALN or H-PTH bone regions. Bone surfaces of AC, OVX and H-PTH treated rats were 13, 18 and 12% less mineralized than their interstitial bone regions ($p<0.05$). ALN-treated rats had no differences across bone regions ($p>0.05$). H-ALN treated rats had bone surfaces that were 32% more mineralized than OVX and 18% more mineralized than H-PTH bone surfaces ($p<0.05$). Bone surfaces of AC, OVX and H-PTH treated rats had 4, 6.5 and 7% lower elastic moduli and H-PTH had 9% lower tissue hardness when compared to their interstitial bone regions ($p<0.05$). H-ALN treated rats had no difference in mechanical properties across bone regions ($p>0.05$). H-ALN treated rats had bone surfaces with 17% higher elastic moduli than OVX bone surfaces and 25% higher elastic moduli than H-PTH bone surfaces ($p<0.05$). Bone chemistry weakly correlated to changes in micro-mechanical properties. Bone tissue mineralization (FTIR) positively correlated to tissue elastic moduli (nanoindentation) ($R^2=0.05$, $m=0.82$, $p<0.01$), and to tissue hardness ($R^2=0.03$, $m=0.78$, $p<0.05$). Collagen cross-linking negatively correlated to tissue elastic moduli ($R^2=0.02$, $m=-0.68$, $p<0.05$), but not to tissue hardness. Crystallinity and carbonate did not correlate to changes in micro-mechanical properties.

These data demonstrate the drug-specific modulation in tissue material properties and how properties vary across the bone matrix. Through suppression of remodeling, ALN increases the mineralization and tissue mechanical properties of bone surfaces while PTH increases bone formation and leads to bone surfaces with reduced mineralization and mechanical properties. The

modest reduction in interstitial bone properties by PTH suggests that long term treatment may lead to an overall reduction in tissue properties which could result in decreased bone strength. Both treatments successfully mitigate osteoporotic bone loss, but their effects on tissue properties could negatively affect bone strength, particularly during long term drug use.

3.2 Introduction

Bone strength is derived from an accumulation of factors including, bone mass, structure geometry, microarchitecture, the rate of metabolic activity, and tissue mineral density which is inherently derived from its chemical properties. Osteoporosis related bone loss alters each of these parameters, but most studies focus on changes to bone mass, geometry and architecture. The effects of osteoporosis-induced changes to tissue level properties including tissue mineral density, chemical composition and tissue mechanical properties still remain unclear. These properties can also be altered by drug treatments used to prevent bone loss.

Ovariectomized rat models are commonly used to study the effects of estrogen related bone loss [169]. The removal of ovaries causes drastic reduction in circulating estrogen inducing changes to the skeletal system similar to post menopausal osteoporosis. Ovariectomy reduces bone mass, microarchitecture, and tissue mineral content [170]. Osteoporosis is a result of a change in the bone remodeling process where bone resorption outweighs formation leading to a net loss in bone. The coupled nature of resorption and formation leads to an overall increase in the metabolic activity of bone where increased resorption is accompanied by increased formation. Pharmaceuticals used to treat osteoporosis mitigate bone loss by targeting the mismatch in remodeling. Drugs target different mechanisms of the remodeling process by preventing bone resorption through bisphosphonates (e.g., alendronate) [59, 171] or increasing

bone formation through anabolic agents (e.g., intermittent parathyroid hormone) [80, 172]. However, the differential ways in which bone mass is preserved can lead to changes in the matrix material properties.

Bone mineral density distribution describes the rate at which bone tissue is mineralized across the trabecular landscape. The method and rate at which bone tissue becomes calcified is a complex process which is tightly regulated to maintain an organized distribution of mineral throughout the matrix [173]. Tissue mineralization is a two phase process with an initial rapid mineralization of up to 70% of its total mineral content, that occurs directly upon the onset of bone formation [174]; this can happen within days [1]. A slow secondary mineralization process follows, where mineral crystals undergo maturation which can take up to several years for the tissue to fully mineralize [174]. Physiologic conditions, such as age, drug status and genetics alter bone metabolism and formation rates; which affect the rate of tissue mineralization. This may indicate that drugs with different modes of targeting bone remodeling may drastically affects bone mineral density distribution.

Intermittent PTH therapy applied for up to 3 years in osteoporotic women, significantly increased bone mass [172]. Histological analysis shows PTH increases bone mass by increasing the number of mineralizing surfaces and increasing mineral apposition rates thereby thickening the trabeculae [175]. Rapid bone formation by PTH induces a greater amount of new bone on marrow exposed trabecular and cortical surfaces [176].

With intermittent PTH treatment, new bone is constantly being formed and with high enough doses new bone is laid down very rapidly which could perturb normal mineralization. High resolution analysis is needed of the trabeculae and cortical surfaces, which are undergoing remodeling elucidate drug induced changes to tissue quality. Thus far, studies on the

mineralization of bone after PTH therapy have been promising. Studies have shown that there is adequate mineralization after intermittent PTH administration in aged rats [176], and treatment did not compromise its micro-mechanical properties [177]. Proper tissue mineralization could lead to reduced bone properties and/or material properties that differ across the tissue matrix.

Alternatively, alendronate maintains bone mass by blocking resorption, even the natural turnover that occurs during healthy remodeling. Remodeling is necessary for the removal of damaged bone and for the natural excretion of calcium into the blood stream upon demand. By suppressing the remodeling process, alendronate alters the material properties and increases tissue stiffness [160]. Increased tissue stiffness could increase bone brittleness and raise the susceptibility to fracture [178].

A recent clinical study of alendronate administration in osteoporotic women demonstrated that drug-induced increases in BMD scores, collected through Dual X-ray absortiometry (DXA), were the result of increased tissue mineralization and not increased in bone mass [179]. In a long-term animal study, bisphosphonates did not affect the rate of secondary mineralization [180]. Together, these data imply that the alendronate-induced alterations to BMD are caused by increased mineralization of bone surfaces through the suppression of natural turnover. Alendronate and PTH induced changes to bone material properties may influence bone mineral density distribution caused by changes in chemical composition that differ across the bone matrix.

Fourier transform infrared microspectroscopy (FTIR) analysis has been used to measure tissue level chemical distribution of bone [157]. Bone chemistry varies across skeletal sites, and throughout bone tissue matrix [178]. New bone is different in its chemical makeup from mature bone, it has reduced collagen content and lower crystal maturation which lowers mineralization

[181]. Nanoindentation has been used to measure tissue level micro-mechanical properties of bone. Discrepancies between studies have found that ovariectomy induced no change in tissue material properties [182], or reduced material properties [161]. Changes in bone chemistry have been shown to correlate to alterations in mechanical properties. Collagen structure and collagen cross-linking can modulate bone elasticity [183], [20]. Mineral content, crystal size, orientation and maturation as well as crystalline perfection have been shown to modulate bone hardness and stiffness [184], [185]. The effects of OVX and drug treatments on bone material properties at remodeling sites compared to more mature bone is still unclear. Understanding these effects may help to elucidate spatially localized alterations in chemical composition and its effect on bone. As osteoporosis drugs differentially target bone metabolism, the localized bone changes in chemistry during bone formation is particularly important.

Current research on the effects of osteoporosis drug treatments on tissue material properties are contradictory, where some have indicated bisphosphonates reduce tissue mechanical properties [151], while others measure no such effect [186] and some demonstrate an increase in properties [177, 187]. The bisphosphonate risedronate has been shown to decrease mineral crystal size and reduce maturation of collagen fibers [188].

Defining the drug-induced changes in the chemistry of the bone matrix and its influence on mechanical behavior will provides novel information to the role of drug treatment on bone quality. Special attention needs to be made to site-specific modification of bone chemistry, particularly in regions of new bone formation in order to elucidate drug-specific modifications of bone tissue quality. We hypothesize that alendronate and PTH will have dose-dependent but differential affects on bone metabolism, leading to differences in the spatial distribution of tissue chemical composition (FTIR) and micromechanical properties (nanoindention).

3.3 Materials and Methods

Experimental design

All procedures were reviewed and approved by the Institutional Animal Care and Use Committee of Stony Brook University. All rats were individually housed in standard cages and allowed free access to standard rodent chow and tap water and were weighed twice weekly to monitor changes in body mass. Adult five-months-old female Sprague-Dawley rats were ovariectomized and weight-matched into normal age matched controls (AC), ovariectomized controls (OVX), and ovariectomized rats treated with either alendronate (ALN) or parathyroid hormone (PTH) at three different doses.

At 6 months of age, 10 age matched and 10 OVX rats were sacrificed as baseline controls, drug treatment began and continued for six months . Alendronate was injected subcutaneously twice per week; high-dose rats received 2 mg/kg (H-ALN), medium-dose rats received 100 µg/kg (M-ALN), and low-dose rats received 10 µg/kg) (L-ALN). Parathyroid hormone was injected subcutaneously five times per week: high at 75 µg/kg (H-PTH), medium at 15 µg/kg (M-PTH), and low at 0.3 µg/kg (L-PTH). Drugs were administered at the dosages listed, per injection. Treatment doses were determined based on previous literature for the clinically relevant dose (medium), the maximum tolerable dose without known evidence of cytotoxicity (high) and a dose low enough to induce minor improvements compared to OVX controls.

All animals, with the exception of AC controls, were ovariectomized at 5 months of age. Animals were sacrificed at baseline, at 6 months of age, and after 6 months of treatment, at 12 months of age.

Dynamic Histomorphometry

Dynamic histormorphometry was conducted to determine the metabolic activity of bone of the tibial metaphysic. Animals were injected with calcein 10 and 9 days prior to sacrifice, and again a week later at 4 and 3 days prior to sacrifice. This created a region of double labeled new bone formation on the bone surfaces. After sacrifice, the left tibiae were extracted, cleaned of soft tissue and dehydrated in ethanol (70%, 80%, 90%, 100% - 3-4 days each). The dehydrated left tibiae were embedded in poly methyl-methacrylate by previously described methods [189]. The metaphyseal regions of the tibiae were sectioned in the coronal plane at 8 µm section thickness (Leica, RM 2165 microtome, Leica Microsystems, Wetzler, Germany). The entire metaphyseal regions, from growth plate to diaphysis, were imaged at 10x magnification with a Zeiss Microscope with a FITC fluorescence filter to capture bone with its double labeled surfaces. Collected images were superimposed together using imaging software (Adobe Photoshop) to create a map of the metaphyseal section. Maps were analyzed using Osteomeasure software(OsteoMetrics, Decatur Georgia). Output parameters from dynamic histomorphometry included bone area, trabecular number, trabecular separation, trabecular thickness, mineral apposition rate, mineralizing surface rate and bone formation rate.

Fourier Transform Infrared Microspectroscopy (FTIR)

The tibial metaphyseal bone blocks that remain after sectioning were analyzed using synchrotron-based Fourier transform infrared microspectroscopy imaging. The analysis was used to determine chemical composition of bone surfaces (new – (< 10 day old) within by intra-calcein label) or interstitial bone from both cortical and trabecular bone regions. The exposed bone embedded within PPMA that remained after microtome sectioning was polished using

abrasive silicon carbide papers of decreasing particle size (600 μm, 800 μm and 1200 μm) and was then polished with a series of diamond suspension polishing solutions (3 μm, 1 μm, 0.25 μm and 0.05 μm) to create a highly reflective surface.

Bone blocks were mounted and analyzed with FTIR in reflective mode at Brookhaven National Labs U2B beamline to determine the chemical composition of bone. A spectrophotometer, equipped with a fluorescence microscope, with an IR microscope and MCT-A detector was used in a frequency range of 650 to 4,000 cm with an aperture size of 20 um x 20 μm. Spectra were collected at 128 scans per point. Collected data was processed using Omnic software. Decay of the current of the synchrotron light source was corrected by beam current normalization for each spectral point. Background scans were collected on a cesium iodide window to reduce beam noise before and after each bone. At least 20 spectra were collected and averaged for each region of interest: 1. cortical bone surfaces, 2. cortical interstitial bone, 3. trabecular bone surfaces, and 4. trabecular interstitial bone (**Figure 3.1a**). The fluorescence microscope, equipped with a camera mercury arc lamp and FITC filter cube, was used to localize spectral data collection points to active remodeling sites of new bone formation (i.e. within the double labeled band, **Figure 3.1b**). Points of interest were selected visually from at least two separate locations for all 4 tissue types previously described. Any spectral data with the characteristic PMMA peak at 1660 were eliminated from the data pool, which occurred when the aperture was placed too close to the bone surface.

Reflective data was transformed into absorbance data using a Kramer's Kronig transformation algorithm [157]. Absorbance data was analyzed using Cytospec software to determine mineralization (phosphate/protein ratio 900-1200/1600-1700), collagen cross-linking

(1659-1661/1689-1691), crystallinity (1034-1036/1024-1026), carbonate substitution (1414-1424/900-1200), protein content (1600-1700) and phosphate content (900-1200).

Nanoindentation

Tissue level mechanical properties were determined through nanoindentation on the tibial metaphysis on both cortical and trabecular bone, to determine site-specific and tissue-specific differences in micro-mechanical properties. The metaphyseal bone blocks, which were previously polished and analyzed through non-destructive FTIR analysis, were used for nanoindentation. The bottom of the bone block was mounted to magnetic metal disks with cyanoacrylate glue and sonicated to thoroughly clean the bone surface of residue. The highly polished surfaces of metaphyseal bone were indented using a nanoindenter system (Triboindenter; Hysitron, Minneapolis, MN) with a Berkovich indenter tip. Bones were indented using a trapezoidal load function at a constant loading rate of 100 μN/s for ten seconds followed by a constant 1,000 μN hold load for 10 seconds, followed by a constant unloading rate of -100 μN/s for ten seconds.

Isotropic silica was used to calibrate the tip area function. The optic-probe tip calibration was performed regularly to calibrate the offset between the probe tip and the optics focal point. The reduced elastic modulus was calculated by the standard Oliver-Phar method which has been described in detail [155]. Indentation regions of interest were selected visually and included: 1. cortical bone surfaces, 2.cortical interstitial bone, 3. trabecula bone surfaces, and 4. trabecular interstitial bone. Ten indents per tissue region were tested and averaged for each of the four tissue types for each sample. Individual indents that were greater than 2 standard deviations from the sample mean were removed as outliers. A force displacement curve was generated for each

indent, and Hysitron software calculated the elastic response (Young's modulus), and tissue hardness, from the 20-90% portion of the unloading curve using calculations previously described [155].

Statistical Analysis

All values are presented as means +/- standard deviations. Statistical significance between groups were determined using a One-Way ANOVA followed by a Tukey post-hoc test, and were reported with their associated p-values. Measures of bone chemistry were regressed against bone micro-mechanical properties using Pearson product correlations to evaluate the associations between bone chemical and micro-mechanical properties. R^2 and p values were reported when significance is detected. A multivariate analysis was used to determine the combined contribution of chemical properties to tissue micro-mechanical properties. Paired-wise Student t-tests were conducted to determine differences between bone surface properties and interstitial bone properties for individual groups.

3.4 Results

Bone microarchitecture of the tibial metaphysis:

Trabecular micro-architecture was altered differentially by PTH an ALN treatments in a dose-dependent manner. At 12 months, after 7 months of OVX, trabecular number was 65% lower with 174% greater trabecular separation than AC controls ($p<0.05$). 6 months of PTH and ALN treatments differentially modulated trabecular architecture. H-PTH-treated rats had 108% thicker trabeculae than OVX controls ($p<0.001$), while ALN-treated animals had 1.4x (L-ALN) 1.8x (M-ALN) and 2.5x (H-ALN) more trabeculae than OVX controls (all $p<0.05$, **Figure 3.2**).

Similarly, all doses of ALN reduced trabecular separation as did M- and H-PTH. Together these changes in bone architecture led to dose-dependent increases in total trabecular bone area.

Bone metabolism of the tibial metaphysis:

Changes to trabecular bone architecture were caused by dose-dependent and differential effects of PTH and ALN treatments on bone metabolism. At 12 months of age, OVX controls had a 112% greater percentage of mineralizing trabecular surfaces than AC controls ($p<0.05$). PTH-treated rats had 171% (L-PTH), 280% (M-PTH) and 261% (H-PTH) more mineralizing trabecular surfaces than AC controls ($p<0.001$). ALN-treated rats had 27% (L-ALN, $p>0.05$), 59% (M-ALN, $p<0.05$) and 81% (H-ALN, $p<0.001$) less mineralizing trabecular surfaces than OVX controls (**Figure 3.3a**).

OVX controls had 39% higher mineral apposition rates than AC controls ($p<0.05$). PTH-treated rats had 14% (L-PTH, $p>0.05$), 14% (M-PTH, $p>0.05$) and 42% (H-PTH, $p<0.001$) higher mineral apposition rate than AC controls. ALN-treated rats had 28% (L-ALN, $p>0.05$), 69% ($p<0.05$, M-ALN) and 60% ($p<0.05$, H-ALN) lower mineral apposition rates than OVX controls ($p<0.05$) (**Figure 3.3b**).

OVX controls had 176% higher bone formation rates than AC controls ($p<0.05$), PTH-treated animals had 207% (L-PTH), 341% (M-PTH) and 399% (H-PTH) higher bone formation rates than AC ($p<0.001$). Additionally, M-PTH and H-PTH had 60% (M-PTH, $p<0.05$) and 80% (H-PTH, $p<0.001$) higher bone formation rates than OVX controls. ALN-treated animals had 44 % (L-ALN, $p>0.05$), 85% (M-ALN, $p <0.001$) and 90% (H-ALN, $p<0.001$) lower bone formation rates than OVX controls (**Figure 3.3c**).

Similar OVX and drug related effects on bone metabolism were seen on the endosteal surfaces of cortical bone. The percentage of endosteal mineralizing surfaces increased by 165% with OVX, and increased by 121% (L-PTH) 171% (M-PTH) and 189% (H-PTH) compared to AC controls ($p<0.01$). Inversely, ALN had 13% (L-ALN, $p>0.05$) 71% (M-ALN, $p<0.05$) and 80% (H-ALN, $p<0.001$) lower mineralizing surfaces than OVX controls ($p<0.001$, **Figure 3.4a**) H-PTH treated rats had mineral apposition rates that were 62% higher than L-PTH ($p<0.05$). ALN-treated rats had mineral apposition rates that were 49% (M-ALN, $p<0.05$) and 60% (H-ALN, $p<0.01$) lower than OVX controls (**Figure 3.4b**). Bone formation rates of OVX rats were 184 % higher than AC controls ($p<0.05$). PTH treated rats had 75% (L-PTH, $p>.05$), 176% (M-PTH, $p<0.05$) and 246% (H-PTH, $p<0.001$) higher bone formation rates than AM controls. ALN-treated rats had 17% (L-ALN, $p>0.05$), 87% (M-ALN, $p<0.001$) and and 92% (H-ALN, $p<0.001$) lower bone formation rates than OVX controls ($p<0.001$, **Figure 3.4c**).

Cortical and trabecular chemistry of bone surfaces and interstitial bone:

FTIR analysis of the cortical and trabecular bone analyzed at both bone surfaces and interstitial bone revealed little differences in chemical composition with OVX or drug treatments. After 7 months of OVX, and 6 months of high doses of ALN or PTH treatment there were no differences in Crystallinity, collagen cross-linking or carbonate substitution between AC, OVX, H-ALN or H-PTH (**Figure 3.5**). Yet, there were significant differences in tissue mineralization depending on bone tissue and region of interest.

The cortical and trabecular bone surfaces of OVX bone were 29% and 33% less mineralized than AC interstitial bone ($p<0.05$). The metabolic affects of ALN and PTH treatments were apparent in their bone surface chemistries: H-ALN cortical and trabecular

interstitial bone regions were 36% and 47% more mineralized than OVX trabecular bone surfaces ($p<0.05$). While H-PTH trabecular bone surfaces were 23% less mineralized than AC interstitial bone, 23% less mineralized than the bone surfaces of H-ALN and 24% less mineralized than the interstitial bone of H-ALN treated rats ($p<0.05$, **Figure 3.6**).

The chemical data of trabecular and cortical bone surfaces was averaged together, as was the trabecular and cortical interstitial bone data. These two groups were compared to answer the direct question of tissue-age related changes in bone chemistry. Bone surfaces of AC, OVX and H-PTH treated rats were 13, 18 and 12% less mineralized than their interstitial bone regions ($p<0.05$ pair-wise Student t-test). ALN induced changes to bone surface chemistry where the bone surfaces of ALN treated rats were no different than the interstitial bone ($p>0.05$), potentially through cessation of bone turnover. H-ALN treated rats had bone surfaces that were 32% more mineralized than OVX bone surfaces and 18% more mineralized than H-PTH bone surfaces ($p<0.05$, One-Way ANOVA, Tukey post hoc, **Figure 3.7**)

The micro-mechanical properties of cortical and trabecular bone surfaces and interstitial bone:

Nanoindentation of cortical and trabecular bone, indented at both bone surfaces and interstitial bone regions revealed small changes in micro-mechanical properties after OVX or drug treatments. The cortical bone surface of OVX rats had 16% lower tissue hardness than AC controls ($p<0.05$). The metabolic affects of ALN and PTH treatments were apparent in their bone surface micro-mechanical properties. The cortical bone surfaces of H-PTH treated rats had 21% lower elastic moduli and 16% lower tissue hardness than AC bone surfaces ($p<0.01$). H-PTH elastic moduli were also lower than the bone surfaces of L-PTH (18%, $p<0.05$), M-ALN (19%,

$p<0.05$) and H-ALN treated rats (22%, $p<0.01$). The trabecular bone surfaces of H-ALN treated rats had 22% higher elastic moduli than OVX controls ($p<0.05$) and 22% higher than PTH treated rats ($p<0.05$). The cortical interstitial bone of OVX controls had 15% lower tissue hardness than AC controls ($p<0.05$). The interstitial cortical bone of H-PTH treated rats had 16% lower elastic moduli than AC controls ($p<0.05$). There were no differences in trabecular interstitial bone properties (**Figure 3.8 and Figure 3.9**)

The averaged bone surface data from cortical and trabecular regions provided a more direct answer to the question of tissue age on bone micro-mechanical properties. Bone surfaces of AC, OVX and H-PTH treated rats had 4, 6.5 and 7% lower elastic moduli and PTH had 9% lower tissue hardness than their interstitial bone regions ($p<0.05$ pair-wise Student t-test). ALN treated rats (through blocked bone remodeling) had no difference in mechanical properties of the bone surface and the interstitial bone ($p>0.05$). H-ALN treated rats had bone surfaces with 17% higher elastic moduli than OVX bone surfaces and 25% higher elastic moduli than H-PTH bone surfaces ($p<0.05$, **Figure 3.10**)

Bone chemistry weakly correlated to changes in micro-mechanical properties. Bone tissue mineralization (FTIR) positively correlated to tissue elastic moduli (nanoindentation) ($R^2=0.05$, $m=0.82$, $p<0.01$), and to tissue hardness ($R^2=0.03$, $m=0.78$, $p<0.05$). Collagen cross-linking negatively correlated to tissue elastic moduli ($R^2=0.02$, $m=-0.68$, $p<0.05$), but not to tissue hardness. Crystallinity and carbonate did not correlate to changes in micro-mechanical properties (**Table 3.4**).

3.5 Discussion

PTH and alendronate dose-dependently improved bone architecture through differential modulation of bone metabolism. Alendronate's mechanism of suppressed resorption was seen by a higher trabecular number with trabecular and cortical bone surfaces that had increased tissue mineralization and higher mechanical properties compared to OVX controls. While the anabolic action of PTH led to increased bone formation rates, a higher percentage of remodeling surfaces, increased trabecular thickness, and decrease in bone surface mineralization and tissue mechanical properties, as well as slight decreases in interstitial properties. The drug-specific changes to tissue mineralization positively correlated to micro-mechanical properties.

Preservation of bone structure and microarchitecture is critical in the prevention of osteoporotic fractures. It has been demonstrated that reductions to architecture correlates to decreased bone mechanical properties [190, 191]. Here we demonstrate the efficacy of PTH and ALN with dose-dependent improvements to tibial metaphysis bone architecture when compared to untreated OVX controls (**Figure 3.2**). Therefore the drugs were effective at preserving a main component of bone quality.

However, drug-induced modulation of tissue material properties is a concern when treating patients with osteoporosis, particularly during long term drug use. Although alendronate is one of many bisphosphonates commonly used to prevent bone loss, these drugs have recently been linked to an increase in atypical low energy femoral fractures. The cause of this type of fracture is somewhat unclear. It has been suggested that it may be due to a change in structural properties like a thickening of the cortex [192], accumulation of microcracks and reduced toughness [62], or drug-induced increases in material properties such as tissue hardness and crystallinity [193].

In general, bisphosphonates do more good than harm and should still be used, but these changes in surface properties may provide insight into why bone is failing after bisphosphonate use. We hypothesize that more elastic bone surfaces are necessary for energy dissipation during dynamic loading. PTH showed a similar difference in bone surface properties as AC controls, demonstrating a normal material property distribution across the matrix. Since bone is an anisotropic viscoelastic material, it is possible that variability in the bone matrix provide a compensatory mechanism to distribute the strain through the tissue. As the bone is loaded through its cortex and subsequently through the trabeculae, reduced surface material properties may allow strain energies to dissipate through the material more readily and through the bone. If this surface material is as stiff as its interstitial counterparts it could result in bone brittleness and cause a reduction in viscoelastic response. Recent whole bone studies suggest the increased tissue material properties improves bone's structural mechanical properties [194, 195], yet it has also been shown that despite improvements to structural mechanical properties, bisphosphonates did not improve fracture toughness [195].

Nanoindentation techniques have been criticized due to the relatively small differences observed in tissue material properties. Measureable changes in material properties may be localized to regions of skeletal remodeling where major differences in bone chemistry can be observed, such as within regions of new bone formation., if the bone surface is blindly probed with a small surface area tip (<1 μm), indentations could occur within cement lines, on a pocket of phosphatase crystals, or within a collagen fibril which all have different material properties [196]. Therefore, nanoindentation is not appropriate tool to accurately measure bone's tissue response as a constitutive material, or the overall changes in bone strength. For small resolution

characterization of tissue material properties, nanoindentation does provide the sensitivity to test and determine differences in mechanical properties along bone surfaces.

Ultimately, high resolution analysis of tissue material properties by FTIR and nanoindentation allowed the site-specific analysis of bone surfaces compared to interstitial bone. This study provided valuable insight into material changes that differ across the bone matrix after PTH and ALN treatment. Future work should be done on structural mechanical loading of metaphyseal bone to measure the strain distribution throughout the matrix in treated rats. This would provide additional information about how the mechanical energy is dissipated through tissue with varying chemical and mechanical properties.

3.6 Figures

Figure 3.1. A.) A representative spectral point obtained during U2B - FTIR analysis of bone showing the spectra of the cortical bone surface (blue), cortical interstitial bone (red) trabecular bone surface (pink) and trabecular interstitial bone (purple) with the characteristic carbonate, phosphate, and protein peaks defined. B.) An example of placement of the aperture within double labels obtained during FTIR analysis of bone surfaces.

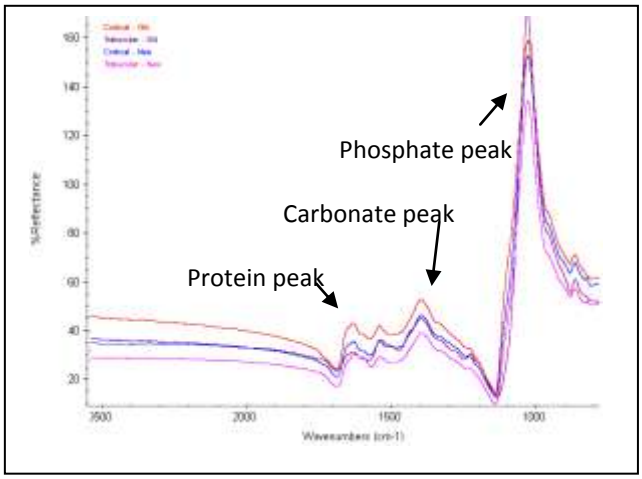

A.

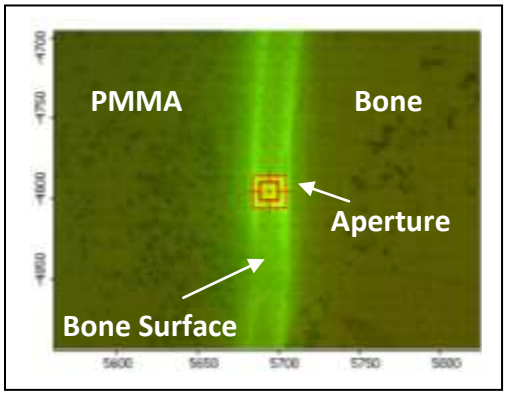

B.

Figure 3.2. Static histomorphometry determined trabecular A.) Bone area/total area (Tb.BA/TA) B.) Thickness (Tb.Th) C.) Separation (Tb.Sp) and D.) Number (Tb.N) for age-matched (AC-black), ovariectomized (OVX-white), alendronate-treated at low (L), medium (M), or high (H) doses (ALN - light gray) and PTH-treated at low (L), medium (M), or high (H) doses (PTH - dark gray) with 6 mo old baseline animals (- - -).

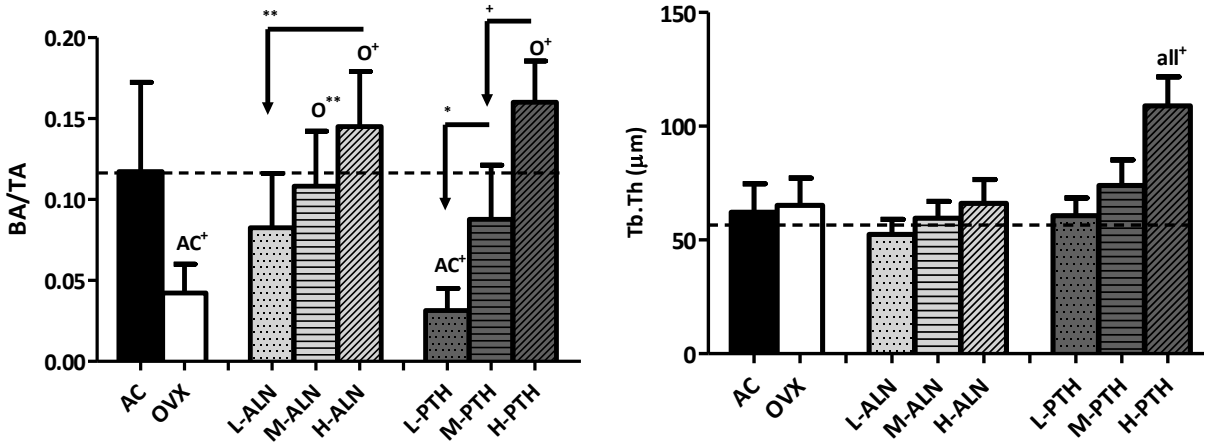

A.

B.

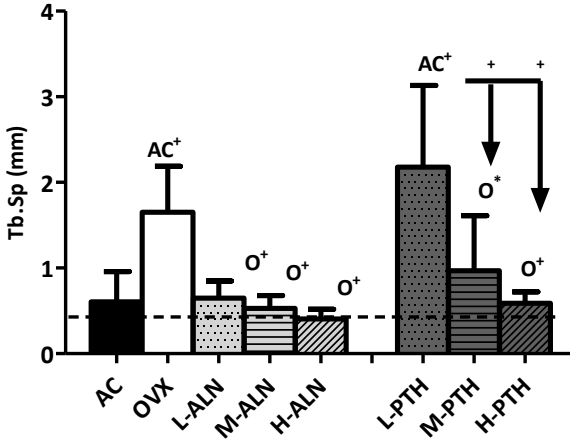

C.

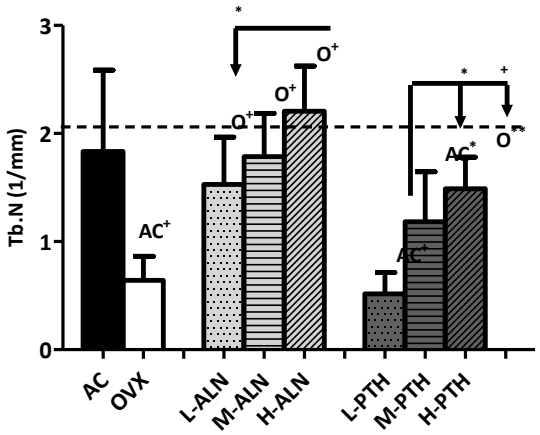

D.

Figure 3.3. Dynamic histomorphometry of the trabecular bone within the tibial metaphysis sectioned longitudinally determined trabecular A.) mineralizing surface/bone surface (Tb. Mineralizing Surface/BS) B.) mineral apposition rate (Tb.MAR) and C.) bone formation rate/bone surface (Tb.BFR/BS) for age-matched (AC-black), ovariectomized (OVX-white), alendronate-treated at low (L), medium (M), or high (H) doses (ALN - light gray) and PTH-treated at low (L), medium (M), or high (H) doses (PTH - dark gray) with 6 mo old baseline animals (- - -).

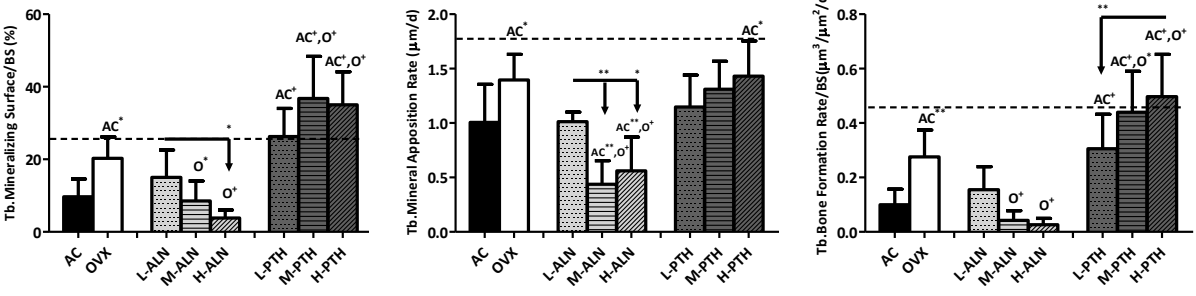

A. **B.** **C.**

Figure 3.4. Dynamic histomorphometry of the cortical bone of the tibial metaphysis sectioned longitudinally determined Endosteal A.) mineralizing surface/bone surface (Ec. Mineralizing Surface/BS) B.) mineral apposition rate (Ec.MAR) and C.) bone formation rate/bone surface (Ec.BFR/BS) for age-matched (AC-black), ovariectomized (OVX-white), alendronate-treated at low (L), medium (M), or high (H) doses (ALN - light gray) and PTH-treated at low (L), medium (M), or high (H) doses (PTH - dark gray) with 6 mo old baseline animals (- - -).

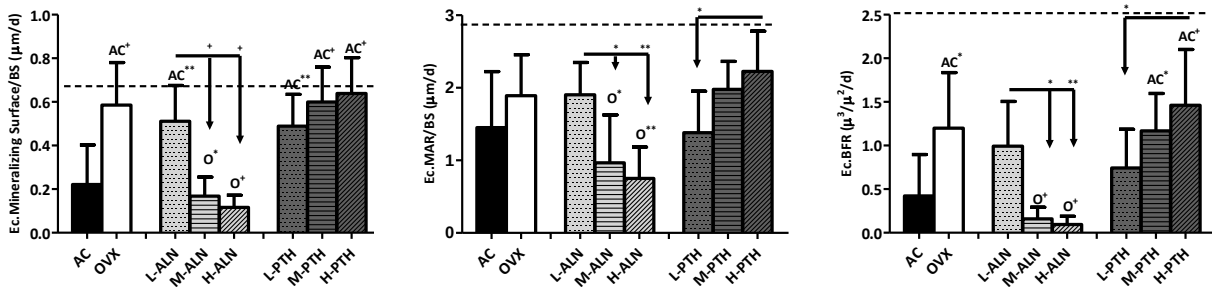

A. **B.** **C.**

Figure 3.5. FTIR analysis on the bone surfaces of the tibial metaphysis revealed Tissue A.) Mineralization (900-1200/1600-1700) B.) Crystallinity (1034-1036/1024-1026) C.) Collagen cross-linking (1659-1661/1689-1691) and D.) Carbonate Incorporation (1414-1424/900-1200) E.) Protein content (1600-1700) and F.) Phosphate content (900-1200) for age-matched (AC-black), ovariectomized (OVX-white), alendronate-treated for high dose alendronate (H-ALN - light gray) and high dose PTH-treated (H-PTH - dark gray) on the cortical surface, cortical interstial region, trabecular surface and trabecular interstitial region, statistically compared regional differences within a treatment group.

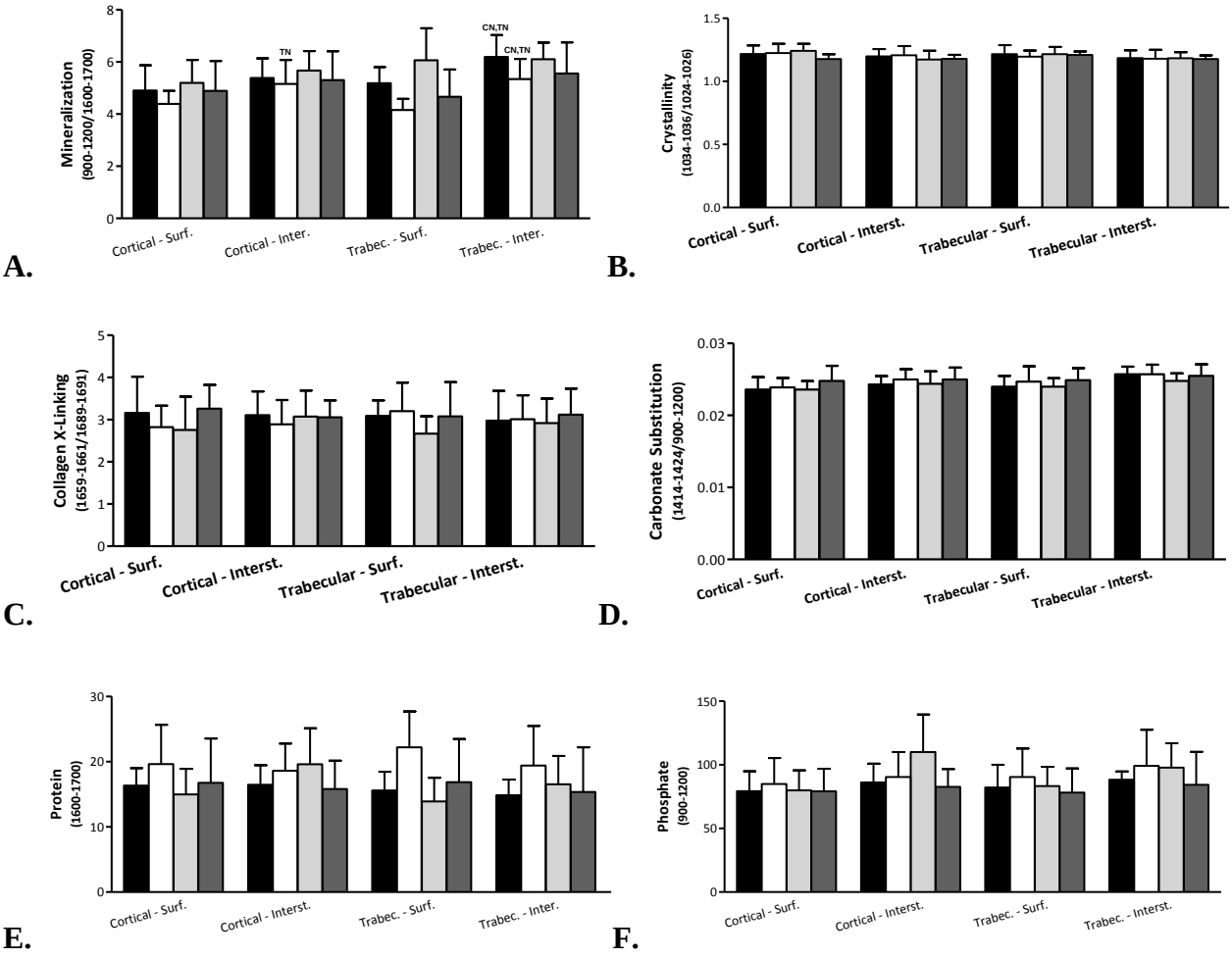

CN – Cortical New
CO – Cortical Old
TN – Trabecular New
TO – Trabecular Old

AC
OVX
H-ALN
H-PTH

Figure 3.6. FTIR analysis revealed tissue mineralization (900-1200/1600-1700) at the A.) Cortical bone surface (far left), cortical interstitial space (middle left), trabecular bone surface (middle right) and trabecular interstitial space (far right) for age-matched (AC-black), ovariectomized (OVX-white), H-alendronate-treated (H-ALN - light gray) and H-PTH-treated rats (H-PTH - dark gray) statistically compared across treatment groups and bone regions.

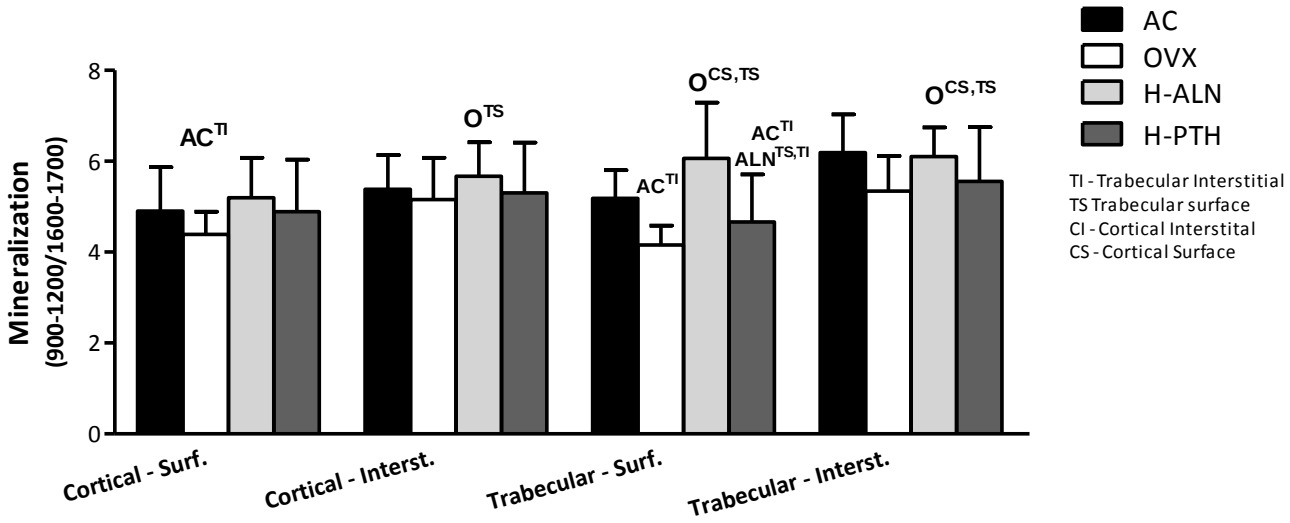

Figure 3.7. FTIR analysis of bone surfaces (gray) and interstitial bone (black) revealed tissue mineralization (900-1200/1600-1700). Statistical differences within a group were determined with a paired-wise Student t-test comparing bone surface properties (gray) to interstitial properties (black).

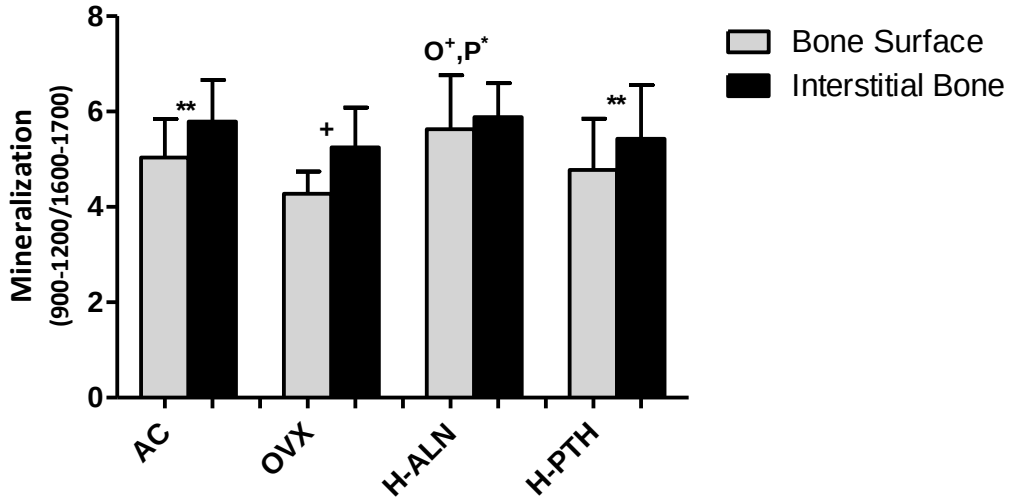

Figure 3.8. Nanoindentation of the tibial metaphysis to determine elastic moduli (E) of A.) Cortical bone surfaces B.) Cortical interstitial bone, C.) Trabecular bone surfaces and D.) Trabecular interstitial bone for age-matched (AC-black), ovariectomized (OVX-white), alendronate-treated at low (L), medium (M), or high (H) doses (ALN - light gray) and PTH-treated at low (L), medium (M), or high (H) doses (PTH - dark gray).

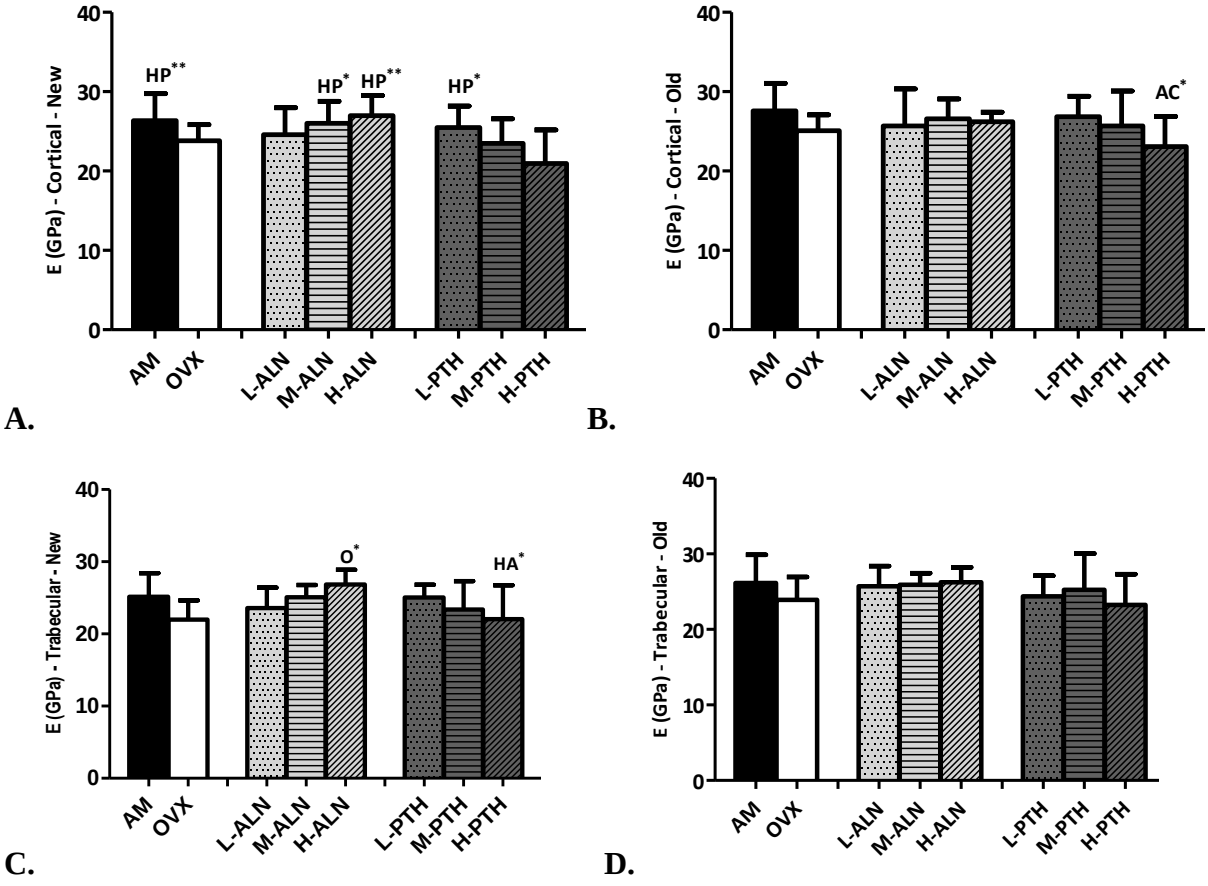

Figure 3.9. Nanoindentation of the tibial metaphysis to determine tissue hardness of A.) Cortical bone surfaces B.) Cortical Interstitial bone, C.) Trabecular bone surfaces and D.) Trabecular interstitial bone for age-matched (AC-black), ovariectomized (OVX-white), alendronate-treated at low (L), medium (M), or high (H) doses (ALN - light gray) and PTH-treated at low (L), medium (M), or high (H) doses (PTH - dark gray).

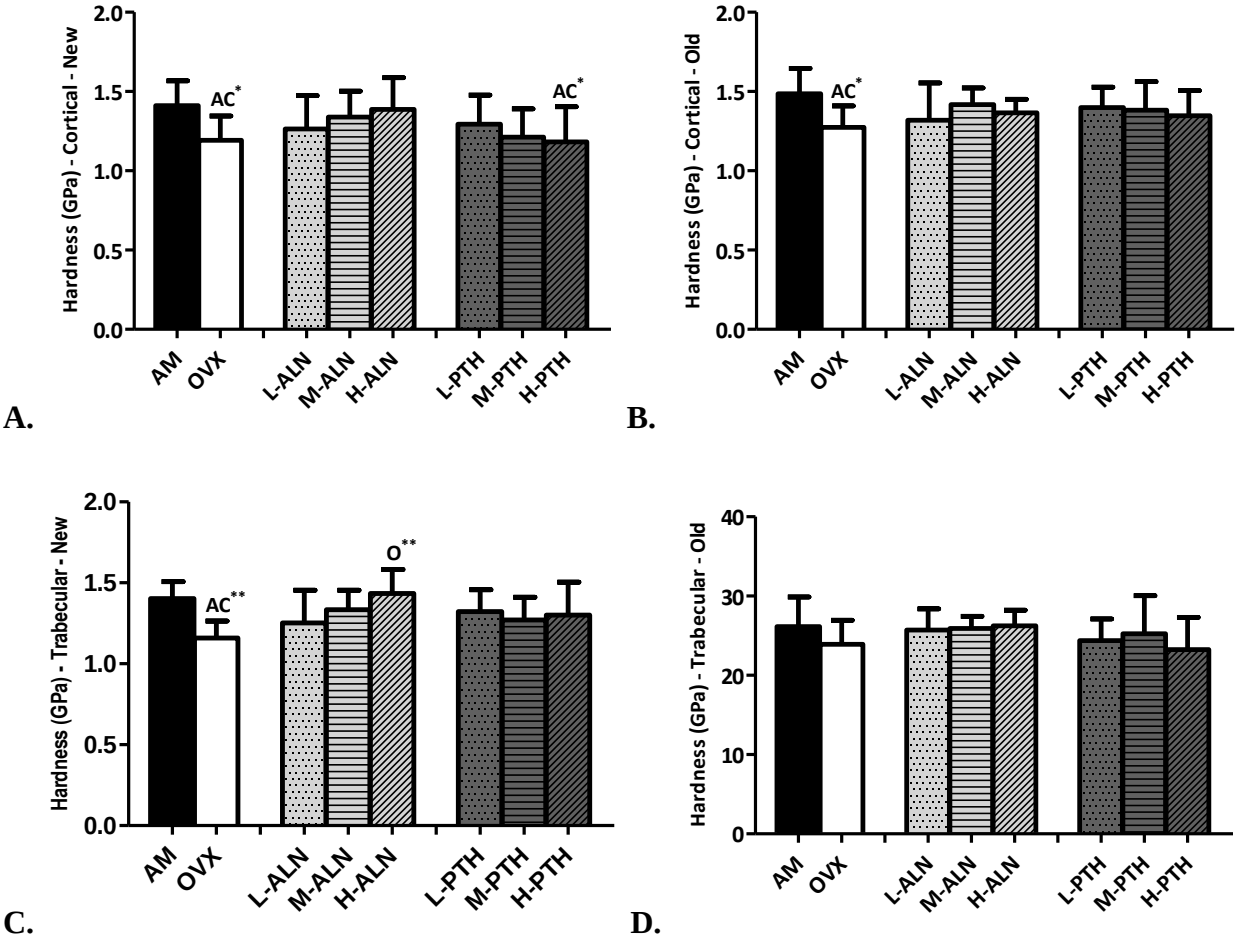

Figure 3.10. Nanoindentation of bone surfaces (gray) and interstitial bone (black) revealed A.) Elastic moduli and B.) Tissue hardness for age matched controls (AC), OVX controls (OVX), high alendronate treated (H-ALN) and high PTH treated (H-PTH) rats.

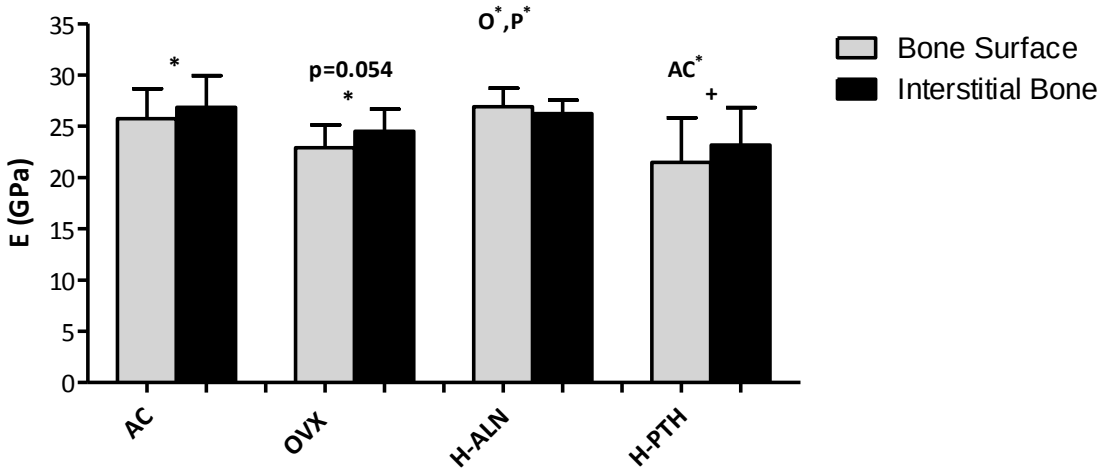

A.

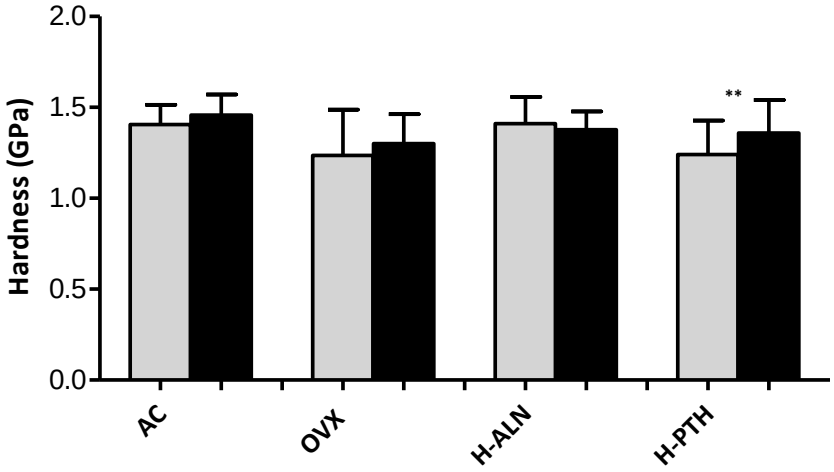

B.

3.7 Tables

Table 3.1. Histomorphometric analysis of the tibial metaphysis at 12 months of age after 6 months of drug treatment

		AC	OVX	L-ALN	M-ALN	H-ALN	L-PTH	M-PTH	H-PTH
Trabecular Bone	**Tb.BA** [mm^2]	**4.12±1.52** O LA MA LP MP	**1.43±0.78** AC HA HP	**2.82±1.09** AC HA	**3.55±1.30** AC HA	**5.39±1.52** O LA MA	**1.01±0.51** AC HP	**3.08±1.87** AC HP	**5.29±1.01** AC LP MP
	BA/TA	**0.12±0.06** O LA MA LP MP	**0.04±0.02** AC MA HA MP HP	**0.08±0.03** AC HA	**0.10±0.04** AC O HA	**0.15±0.04** O LA MA	**0.03±0.02** AC MP HP	**0.09±0.03** AC O LP HP	**0.16±0.03** AC O LP MP
	Tb.N [1/mm]	**1.83±0.75** O LP MP	**0.64±0.22** AC LA MA HA HP	**1.53±0.44** AC HA	**1.79±0.40** O	**2.21±0.42** O LA	**0.52±0.20** AC HP	**1.18±0.46** AC HP	**1.49±0.29** O LP MP
	Tb.Th [µm]	**62.2±12.5** HP	**65.2±12.0** HP	**52.5±6.5**	**59.5±7.4**	**66.0±10.5**	**60.7±7.7** HP	**73.9±11.3** HP	**109.0±12.7** AC O LP MP
	Tb.Sp [mm]	**0.603±0.353** O LP	**1.652±0.537** AC LA MA HA MP HP	**0.650±0.198** O	**0.529±0.151** O	**0.406±0.112** O	**2.178±0.952** AC HP	**0.969±0.643** O HP	**0.588±0.135** O LP MP
	Tb.MS/BS [1/µm]	**9.69±4.9** O MA HA LP MP HP	**20.26±5.9** AC MA HA MA HP	**0.836±0.30** HA	**15.05±7.5** O	**8.52±5.5** O LA	**26.26±7.8** AC	**36.78±11.6** AC O	**35.02±9.1** AC O
	Tb.MAR [µ/d]	**1.01±0.35** O MA HA HP	**1.40±0.24** AC MA HA	**1.01±0.09** HA	**0.44±0.22** AC O LA	**0.56±0.31** AC O LA	**1.15±0.29**	**1.31±0.26**	**1.43±0.32** AC
	Tb.BFR/BS [μ^3/μ^2/d]	**0.10±0.058** O MA HA LP MP HP	**0.28±0.10** AC MA HA MP HP	**0.16±0.09**	**0.04±0.04** O	**0.02±0.02** O	**0.31±0.13** AC HP	**0.44±0.15** AC O	**0.50±0.16** AC O LP
Cortical Bone	**Ec.Ms/BS** [1/µm]	**0.22±0.18** O LA LP MP HP	**0.59±0.20** O MA HA	**0.51±0.16** AC HA	**0.17±0.09** O LA	**0.12±0.06** O LA	**0.49±0.15** AC	**0.60±0.16** AC	**0.63±0.16** AC
	Ec.MAR [µ/d]	**1.45 ±0.77**	**1.89±0.57** MA HA	**1.90±0.45** MA HA	**0.97±0.66** O LA	**0.75±0.43** O LA	**1.38±0.57** HP	**1.98±0.38**	**2.23±0.56** LP
	Ec.BFR/BS [μ^3/μ^2/d]	**0.42±0.47** O MP HP	**1.20±0.64** AC MA HA	**0.99±0.51** MA HA	**0.16±0.13** O LA	**0.10±0.09** O LA	**0.74±0.44** HP	**1.17±0.43** AC	**1.46±0.64** AC LP

Data are mean ± standard deviations. Difference in letters denominate significant differences to given groups: AC – age matched controls, O – OVX controls, LA(low)/MA(medium)/HA(high) – Alendronate, LP(low)/MP(medium)/HP(high) – PTH. (ANOVA and Tukey)

Table 3.2. Correlations of chemistry (FTIR) and tissue mechanics (nanoindentation) of the tibial metaphysis regressed for all individual data points collected for each individual animal (n=40 points/treatment, top) for average tissue regions within each group (n=4 points/treatment, middle) or regressed for averages for each treatment group (n=1 point/treatment group, bottom) at 6 and 12 months of age

	Mineralization **(900-1200)/(1600-1700)**	**Crystallinity** **(1034-1036)/(1024-1026)**	**Collagen Cross Linking** **(1659-1661)/(1689-1691)**	**Carbonate Substitution** **(1414-1424)/(900-1200)**	**Protein** **(1600-1700)**	**Phosphate** **(900-1200)**
Elasticity [GPa]	$R^2=0.03^*$ $R^2=0.13^*$ $R^2=0.09$	$R^2=0.00$ $R^2=0.02$ $R^2=0.09$	$R^2=0.02$ $R^2=0.11^*$ $R^2=0.20^*$	$R^2=0.01$ $R^2=0.16^*$ $R^2=0.14^*$	$R^2=0.00$ $R^2=0.01$ $R^2=0.00$	$R^2=0.02$ $R^2=0.15^*$ $R^2=0.40^*$
Hardness [GPa]	$R^2=0.03^*$ $R^2=0.18^*$ $R^2=0.01$	$R^2=0.00$ $R^2=0.16^*$ $R^2=0.33^*$	$R^2=0.00$ $R^2=0.00$ $R^2=0.03$	$R^2=0.01$ $R^2=0.22^*$ $R^2=0.21^*$	$R^2=0.02$ $R^2=0.03$ $R^2=0.00$	$R^2=0.00$ $R^2=0.10^*$ $R^2=0.16^*$

*Denotes significantly non-zero slope of the regression line.

Chapter 4

BONE AND FAT ARE PERTURBED IN AN OSTEOPOROTIC RAT MODEL BUT NORMALIZED WITH PARATHYROID HORMONE AND ALENDRONATE TREATMENT

4.1 Abstract

30% of the U.S. population is affected by osteoporosis and obesity, and as we discover more about the role of fat mass on skeletal health it is becoming clear that there is an inherent connection between bone and fat. Post-menopausal osteoporosis is associated with increased body mass and abdominal adiposity, factors that can pose a secondary risk to skeletal health. Alendronate (ALN) and parathyroid hormone (PTH) treatment target bone loss but their effects on adiposity, metabolism, and the interrelationship between bone and fat are largely unknown. Adult OVX rats were subjected to short-term (2 months) and long-term (6 months) treatments of different doses of ALN and PTH. Bone morphology of the tibia and L4 vertebra was assessed by μCT and associated with body mass, abdominal fat and lean volume, marrow adiposity, indices of fat metabolism, and transcriptional levels of osteogenic, adipogenic and osteoclastic genes in bone marrow populations. Bone mass and tissue architecture deteriorated with OVX while both PTH and ALN provided benefits in a dose-dependent manner. Abdominal fat increased with age independent of OVX or drug-status but OVX induced increases in marrow adiposity and fat metabolism were reduced by ALN and PTH. Bone mass and microarchitecture negatively correlated to changes in fat composition and marrow adiposity. Wnt-9 transcriptional levels were greater in ALN than in controls. Perturbation of the OVX induced bone and fat phenotypes were normalized by moderate to high doses of ALN and PTH. Through their effects on adiposity,

both drugs may help to reduce the incidence of the metabolic syndrome and tissue fat accumulation that often accompanies post-menopausal osteoporosis.

4.2 Introduction

Post-menopausal osteoporosis, a result of estrogen withdrawal, is associated with reduced bone mass [26], deterioration of bone microarchitecture [147, 197] and altered tissue-level material properties [198, 199], ultimately increasing the risk of skeletal fracture [6, 94, 200]. The consequences of estrogen withdrawal are not confined to the skeleton but are also manifested in the perturbation of metabolic health [45]. The loss of estrogen increases visceral fat accumulation [106] and promotes fat infiltration in the bone marrow, skeletal muscle and the liver [102, 201]. Through the intricate linkage of bone and fat [202], metabolic factors are not only primary risk factors for type 2 diabetes and cardiovascular disease [46, 203] but can also lead to bone degradation [101, 204] and increase susceptibility to fracture [205].

The positive relationship between body mass and bone mass [206-209] associated with the increase in mechanical demand [81] is well known but the precise role that body fat plays in modulating bone mass is ambiguous. Discrepancies between studies that found a positive [207, 210-213], negative [85, 88], or no [84] influence of fat on bone mass may be associated with differences in the locale of *in vivo* body compositional measurement, error in imaging modalities due to poor resolution [214] or a lack of normalization by body mass, differences in race, or menopausal status [84, 207, 215, 216]. Most recent studies suggest negative effects of fat metabolism on bone health as highlighted by the negative association between bone mineral density and visceral fat [85] as well as serum lipid levels [217].

Osteoblastogenesis and adipogenesis are closely linked because osteoblasts and adipocytes differentiate from a common progenitor, the mesenchymal stem cell. Not surprisingly, there is an inverse relationship between osteoblasts and adipocytes within the bone marrow [218]. Mesenchymal differentiation into adipocytes is due to the activation of the peroxisomeproliferator-activated receptor-gamma (PPARγ) coupled with a down regulation of Wnt/B-catenin signaling pathways [219]. Additionally, diet-induced obesity models have demonstrated that adipogenesis negatively effects bone mass due to the accumulation of adipocytes in the bone marrow microenvironment [220] which increases osteoclastogenesis NFkB(RANKL)/OPG pathways [221-224] and may enhance osteoclast survival [225], ultimately elevating bone resorption and further reducing bone mass.

Pharmaceuticals used to treat osteoporosis can mitigate bone loss through different mechanisms by preventing bone resorption through bisphosphonates (e.g., alendronate) [59, 171] or increasing bone formation through anabolic agents (e.g., intermittent parathyroid hormone) [80, 172] Although pharmaceuticals have been used successfully to prevent bone loss [172, 226], little is known about their influence on bone-fat interactions. Bisphosphonates may reduce marrow adiposity in post-menopausal women [227]. When applied to preadipocytes and preosteoblasts in culture, PTH increases osteoblastic differentiation while simultaneously reducing adipogenesis [228, 229]. Different forms of bisphosphonates have been shown to have effects on adiposity; residronate treatment blocks adipogenic differentiation of marrow-derived mesenchymal stem cells [230] while strontium ranalate decreased bone marrow adiposity in mice [231]. The impact of anabolic and anti-catabolic pharmaceuticals on metabolic health, adiposity, and body compositional relationships between bone and fat are largely unknown. Here, using the OVX rat model, PTH and alendronate will differentially target bone loss and we

hypothesize that both drugs will prevent fat accumulation, thereby normalizing the bone-fat interaction and prevent the perturbation of fat metabolism that occurs during estrogen withdrawal.

4.3 Materials and Methods

Experimental design

All procedures were reviewed and approved by the Institutional Animal Care and Use Committee of Stony Brook University. All rats were individually housed in standard cages and allowed free access to standard rodent chow and tap water and were weighed twice weekly to monitor changes in body mass. Adult five-months-old female Sprague-Dawley rats were ovariectomized and mass-matched into normal age matched controls (AC), ovariectomized controls (OVX), and ovariectomized rats treated with either alendronate (ALN) or parathyroid hormone (PTH) at three different doses.

At 6 months of age, 10 normal and 10 OVX rats were sacrificed as baseline controls, drug treatment began. Alendronate was injected subcutaneously twice per week; high-dose rats received 2mg/kg (H-ALN), medium-dose rats received 100µg/kg (M-ALN), and low-dose rats received 10µg/kg) (L-ALN). Parathyroid hormone was injected subcutaneously five times per week: high at 75µg/kg (H-PTH), medium at 15 µg/kg (M-PTH), and low at 0.3 µg/kg (L-PTH). Drugs were administered at the dosages listed, per injection. Treatment doses were determined based on previous literature for the clinically relevant dose (medium), the maximum tolerable dose without known evidence of cytotoxicity (high) and a dose low enough to induce minor improvements compared to OVX controls.

All animals, with the exception of AC controls, were ovariectomized at 5 months of age. Animals were sacrificed at baseline (6 months of age), after short term (2 months) treatment at 8 months of age and after long term (6 months) treatment at 12 months of age. Upon sacrifice, L4 vertebrae were extracted and stored in 70% ethanol at -20°C. The left tibiae were extracted, cleaned of soft tissue and dehydrated in ethanol (70%, 80%, 90%, 100% - 3-4 days each). Gonadal fat pad and livers were extracted, weighed and stored at -80°C. Whole blood was collected by cardiac puncture, and centrifuged. Serum was stored at -80°C. Tibial bone marrow was flushed from the diaphysis using 3mL of RNALater solution (Ambion, Foster City, CA, USA) and stored at -80°C.

In vivo micro computed tomography (in vivo µCT)

Animals from the long term treatment group, that were scheduled for sacrifice at 12mo of age were longitudinally scanned by *in vivo* micro-computed tomography µCT at 6, 8 and 12 months of age (VivaCT 75, Scanco Medical, Switzerland, **Figure 4.1**). Prior to each scan, rats were anesthetized with isofluorane. Scans were acquired at an isotropic voxel size of 156 µm (45kV, 133µA, 300-ms integration time). To measure changes in body composition, the abdomen was scanned between the proximal end of the L-1 vertebral body to the distal end of the L-4 vertebral body. An automated script was used to determine visceral and subcutaneous fat content, vertebral bone volume and vertebral bone apparent mineral density [232]. Lean tissue volume was calculated by subtracting bone and fat volume from total tissue volume.

Ex vivo micro computed tomography (ex vivo µCT)

Vertebrae were scanned by desktop µCT (µCT40, Scanco Medical). Scans were acquired at an isotropic voxel size of 36µm to measure trabecular architecture of the vertebral body (45kV, 133µA, 300ms integration time). The trabecular bone within the L-4 vertebral body was separated from the cortical shell and analyzed for bone volume fraction (BV/TV), trabecular thickness (Tb.Th.), trabecular separation (Tb.Sp.), trabecular number (Tb.N) and tissue mineral density (TMD).

Bone marrow histology

The dehydrated proximal tibia was embedded in poly-methyl methacrylate for histological sectioning. Metaphyseal sections were cut in the coronal plane at 8 µm (RM 2165 microtome, Leica Microsystems, Wetzler, Germany), deplasticized in acetone and stained with Giemsa and Toluidine Blue O (Sigma-Aldrich, St. Louis MO, USA). Five fields of view chosen along the boundry of the growth plate were imaged at 10x magnification (Carl Zeiss microscope). Adipocyte number and average size were determined using ImageJ particle analyzer for objects that were between 60 to 1,000 pixels in size with a circularity >0.6. (ImageJ, National Institute of Health, Bethesda MD, USA). Trabecular bone area (Tb.B.Ar) was determined by tracing individual trabeculae within the metaphyseal area from growth plate to diaphysis for one histological section per animal using Osteomeasure software (Osteometrics, Decatur, GA, USA).

Serum, bone marrow and liver biochemistry

Serum was thawed and total triglyceride (TG, total mg in tissue) and nonesterified free fatty acid (NEFA, total mmol in tissue) were measured in whole serum, the lipid extracts of the bone

marrow and liver tissue using enzymatic colorimetric kits (TG Kit: Sigma-Aldrich, St. Lois, MO, USA and NEFA: HR Series NEFA-HR(2), Wako Diagnostics, Richmond VA, USA). Samples were analyzed in duplicate with a 96-well plate reader according to standard assay protocols. Leptin levels of the serum were determined using ELISA assays (University of Cincinnati Mouse Metabolic Phenotyping Center, Cinncinnati OH, USA). Total lipids were extracted from the liver and bone marrow and purified through chloroform-methanol extraction.

Gene expression- RNA extraction and real-time RT-PC

Total RNA was isolated from the tibial bone marrow with an RNeasy Total RNA isolation kit (Qiagen, Valencia, CA, USA) according to manufacturer's instructions. After digestion with RNase-free DNase set (Qiagen, Velencia, CA, USA), total RNA was quantified (Nanodrop spectrophotometer, ThermoFischer Scientific, Waltham MA, USA). RNA purity was confirmed on an electrophoresis agarose gel. cDNA was reverse-transcribed using a high capacity cDNA reverse transcription kit (Applied Biosystems, Carlsbad, CA, USA) Expression levels of candidate genes Wnt-9, RUNX2, PPAR-γ, and TNFS-11 (TaqMan probes, **Table1**) were quantified using StepOnePlus Real-Time PCR (Applied Biosystems, Carlsbadm CA, USA) following the manufacturer's instructions. The mRNA levels were normalized to those of β–Actin (control gene) and changes in gene expression were measured as fold changes from measured standard curves.

Statistical Analysis

Longitudinal differences within groups were compared with repeated measures Two-Way ANOVA to determine the interaction of time and treatment and their relative contribution to

changes invertebral bone and abdominal fat. A Student t-test compared baseline organ masses, metabolic parameters and histological data between AC and OVX controls. A One-Way ANOVA with a Dunnett post-hoc test compared endpoint organ masses, metabolic parameters and histological data to OVX controls within a time point at 8 or 12 months. Linear regressions tested for associations between endpoint vertebral bone and measures of fat adiposity. R-squared values were reported with their associated p values. ANCOVA was used to determine differences in slopes among treatment groups. All values were reported as means +/- standard deviations. P-values less than 5% were considered significant. Outliers were removed using a one-sample t-test with a-value equal to 0.05.

4.4 Results

Body mass increases with age:

At 6 months of age, prior to the start of treatment, and after one month of ovariectomy, all OVX groups had 19% greater body mass than AC ($p<0.05$). At 8 months of age, OVX controls were 10% heavier than AC, PTH-treated animals were % (low dose), % (medium dose), % (high dose) heavier than AC, and ALN-treated animals were % (low dose), % (medium dose) and % (high dose) heavier than AC (all $p<0.05$). By 12 months of age, there were no significant differences in body mass between groups ($p>0.05$). AC controls gained 18% body mass from 6 months of age to 8 months of age ($p<0.05$) and 35% from 6 to 12 months ($p<0.001$) where OVX controls only gained 8% body mass from 6 to 8 months ($p<0.05$), and 25% from 6 to 12 months ($p<0.001$). Treated animals gained mass similarly to OVX controls; PTH treated animals gained 11+/-2% from 6 to 8 months ($p<0.05$) and 22+/-3% from 6 to 12 months ($p<0.001$). ALN treated animals gained 12+/-2% from 6 to 8 months ($p<0.01$) and 19+/-6% from 6 to 12 months ($p<0.001$).

These data demonstrate a strong age-related effect on body mass, regardless of estrogen deficiency (**Figure 4.2**).

Vertebral bone morphology:

Longitudinal *in vivo* μCT analysis revealed OVX and drug-induced differences in vertebral bone volume and apparent mineral density. At six months of age, one month after ovariectomy and prior to the start of treatment, all ovariectomized animals had 12.9% less vertebral bone volume (BV) than AC controls ($p<0.001$). From 6 to 12 months of age, vertebral BV did not change in AC controls or in OVX controls ($p>0.05$). In contrast, BV in ALN rats increased (all $p<0.05$) by 11% (low dose), 15% (medium), and 23% (high) from 6 to 12mo. BV in H-PTH increased by 26% ($p<0.001$) from 6 to 12mo. No changes in BV were observed in L- and M-PTH rats (**Figure 4.3a**).

At six months of age, one month after ovariectomy and prior to the start of treatment, all ovariectomized animals had 6.9% lower vertebral apparent mineral density (App.MD) than AC controls ($p<0.001$). From 6 to 12 months of age, vertebral App.MD did not change in AC ($p>0.05$). Yet, vertebral App.MD decreased by 10% in OVX rats ($p<0.001$). Vertebral App.MD increased longitudinally in M- and H-ALN treated animals by 7 and 9% ($p<0.01$) and did not change in L-ALN ($p>0.05$). Vertebral apparent mineral density increased in M- and H-PTH treated animals by 6 and 12% ($p<0.05$), but decreased in L-PTH by 10% ($p<0.05$, **Figure 4.3b**). Changes in bone volume and apparent density measured by *in vivo* microCT were supported by high-resolution *ex-vivo* μCT scans at the 12mo endpoint. Compared to AC, trabecular micro-architecture was degraded in OVX, but PTH and ALN dose-dependently normalized trabecular micro-architecture. OVX had 92% lower BV/TV than AC ($p<0.01$). L-, M- and H- ALN had 90,

96, and 117% higher BV/TV compared to OVX ($p<0.05$). M- and H-PTH had 118 and 170% higher BV/TV compared to OVX ($p<0.001$, **Figure 4.4a**). Greater BV/TV in the drug treated groups was due to an increase in trabecular number and thickness (**Figure 4.4b and 4.4c**).

Adiposity increases with age and positively correlates to body mass:

Longitudinal *in vivo* μCT separated abdominal fat into visceral and subcutaneous fat compartments, and revealed longitudinal increases in abdominal fat; all animals gained 103+/-37% fat volume from 6 to 8 months and 140+/-43% from 8 to 12 months (**Figure 4.5**). At 6 months of age, there were no differences in total fat, subcutaneous fat or visceral fat volumes between groups (*in vivo* μCT, One-Way ANOVA, Tukey post hoc, $p>0.05$). Similarly, at 6 months of age there were no differences in extracted gonadal fat pad mass at sacrifice between baseline intact animals or baseline ovariectomized animals (unpaired Student t-test, $p>0.05$). (**Disclaimer:** These were a separate set of animals that were not part of the *in vivo* scanning analysis.)

At 8 months of age, there were no differences in total, subcutaneous or visceral fat volumes between groups (*in vivo* μCT, One-Way ANOVA, Tukey post hoc, $p>0.05$). The sacrificed animals from the 8 months time point, after two months of treatment, had differences in their gonadal fat pad masses, where PTH-treated rats had 58% (L-PTH, $p<0.01$), 38% (M-PTH, $p<0.05$) and 38% (H-PTH, $p<0.05$) smaller gonadal fat pads than AC controls and L-ALN treated rats had 42% smaller gonadal fat pads than AC controls (fat mass, One-Way-ANOVA, Tukey post hoc, $p<0.01$). (**Disclaimer:** These were a separate set of animals that were not part of the *in vivo* scanning analysis.)

At 12 months of age, after 6 months of treatment, H-ALN treated rats had 21% less visceral fat and 38% less subcutaneous fat than AC ($p<0.05$), all other groups had similar amounts of visceral and subcutaneous fat ($p>0.05$, One-Way ANOVA, Tukey post hoc, **Figure 4.6**). The extracted fat pads from the longitudinally scanned animals showed that after 6 months of treatment, H- and L-ALN, and H-PTH and M-PTH had smaller gonadal fat pads than OVX controls ($p<0.05$, **Table 4.3**). The gonadal fat pad mass of 12 month old animals positively correlated to body mass and to visceral fat volume (BM: $R^2=0.26$, $p<0.001$, VAT: $R^2=0.37$, $p<0.001$, **Figure 4.7**).

Vertebral bone volume was positively associated with body mass , as well as total fat volume (TAT) and visceral fat (VAT) volume independent of body mass, (Linear Regression Analysis- BW: $R^2=0.11$, ANCOVA- TAT: $R^2=0.27$, ANCOVA: VAT: $R^2=0.13$, $p<0.05$, **Figure 4.8a**). Body mass, total fat volume (TAT) and visceral fat volume (VAT) were poorly associated with vertebral apparent mineral density (BW: $R^2=0.02$, $p<0.05$, TAT: $R^2=0.00$ $p>0.05$, VAT: $R^2=0.01$ $p=0.07$, **Figure 4.8b**).

Liver adiposity increases with age, accumulation reduced with drug treatments:

At baseline, one month after ovariectomy, there were no differences in liver mass between intact or ovariectomized animals. At eight months, after short term treatment (2 months), all OVX groups had smaller livers than AC controls, but differences were not yet significant ($p>0.05$). At 12 months, after long term treatment (6 months), ALN-treated rats had 22% (L-ALN, $p<0.001$), 17% (M-ALN, $p<0.01$) and 17% smaller livers than AC controls. Similarly, PTH-treated rats had 20% (L-PTH, $p<0.001$) 22% (M-PTH, $p<0.001$) and 10% (H-PTH, $p>0.05$) smaller livers than AC controls (**Table 4.3**).

Bone histology and marrow adiposity of the tibia:

Histological analysis of the tibial metaphyseal trabecular bone after 6mo of treatment was consistent with results from the vertebral trabecular data analysis. Bone area of the tibia positively correlated with BV/TV of vertebral bone (R^2=0.44, $p<0.05$). OVX controls had 206% less trabecular bone than AC ($p<0.001$). There were dose-dependent increases in trabecular bone with both PTH and alendronate treatments. L-ALN and L-PTH did not have more trabecular bone than OVX controls. M- and H-ALN had 167 and 268% more bone than OVX ($p<0.01$). M- and H-PTH had 126 and 283% more bone than OVX ($p<0.05$, **Figure 4.9**).

After 6 months of treatment, bone marrow histology of the tibial metaphysis revealed increased adipogenesis with ovariectomy but a reduction by treatment. OVX controls had 104% more adipocytes than AC controls in the tibial bone marrow ($p<0.001$). There were dose-dependent reductions in the number of adipocytes in the marrow with both ALN and PTH treatment. L-, M- and, H-ALN treated rats had 39, 32 and 60% fewer adipocytes compared to OVX controls ($p<0.01$). M- and H-PTH treated rats had 50 and 73% fewer adipocytes compared to OVX controls ($p<0.001$). L-PTH had 18% fewer adipocytes than OVX controls but the difference was not significant. There were no differences in average adipocyte size ($p>0.05$, **Figure 4.10**).

At twelve months of age, adipocyte number was negatively correlated with bone area within the marrow cavity (R^2=0.45, $p<0.001$). When stratified into treated and non-treated rats, there was a strong negative correlation between tibial bone area and adipocyte number in pooled AC and OVX (R^2=0.79, $p<0.001$) while the slope of this relation was significantly less proportional ($p<0.05$) in both ALN (R^2=0.35, $p<0.01$) and PTH (R^2=0.49, $p<0.001$) (**Figure 4.11**).

Measures of fat metabolism worsened by OVX, improved with drug treatment:

At baseline, OVX had 13 fold greater total liver triglyceride levels than AC ($p<0.001$, Student t-test). After 3 months of OVX and 2 months of treatment, OVX controls and drug-treated rats had elevated triglyceride levels in the liver compared to AC controls which were not significant. Similarly, L-, M- and H-ALN had 2.7x, 3x ($p<0.05$) and 3.6x ($p<0.05$) more liver triglycerides than AC, and L-, M- and H-PTH had 3x ($p<0.05$), 2.1x and 2.4x more liver triglycerides than AC. After 6 months of treatment, OVX controls had 2.3x more liver triglycerides than ACs ($p<0.001$). L-ALN, L-PTH and M-PTH treated rats had 2.7, 2.7 and 2.8x more triglycerides in the liver than AC controls ($p<0.05$), but H-PTH and M- and H-ALN rats did not have significantly different liver triglycerides than AC controls ($p>0.05$). The beneficial effects of PTH and ALN on triglyceride accumulation in the liver were apparent because all treated groups were significantly less than OVX controls ($p<0.01$, **Figure 4.12a, Table 4.4**).

At baseline, OVX had 2.5x more total liver non-esterfied free fatty acids (FFAs) than AC ($p<0.001$, Student t-test). After 3 months of OVX and 2 months of treatment, OVX controls had a trend towards more FFAs in the liver than AC control (1.8x) but the difference was not significant ($p>0.05$), while H-PTH treated rats had 71% lower FFAs in the liver than OVX controls ($p<0.01$). After 6 months of treatment, OVX controls had 56% more FFAs in the liver than AC controls but the difference was not significant ($p>0.05$). ALN and PTH treatments significantly reduced liver FFAs compared to OVX controls, L- and H-ALN treated animals had 50 and 40% less FFAs than OVX ($p<0.01$). L- and M-PTH treated rats had 55.3 and 46.3% lower liver FFAs than OVX ($p<0.001$, **Figure 4.12b**).

At baseline, OVX controls had 19% more TGs in the bone marrow than AC ($p<0.01$). After 3 months of OVX and 2 months of treatment, OVX controls had 12% more marrow TGs

than AC but the difference was not significant ($p>0.05$). However L- and M-ALN both had 18% less TGs in the marrow than OVX controls ($p<0.01$) while L-, M- and H-PTH had 18-19% lower TGs in the marrow than OVX controls ($p<0.01$). After 6 months of treatment, OVX controls had 20% more marrow TGs than AC ($p<0.05$). L- and H-ALN treated animals had 46 and 53% lower marrow TGs than OVX controls ($p<0.05$) H-PTH treated animals had 58% less TGs in the marrow than OVX controls ($p<0.001$, **Figure 4.12c**).

At baseline, OVX controls had 2x more bone marrow FFAs than age matched controls ($p<0.001$, Student t-test). After 3 months of OVX and 2 months of treatment, OVX controls had 49% more FFAs in the bone marrow than AC controls but the difference was not significant ($p>0.05$). L-, M-, and H-ALN had 57, 58 ad 42% less FFAs than OVX controls ($p<0.01$). L-, M-, and H-PTH had 55, 57 and 59% less FFAs than OVX controls ($p<0.01$). After 6 months of treatment, OVX controls had 54% more bone marrow FFAs than AC controls ($p<0.05$). L- , M- and H-ALN treated animals had 57, 48 and 55% less FFAs than OVX controls ($p<0.05$) and M- and H-PTH treated animals had 54 and 58% less FFAs than OVX controls ($p<0.05$, **Figure 4.12d**).

The total triglyceride content of the bone marrow from the right leg was moderately, negatively associated with the bone area of the tibial metaphysis from the left leg ($R^2=0.33$, $p<0.05$), BV/TV from the L-4 vertebral body ($R^2=0.18$, $p<0.05$) and apparent mineral density from the L-4 vertebral body ($R^2=0.35$, $p<0.05$). Similarly, other measures of marrow adiposity were negatively correlated to measures of bone mass and architecture (**Table 4.5**).

There were no drug-specific changes in serum leptin levels after 2 or 6 months of treatment, but there were age-related changes in leptin. At baseline, OVX controls had 76% higher leptin levels than AC controls ($p<0.05$). At 8 months of age, OVX controls only had 20%

higher leptin levels than AC controls ($p<0.05$), and by 12 months of age, OVX controls had 24% higher leptin levels and these differences were no longer significant ($p>0.05$, **Figure 4.13**).

Serum markers of bone formation are modulated with high dose treatments:

After 6 months of treatment, high doses of ALN and PTH lowered IGF-1 levels in the serum, H-ALN had 32% lower and H-PTH had 30% lower IGF-1 than OVX controls ($p<0.05$, One-Way ANOVA, Dunnett post hoc test). After six months of treatment, H-PTH treated rats had 69% higher alkaline phosphatase levels in the serum than AC controls ($p<0.01$, **Figure 4.14**).

Bone marrow osteogenesis and adipogenesis relatively unchanged by OVX and treatment:

After three months of ovariectomy and 2 months of drug treatment, there were no significant changes in osteogenic (RUNX2, Wnt9b), adipogenic (PPAR-γ) or osteoclastic (RANK-L) gene expression in the bone marrow with OVX, nor drug treatment. Anecdotally, L-, M- and H-ALN treated animals had a 2.12, 2.47 and 2.18 fold higher Wnt9b gene expression compared to AC and L-, M- and H-PTH had a 1.50, 1.66 and 1.15 fold higher Wnt9b expression compared to AC controls (**Table 4.6**). When ALN groups were pooled and PTH groups were pooled, ALN groups had 39% higher RANK-L expression than PTH groups ($p<0.01$). ALN groups had 1.25 fold higher Wnt9b expression than OVX controls ($p<0.05$, Dunnett post hoc test, **Figure 4.15**).

4.5 Discussion

We investigated how ovariectomy and different doses of two pharmaceutical countermeasures of bone loss modulate the association between bone morphology and adiposity. Vertebral bone volume and microarchitecture were substantially compromised by OVX, with dose-dependent

gains by either PTH or ALN. Body mass, tissue fat mass and biochemical fat markers were elevated with OVX but normalized, or lowered, with ALN and PTH treatment. Measures of bone mass and architecture were negatively correlated with measures of fat metabolism and fat composition. Similarly, marrow adiposity increased proportionally with the amount of bone loss. After two months of treatment, there were no OVX or drug-induced changes to RUNX2, PPAR-gamma or RANK-L expression. There were moderate increases in Wnt9b signaling with all doses of alendronate treatment and minor increases with all doses of PTH treatment. The differences in gene expression were not as pronounced as expected, which could be due to the timing of bone marrow extraction. After two months of treatment, the differentiation of stromal cells within the bone marrow may have already occurred.

Bone mass and microarchitecture are decreased with OVX, but dose-dependently improved with PTH and ALN treatment:

The rapid effects of OVX were reflected by the decrease in bone density one month after the surgery. This type of decline in tissue microarchitecture is well documented in the OVX rat model [169, 233]. Bone microarchitecture is a main proponent of bone quality, strongly influencing bone strength [33], the loss in bone architecture causes an increased susceptibility to skeletal fractures [234]. PTH and ALN are both clinically proven to prevent bone microarchitecture degradation [59, 75]. The preservation of bone mass and tissue architecture are critical during osteoporosis bone loss. Once architecture is lost, it is difficult, if not impossible to recover. Our model dose-dependently increased bone mass and architecture to establish a population with large variability in bone tissue mass and architecture which helped to elucidate the role of body composition and fat metabolism on skeletal quality.

Fat infiltration was elevated after OVX but prevented with PTH and ALN treatment:

The detrimental effects of OVX on body composition and fat infiltration were rapid, appearing after only one month of ovariectomy. ALN and PTH treatment given for 6 months prevented estrogen-related metabolic health degradation. There was a rapid change to body mass upon the onset of estrogen withdrawal that occurred after one month of ovariectomy. It has previously been reported that estrogen withdrawal leads to increased food intake [235] and changes body composition [50, 236, 237]. In this study the significant alterations to body mass were diminished as natural aging progressed, where AC controls gained more mass throughout the course of the study compared to all OVX animals (**Figure 4.1**). This made it difficult to isolate the ovariectomy effects from aging effects on body composition throughout the course of treatment, but it was clear that there was no measureable alteration in body mass caused by drug treatment. Similar to our findings, others have reported a less drastic effect of estrogen withdrawal on body composition [238], and there is some ambiguity of whether changes after menopause are due to aging or estrogen status [239]. We believe our data are indicative of the strong age-related effects on body mass and body composition [240]. Our results are consistent with the *in vivo* body composition findings where body fat increased longitudinally while lean tissue mass declined (**Table 4.2**). The change in body composition occurred in all groups regardless of OVX status or drug treatment. Similar age-related shifts from lean tissue mass to fat mass have previously been reported in ovariectomized Sprague-Dawley rats [241] and from pre- to post-menopausal women [242].

Although the OVX induced alterations to whole body composition were less pronounced than hypothesized, there were drastic changes to tissue fat accumulation and fat metabolism after only one month of ovariectomy which worsened over the course of the study. Three months after

OVX, livers were smaller than age-matched controls. A reduction in organ masses is common after OVX due to reduced circulating estrogen levels slowing normal organ development [237]. Drug treatments further reduced liver mass which was potentially due to a reduction in the fat infiltration. This hypothesis was supported by the significant increases in fat accumulation, circulating triglycerides and free fatty acids after the induction of ovariectomy which was prevented with both ALN and PTH treatment. Increased fat infiltration, visceral fat accumulation and increased indices of metabolic health are indicators for cardiovascular diseases and type 2 diabetes [45, 243] and are negatively associated with bone health [89, 244]. The prevention of fat infiltration into organs by drug treatment may represent a secondary benefit of osteoporosis therapy. A recent study found a moderate but significant beneficial effect of both PTH and alendronate applied in osteoporotic women on body mass, and measures of metabolism and adiposity, which supports the current findings [245].

Drug-induced changes to marrow adiposity improve bone health:

Bone marrow is rich in multipotential stem cells, growth factors and cytokines, which makes it a key site for osteogenesis and adipogenesis regulation [246]. The marrow is sensitive to hormonal changes and biochemical signaling making it susceptible to change after ovariectomy and drug-treatment. Therefore it is not surprising that the changes to adiposity observed in this study were most significant in the bone marrow.

Estrogen withdrawal induced a large increase in marrow adipose cell number, which was dose-dependently reduced with both ALN and PTH drug treatment (**Figure 4.8**). Similar changes in marrow adiposity have been reported after estrogen withdrawal [247] and marrow adiposity was also reduced after risedronate treatment in osteoporotic women [227]. Our data

demonstrated that the adipogenic marrow population is influenced by both anti-catabolic and anabolic therapies. PTH is an anabolic drug which has been shown to directly influence the bone marrow stromal cell differentiation and down-regulate adipogenesis [42, 228]. Another possible explanation for PTH's beneficial effect on marrow adiposity is through an upregulation of osteocalcin. Osteocalcin has beneficial regulatory effects on energy and fat metabolism and interacts with skeletal health, which has been well documented [248-250]. Studies have shown that Teriparitide can increase the production of osteocalcin in cells [251], diabetic rats [252] and in humans [245]. PTH has even been proposed as a pharmaceutical tool for treating diabetic osteoporosis because of its beneficial effects on fat metabolism.

However, the mechanism of action by which ALN reduces adiposity is less clear. It has previously been reported that strontium renalate (a combinatorial anabolic and anti-catabolic agent) can reduce bone marrow adiposity [231] through PPAR-γ suppression. We did see some suppression in PPAR- γ after 2 months of ALN treatment, although these changes were not significant. Our data is consistent with others who show that upregulation of Wnt signaling is accompanied by a reduction in adipogenesis [253, 254], or inversely, a decrease in Wnt signaling led to an increase in adipogenesis [255].

The lack of effect on gene expression after OVX or with drug treatment in the bone marrow differs from what has previously been reported [256] which could indicate a potential therapeutic window of marrow stromal cell activation by drug therapy. The phenotypic changes to both bone architecture and fat development that were seen by twelve months of age demonstrate the detriment of OVX and the effectiveness of drug-therapy on both of these tissue types. It is possible that the markers chosen for gene expression were not sensitive enough to the linked association of bone and fat or that the changes in these pathways were too subtle to detect

significance. Additionally, the differentiation of these particular genes may have occurred earlier upon the onset of disease (within weeks of ovariectomy). Future work should examine early time points to establish the differential effects of OVX and drug therapy on marrow populations in the rat model.

Fat composition was negatively associated with bone mass and architecture:

The relationship between fat and bone is still unclear. The inconsistency in the literature report a positive [92, 207, 210-212, 257], negative [85, 88], or no [84] relationship between bone and fat [258]. It is apparent that the measurements of fat and how it is related to bone mass and architecture needs standardization. Studies that directly measure visceral adipose tissue through MRI or CT more consistently find a negative association to bone [259]. This relationship is less apparent when body composition is measured through DXA [260], which is not an accurate test for soft tissue analysis [214, 255, 261]. Additionally, the relationship between bone and subcutaneous fat is less pronounced [262]. It is widely accepted that visceral fat plays a detrimental role on skeletal health [50, 258]. The interactions between bone and fat are further complicated by menopause status and by osteoporosis treatment. Most clinical studies for osteoporosis medications focus on bone indices so the effects of drug treatments on metabolism is not well understood. As the relationship between bone and fat is brought to the forefront of the bone field, clinical studies will begin to expand their focus to include measures of adiposity and we will begin to understand the role of drug treatments on the bone-fat interaction.

Our study found no strong relation between total, visceral or subcutaneous fat mass to bone mineral density when measured by *in vivo* μCT. However there was a correlation between bone and fat were measured at a higher resolution, for instance measures of bone architecture

(Tb.N, Tb.Th.) were highly correlative to measures of marrow adiposity (adipocyte #) (**Table 5**). This suggests that the appropriate resolution of imaging and analysis is critical in accurately determining the relationship between bone and fat. This becomes increasingly complicated in clinical studies where biopsies and high resolution imaging are invasive to patients. Future studies should carefully consider their limitation of resolution when drawing conclusions regarding the relationship made between bone and fat based on body composition alone. Future clinical work is needed to determine the role of drug treatment on bone-fat interactions in osteoporotic patients.

Interestingly, we found a very strong negative correlation between trabecular bone area and marrow adiposity in both AC and OVX rats where analysis was conducted at the same skeletal location. The slope of this association was significantly lowered with PTH and ALN treatment indicating a drug-specific effect to the interaction between bone and fat. Similar associations between decreased bone and increased marrow adiposity have previously been reported [263-265]. PTH down-regulates adipogenic differentiation in marrow stromal cells [25]. This data may indicate a potential protective mechanism of drug therapy on the bone-fat interaction within the bone marrow micro-architectural niche where multipotential stromal cells reside. Since osteoblasts and adipocytes arise from the same mesenchymal stem cell population, drug-related effects on differentiation toward one lineage could alter the other's outcome.

There is conflicting evidence regarding the benefit or detriment of excess adipose tissue on bone health. The protective benefits of obesity to skeletal health include increased mechanical loading, resulting in skeletal adaption, increased bone formation, and overall higher bone mass [2, 266] as well as hormonal regulation, such as increased leptin secretion, which increases bone mass [52, 267]. The benefits of high fat mass may be skeletal site dependent where extra

cushioning around the hips may protect bones during falling, but visceral fat has no beneficial effect for vertebral fracture protection [268, 269] and a high fat mass may no longer be considered beneficial when properly normalized by body mass [208, 270, 271]. Emerging evidence suggests higher fat content leads to deterioration in bone quality including a loss in trabecular architecture that puts patients at a higher risk of fracture [272]. At the whole body level, our data showed very small-positive or no association between bone density and body fat composition. At the tissue and cellular levels, we found a consistent negative association between bone mass and architecture and fat composition and metabolism similar to previously reported data [258]. Our data support negative bone-fat interactions. This study also provides evidence that osteoporotic drug therapies play a dynamic role in the interaction between bone and fat.

As patients are frequently prescribed osteoporosis pharmaceuticals, it is important to consider the long-term effects of treatment on not only bone mass and bone quality, but also other systemic effects. Understanding these secondary outcomes could help determine beneficial side effects of bone promoting drugs, such as preventing adiposity. Future osteoporosis clinical studies should attempt to utilize bone biopsy specimens to determine the effect of osteoporosis drug treatment on marrow adiposity and its interaction with bone quality. Attention should be paid when studying large populations of patients focusing on discrepancies in age, race, metabolic health, menopausal status, body mass and body composition as well as drug status. Additional information regarding drug-driven alterations to marrow adiposity will provide insight into drug targets and may suggest new ideas for diagnosing and treating our growing osteoporotic population.

4.6 Figures

Figure 4.1. Representative images from *in vivo* μCT: A.) A scout view of the region of interest scanned (between white lines) B.) The applied script showing the segmented image from a single gray scale slice C.) A segmented 3D image with subcutaneous fat (gray) and visceral fat (pink) separated.

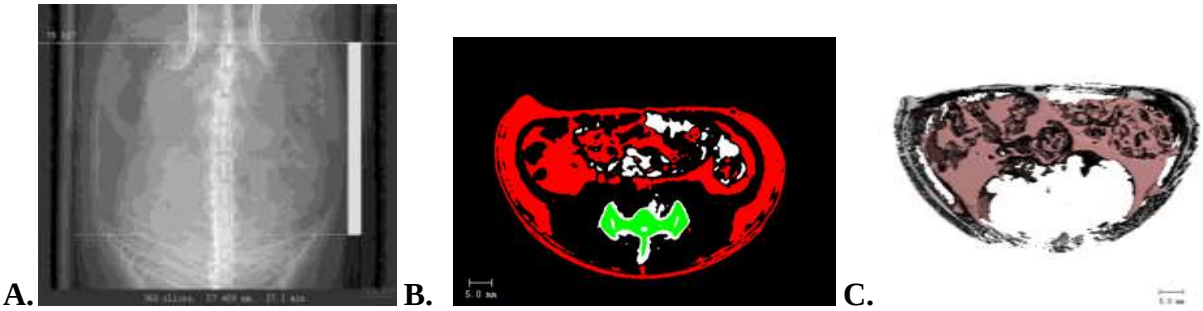

Figure 4.2. Longitudinal change in body mass for age-matched controls (AC- black solid) ovariectomy controls (OVX - dashed gray), OVX + alendronate-treated at low (L - solid black), medium (M – dashed dark gray), or high (H - dotted light gray) doses or OVX + PTH-treated at low (L - solid black), medium (M - dashed dark gray), or high (H - dotted light gray) doses.

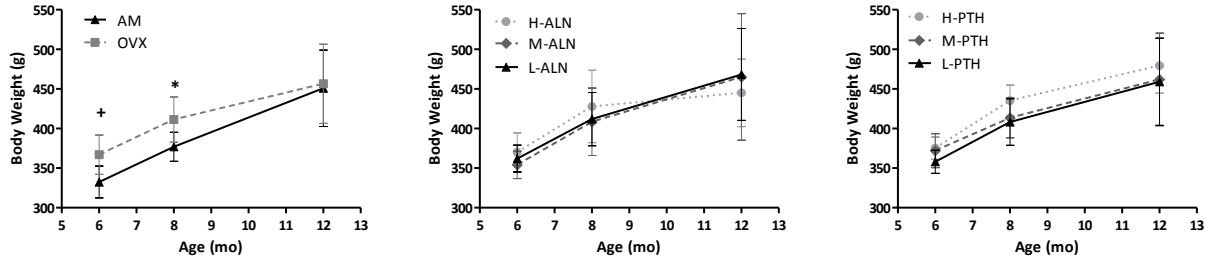

Figure 4.3. *In vivo* microCT of the L4 to the L1 vertebrae scanned at 6, 8 and 12 months of age revealed longitudinal changes in Vertebral A.) bone volume (Vt.BV) and B.) apparent mineral density (Vt.App.MD) for age-matched controls (AC- black solid) ovariectomy controls (OVX - dashed gray), OVX + alendronate-treated at low (L - solid black), medium (M – dashed dark gray), or high (H - dotted light gray) doses or OVX + PTH-treated at low (L - solid black), medium (M - dashed dark gray), or high (H - dotted light gray) doses.

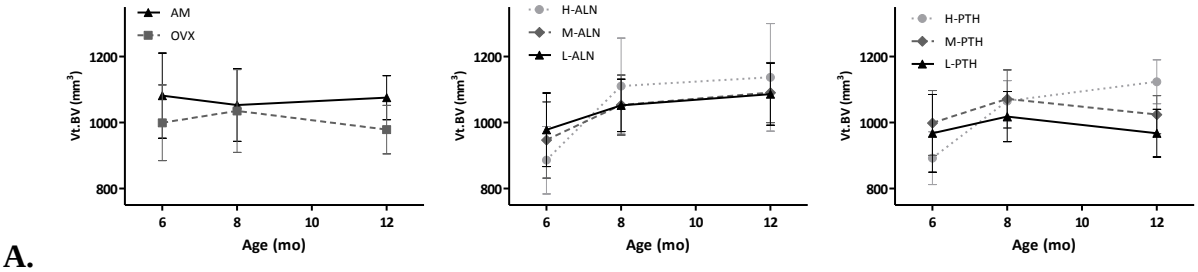

A.

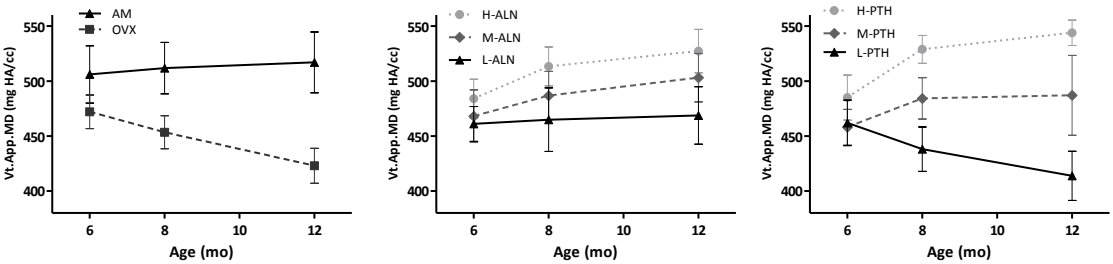

B.

Figure 4.4. Trabecular microarchitecture of the vertebral body from desktop μCT determined Trabecular A.) Bone volume fraction (Tb.BV/TV) B.) Thickness (Tb.Th) C.) Number (Tb.N) D.) Separation (Tb.Sp) E.) Connectivity density (Tb.Conn.D) F.) Apparent mineral density (Tb.AppMD) and G.) Tissue mineral density (Tb.TMD) for age-matched (AC-black), ovariectomized (OVX-white), alendronate-treated at low (L), medium (M), or high (H) doses (ALN - light gray) and PTH-treated at low (L), medium (M), or high (H) doses (PTH - dark gray) with baseline animals represented (- - -) and OVX baseline represented (…).

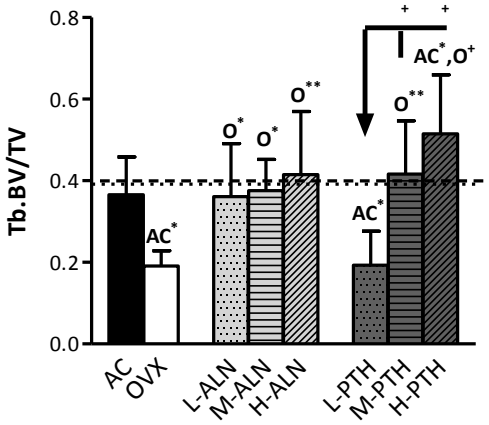

A.

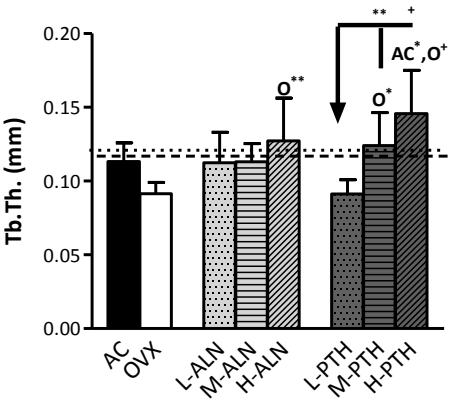

B.

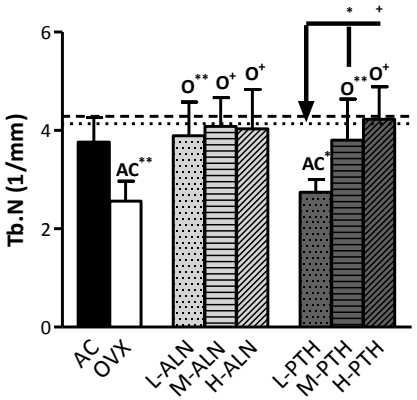

C.

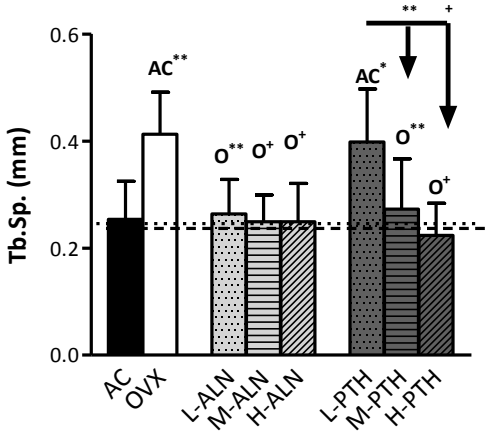

D.

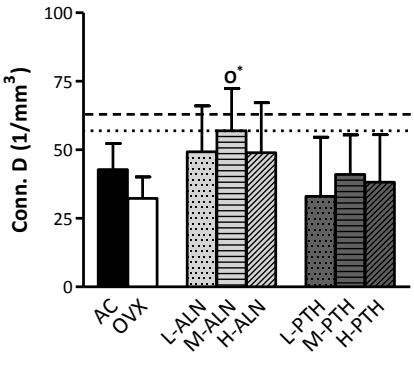

E.

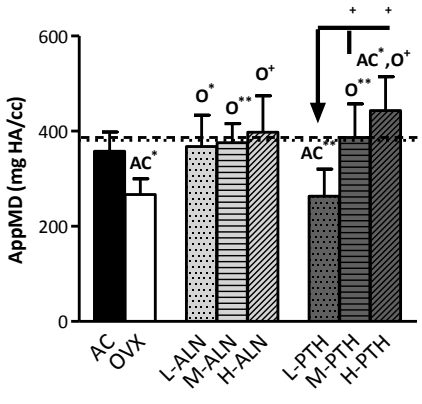

F.

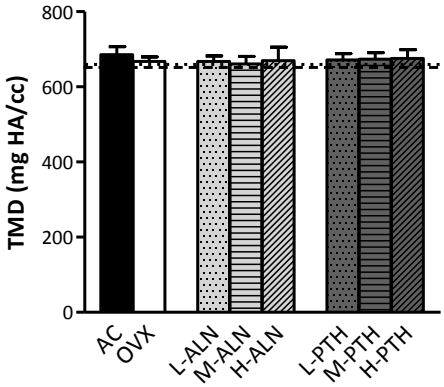

G.

Figure 4.5. In vivo longitudinal µCT scans evaluated abdominal fat volume. Representative images at A.) 6 months old, B.) 8 months old and C.) 12 months old which show the abdominal fat separated into subcutaneous (gray) and visceral (red) fat, with adipose tissue increasing with age.

A. 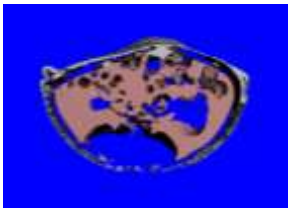 **B.**  **C.** 

Figure 4.6. *In vivo* microCT of the abdomen scanned at 6, 8 and 12 months of age revealed longitudinal changes in A.) Visceral adipose volume (Vis.Adipose V) and B.) Subcutaneous adipose volume (Sub.AdiposeV) for age-matched controls (AC- black solid) ovariectomy controls (OVX - dashed gray), OVX + alendronate-treated at low (L - solid black), medium (M – dashed dark gray), or high (H - dotted light gray) doses or OVX + PTH-treated at low (L - solid black), medium (M - dashed dark gray), or high (H - dotted light gray) doses.

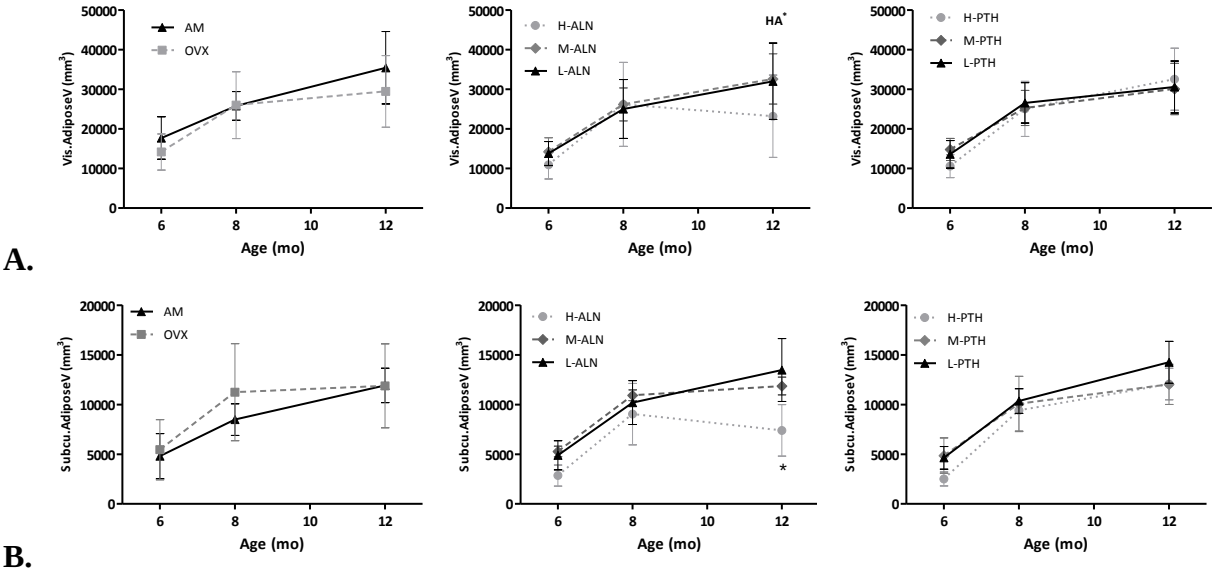

Figure 4.7. A.) Extracted gonadal fat pad mass of all animals correlated to body weight. B.) Fat pad mass of 12 month animals correlated to their 12 month total fat volume (*in vivo* µCT).

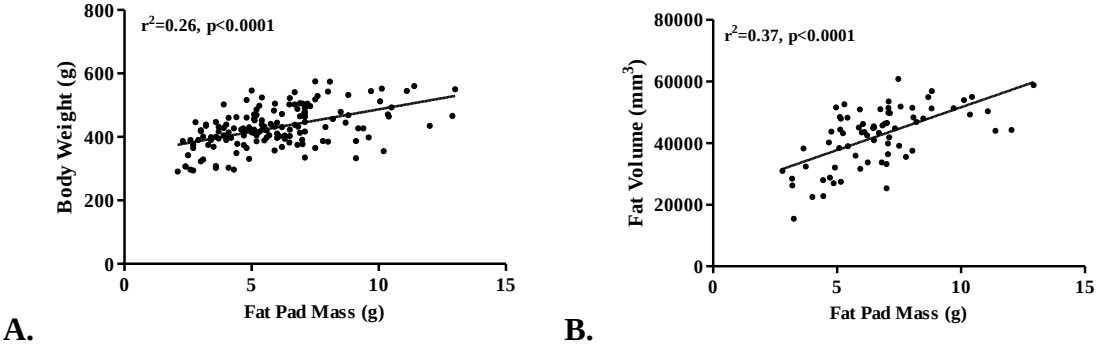

Figure 4.8. Body Mass (BM - diamond), total adipose tissue/body weight (TAT/BW - circle) and visceral adipose tissue/body weight (VAT/BW - triangle) correlated to A.) bone volume, B.) and apparent mineral density (App.MD).

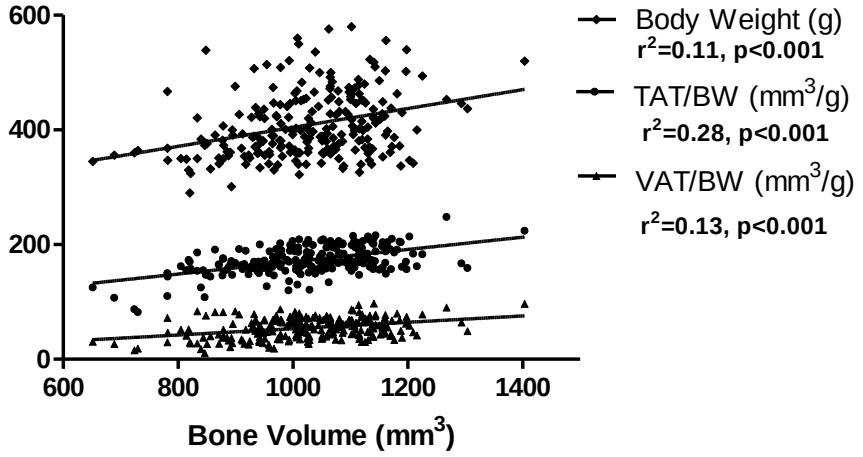

A.

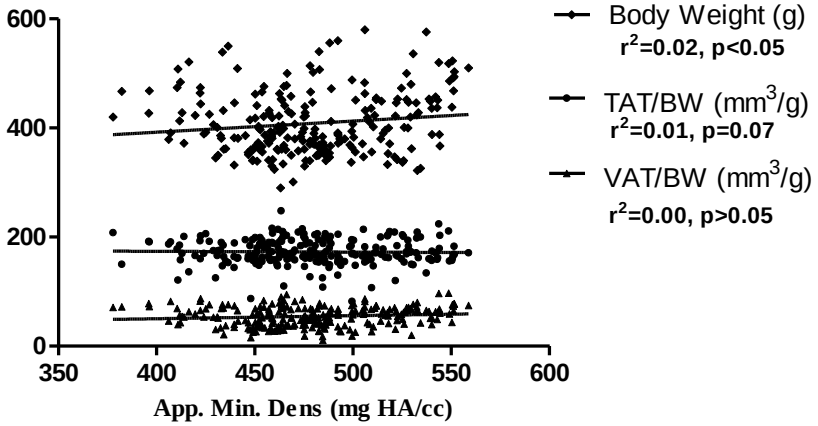

B.

Figure 4.9. Bone area of the tibial metaphysis determined histologically at 12 months through Osteomeasure for age-matched (AC-black), ovariectomized (OVX-white), alendronate-treated at low (L), medium (M), or high (H) doses (ALN - light gray) and PTH-treated at low (L), medium (M), or high (H) doses (PTH - dark gray) with baseline animals represented (- - -) and OVX baseline represented (…).

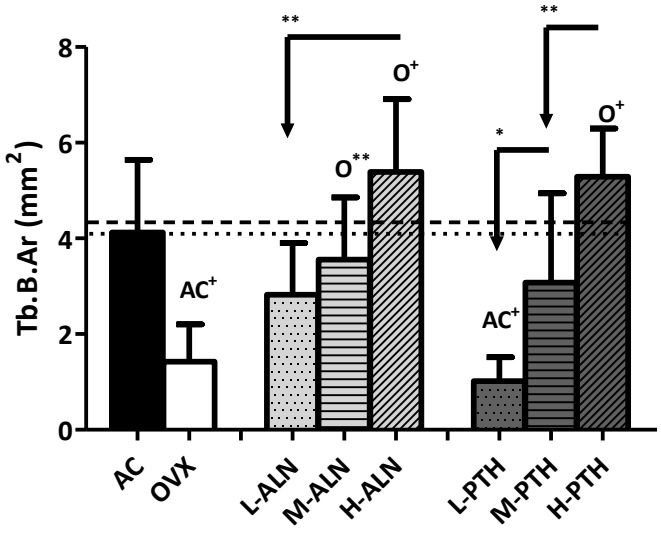

Figure 4.10. A.) Adipocyte number for 5 fields of view within the tibial metaphysis for age-matched (AC-black), ovariectomized (OVX-white), alendronate-treated at low (L), medium (M), or high (H) doses (ALN - light) and PTH-treated at low (L), medium (M), or high (H) doses (PTH - dark gray) with baseline animals represented (- - -) and OVX baseline represented (…). B.) Representative images sectioned at 8 µm, stained with touloudine blue O and Giemsa for AC (top) and OVX (bottom).

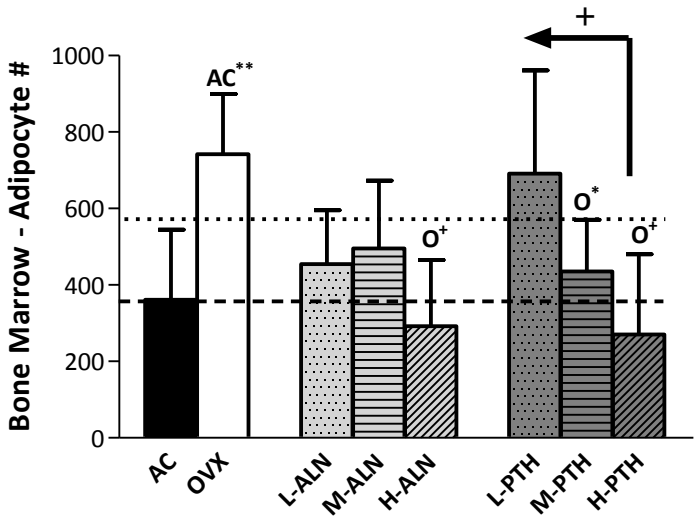

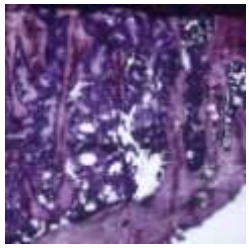

AM

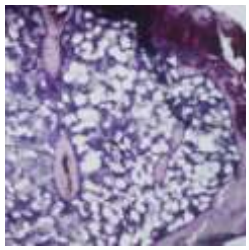

OVX

Figure 4.11. Bone marrow adipocyte number correlated to bone marrow trabecular area determined through histological analysis of the tibial metaphysis for all 12 month old animals (black – dashed), AC and OVX animals (black-square), PTH treated animals (light gray – triangle) and ALN treated animals (dark gray –triangle).

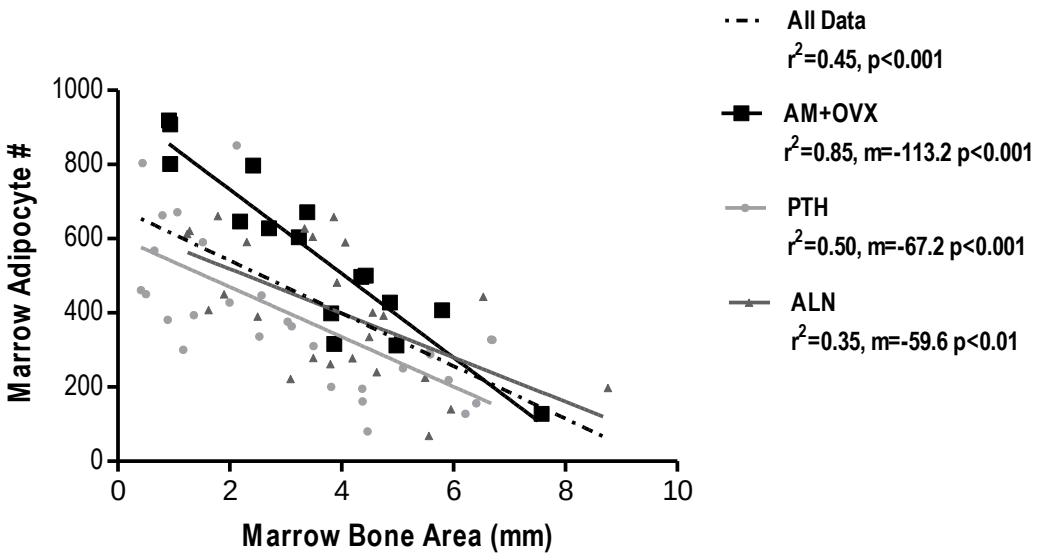

Figure 4.12. A.) Total liver triglyceride (TG) content and B.) Total liver free fatty acid (FFA) content, C.) Bone marrow TG content and D.) Bone marrow FFA content for age-matched (AC-black), ovariectomized (OVX-white), alendronate-treated at low (L), medium (M), or high (H) doses (ALN - light gray) and PTH-treated at low (L), medium (M), or high (H) doses (PTH - dark gray) with baseline animals represented (- - -) and OVX baseline represented (…).

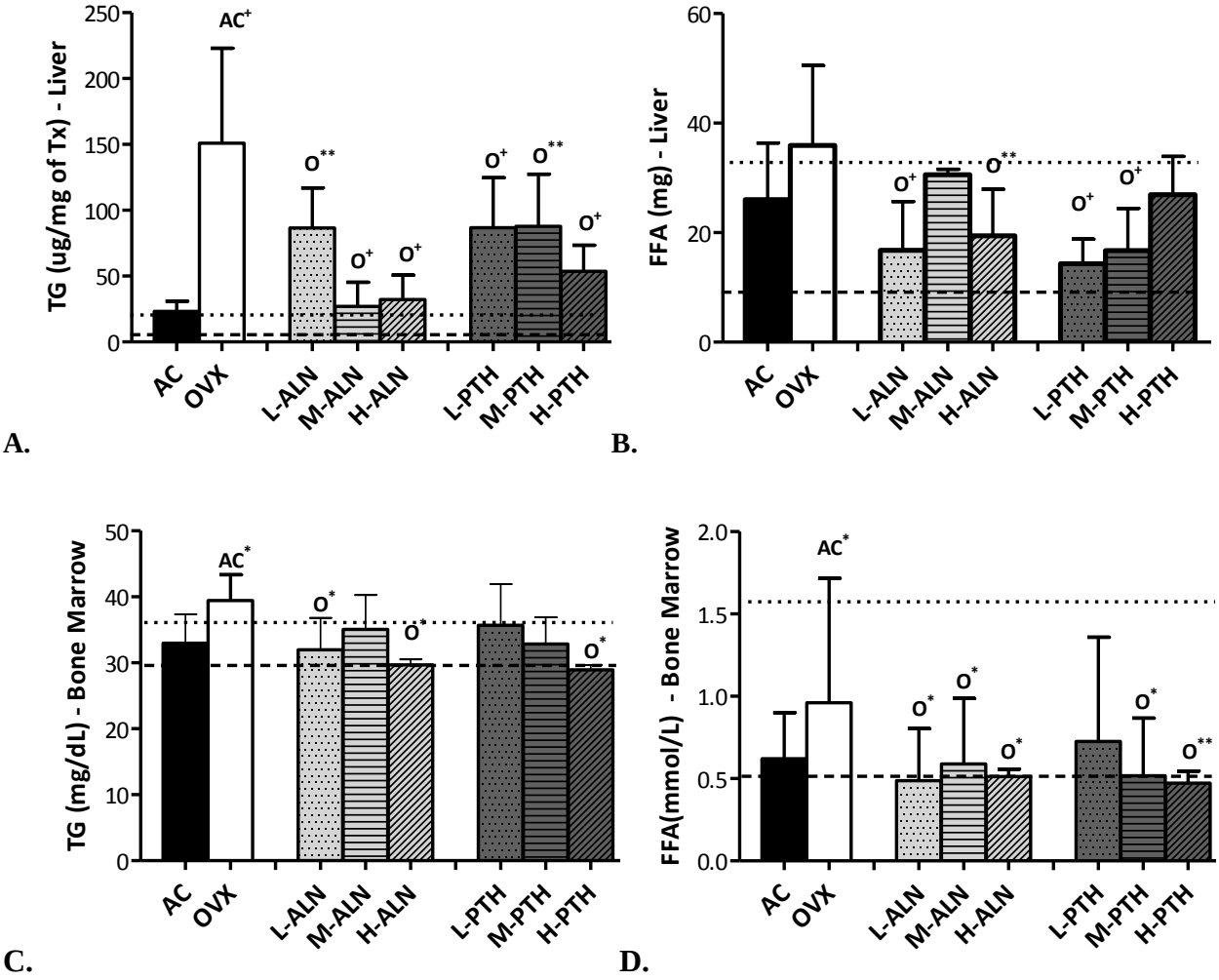

Figure 4.13. Serum leptin concentrations for 6 month (black), 8 month (dark gray) and 12 month (light gray) age-matched controls (AC) and OVX animals.

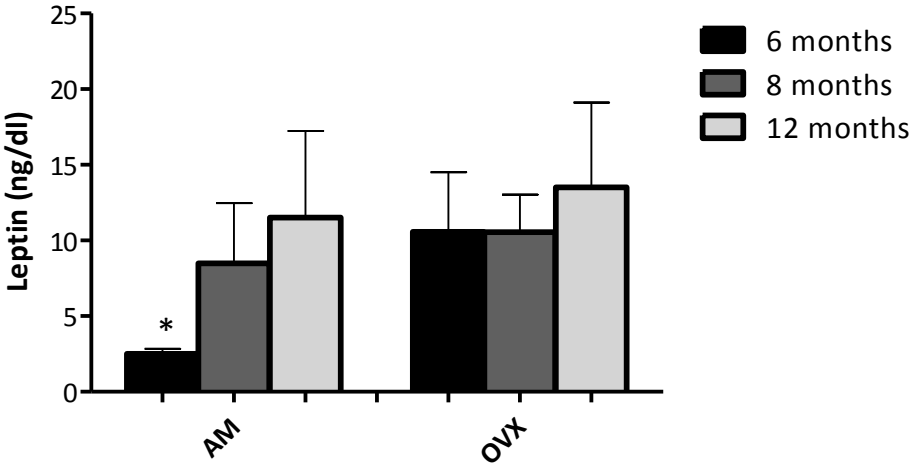

Figure 4.14. Serum A.) IGF-1 concentrations and B.) Alkaline phosphatase concentrations (Alk. Phos) at 12 months of age for age-matched (AC-black), ovariectomized (OVX-white), alendronate-treated at low (L), medium (M), or high (H) doses (ALN - light gray) and PTH-treated at low (L), medium (M), or high (H) doses (PTH - dark gray).

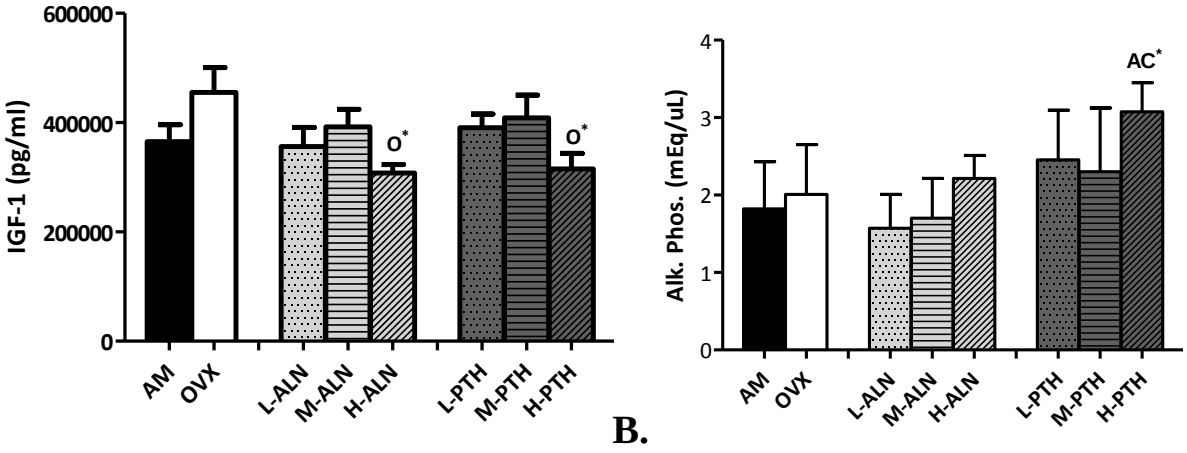

Figure 4.15. RT-PCR analysis from bone marrow 8 month old animals, after 2 months of drug treatment to determine ΔΔCT fold change in gene expression relative to age-matched controls in A.) RUNX2, B.) PPAR-γ, C.) Wnt9b and TNFSF-11 for age-matched (AC-black), ovariectomized (OVX-white), alendronate-treated at low (L), medium (M), or high (H) doses (ALN - light gray) and PTH-treated at low (L), medium (M), or high (H) doses (PTH - dark gray).

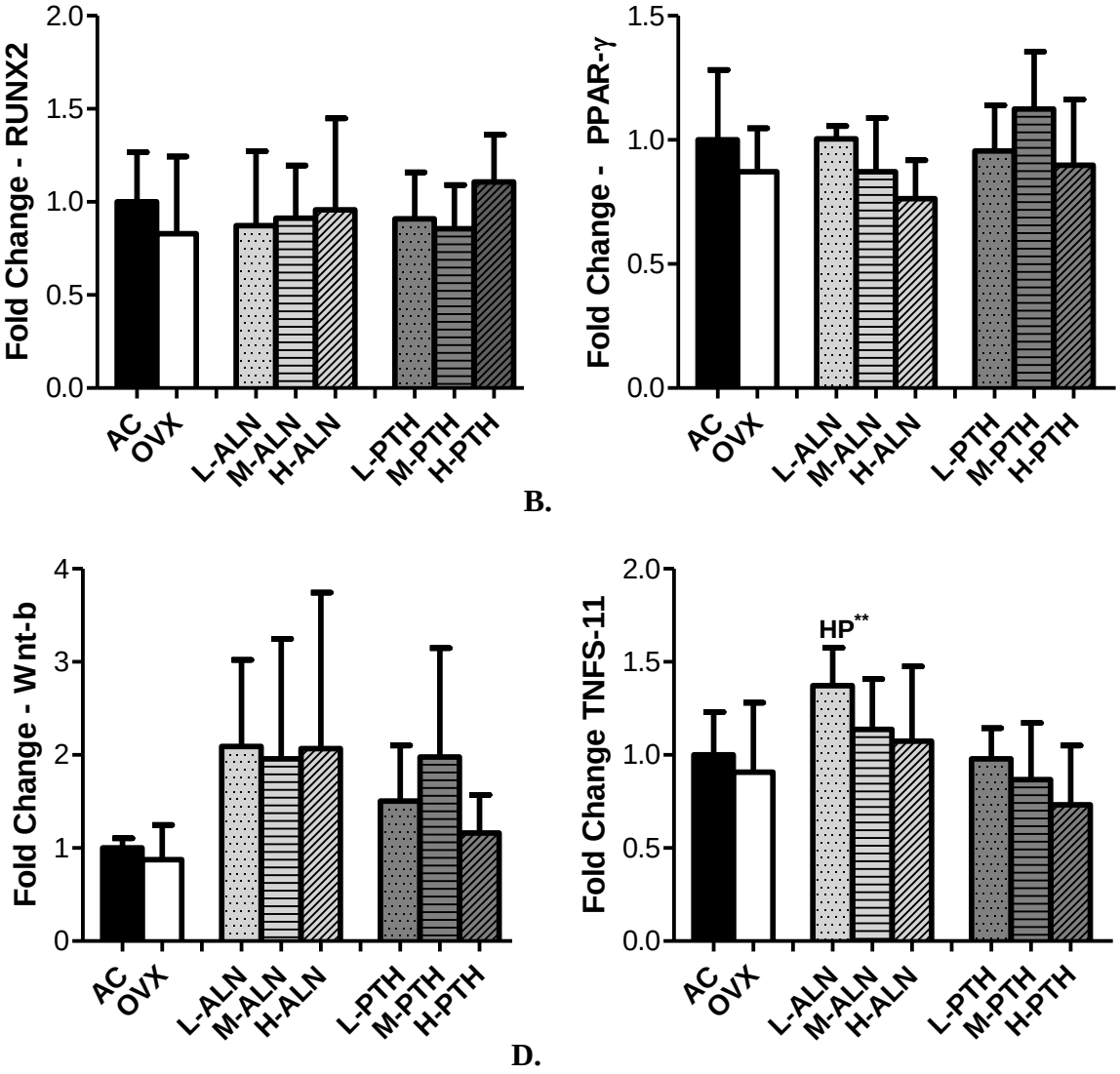

4.7 Tables

Table 4.1. The primers used for RT-PCR in this study

Gene	Target	Probe ID
β-actin	Housekeeping gene	Nm_007393.3
Runx2	Osteoblast differentiation, and maturation	Nm_053470.2
Wnt9b	Osteoblast differentiation	Nm_001107055.1
TNFS11 (RANK-L)	Osteoclast differentiation	Nm_057149.1
PPAR-γ	Adipocyte differentiation	Nm_001145366.1

Table 4.2. Measures of body composition taken longitudinally through *in vivo* microCT at 6, 8 and 12 months of age

		AC	OVX	L-ALN	M-ALN	H-ALN	L-PTH	M-PTH	H-PTH
		6 mo 8 mo 12 mo	6 mo 8 mo 12 mo	6 mo 8 mo 12 mo	6 mo 8 mo 12 mo	6 mo 8 mo 12 mo	6 mo 8 mo 12 mo	6 mo 8 mo 12 mo	6 mo 8 mo 12 mo
	Body Mass at Scan [g]	**329±25** O **377±18** O **451±48**	**367±25** AC **411±29** AC **457±50**	**362±17** AC **412±34** AC **468±58**	**354±17** AC **409±43** AC **465±80**	**370±25** AC **434±48** AC **428±55**	**358±15** AC **408±29** AC **459±55**	**372±22** AC **412.2±24** AC **462±59**	**375±14** AC **446.8±23** AC **492±41**
In vivo microCT of the L1-L4 vertebrae	**BV** [mm^3]	**1021±122** **1054±110** **1076±67**	**999±115** **1035±126** **979±73**	**978±112** **1052±80** **1086±94**	**947±116** **1053±91** **1091±91**	**886±102** **1111±146** **1137±163**	**968±118** **1018±76** **968±72**	**999±98** **1072±88** **1024±58**	**892±80** **1065±62** **1124±67** O
	App.MD [mgHA/cc]	**500±30** **512±23** O **517±28** O	**472±15** **454±15** AC **423±16** AC	**461±16** AC **465±29** AC **469±26** AC O	**469±24** AC **487±22** O **503±22** O	**484±18** **513±18** O **527±20** O	**462±21** AC **438.1±20** AC **413±22** AC	**458±16** AC **484±19** O **487±36** O	**486±21** **529±13** O **544±12** O
	Total FatV [mm^3]	**21.96±8.164** **34.3±4.7** **47.4±10.6**	**19.6±7.3** **37.3±13.1** **41.4±11.6**	**18.7±3.9** **35.2±9.4** **45.5±10.4**	**19.5±5.1** **37.1±5.5** **44.5±6.2**	**13.8±3.8** AC **35.±1.3** **30.6±12.5** O	**18.2±3.9** **36.9±6.0** **44.8±6.9**	**19.7±4.4** **35.4±6.8** **42.1±6.8**	**13.1±3.3** AC **34.5±9.0** **44.6±8.5**
	Visc. FatV [mm^3]	**17.2±6.0** HA HP **25.8±3.6** **35.4±9.1** HA	**14.2±4.6** **26.0±8.4** **29.5±9.0**	**13807±3020** **25037±743** **32035±9656**	**14.2±3.5** **26.2±4.2** **32.6±6.3**	**10.9±3.6** AC **26.2±10.6** **23.2±10.4** AC	**13.6±3.5** **26.6±5.1** **30.6±6.6**	**14.8±2.8** **25.3±4.4** **30.1±6.5**	**10.6±2.9** AC **25.1±7.0** **32.6±7.8**
	Subcu. Fat V [mm^3]	**4.8±2.3** HP **8.5±1.6** **11.9±1.7**	**5.5±3.0** HP **11.2±4.9** **11.9±4.2** HA	**4.9±1.4** **10.2±2.2** **13.5±3.2**	**5.3±1.7** **10.9±1.7** **11.9±2.8**	**2.9±1.1** **9.0±3.1** **7.4±2.6** O	**4.6±1.1** **10.4±1.3** **14.3±2.1**	**4.9±1.8** **10.1±2.8** **12.0±2.0**	**2.5±0.7** AC O **9.4±2.1** **12.1±1.6**
	Lean Tiss.V [mm^3]	**41.2±3.6** **37.9±5.8** **35.7±4.5**	**42.9±7.0** **38.4±5.7** **33.7±4.5**	**40.7±8.2** **37.3±7.3** **33.5±5.1**	**41.9±7.7** **35.0±5.3** **32.0±4.4**	**40.2±8.0** **36.8±6.2** **35.4±1.1**	**41.3±11.5** **36.8±5.2** **32.1±5.6**	**43.5±7.8** **39.4±9.8** **31.8±5.0**	**41.0±8.2** **36.7±3.9** **33.3±3.0**

Data are mean ± standard deviations. Difference in letters denominate significant differences to controls groups: AC – age matched controls, or O – OVX controls (ANOVA and Tukey).

Table 4.3. Body compositional data at sacrifice for animals 6, 8 and 12 months of age

		AC	OVX	L-ALN	M-ALN	H-ALN	L-PTH	M-PTH	H-PTH
		6 mo 8 mo 12 mo	6 mo 8 mo 12 mo	6 mo 8 mo 12 mo	6 mo 8 mo 12 mo	6 mo 8 mo 12 mo	6 mo 8 mo 12 mo	6 mo 8 mo 12 mo	6 mo 8 mo 12 mo
	Body Mass at Sacrifice [g]	305.1±12.3 363.5±30.0 430.2±62.5	376.0±43.6 420.8±46.7 457.4±52.3	.-. 416.1±28.2 467.8±55.9	.-. 471.3±40.2 465.7±76.8	.-. 418.1±13.1 403.3±44.4	.-. 425.0±47.6 459.7±54.1	.-. 424.5±35.2 462.7±58.3	.-. 417.8±25.2 491.2±43.1
Tissue Mass	**Liver** [g]	10.2±0.9 11.8±1.8 12.9±1.6	12.8±2.3 10.0±1.5 11.4±1.2	.-. 10.9±1.2 10.1±1.2	.-. 11.8±1.6 10.7±1.8	.-. 10.7±0.8 10.1±1.5	.-. 11.0±1.5 10.4±1.7	.-. 10.5±0.9 10.1±1.4	.-. 10.9±1.1 11.7±1.4
	Gonadal Fat Pad [g]	3.1±0.7 8.3±2.1 8.9±2.5	3.1±0.6 5.8±1.0 6.7±1.9	.-. 4.2±1.2 7.0±1.5	.-. 6.2±2.3 7.2±2.4	.-. 5.9±1.7 4.0±1.1	.-. 3.0±1.5 7.80±1.8	.-. 4.5±1.4 6.06±1.2	.-. 4.5±1.3 6.02±1.7
	Brown Fat Pad [g]	0.34±0.09 0.48±0.15 0.78±0.26	0.44±0.06 0.44±0.14 0.71±0.35	.-. 0.56±0.23 0.52±0.18	.-. 0.52±0.08 0.57±0.17	.-. 0.43±0.12 0.48±0.17	.-. 0.43±0.06 0.64±0.19	.-. 0.42±0.12 0.54±0.19	.-. 0.52±0.12 0.64±0.11
	Liver TG [µg/mg of Tx]	0.53±0.18 2.03±1.43 3.81±3.51	7.44±3.68 6.39±3.70 12.91±5.47	.-. 7.44±2.86 8.70±2.61	.-. 8.12±1.51 12.22±4.84	.-. 9.40±3.70 3.05±1.41	.-. 8.24±2.86 8.60±4.22	.-. 6.39±3.02 8.69±3.94	.-. 6.81±2.40 4.53±1.50
Fat Metabolism	**B M TG** [mg/dL]	59±04 65±7 66±09	70±5 73±011 79±8	.-. 60±3 64±10	.-. 60±1 70±10	.-. 66±11 59±2	.-. 60±1 71±2	.-. 59±1 66±8	.-. 59±1 58±1
	Liver NEFA [µg/mg of Tx]	0.87±0.85 1.00±0.49 1.99±0.73O	2.83±0.92 1.75±0.77 3.11±1.04	.-. 0.76±0.31 1.57±0.80	.-. 2.00±0.63 3.36±0.32	.-. 0.96±0.43 1.91±0.76	.-. 1.82±0.44 1.39±0.39	.-. 1.43±0.66 1.67±0.77	.-. 0.50±0.29 2.29±0.49
	B M NEFA [mmol/L]	0.052±0.012 0.076±0.029 0.062±0.028	0.156±0.066 0.113±0.087 0.096±0.076	.-. 0.048±0.010 0.049±0.032	.-. 0.047±0.007 0.059±0.040	.-. 0.065±0.024 0.051±0.004	.-. 0.050±0.006 0.073±0.063	.-. 0.048±0.005 0.052±0.035	.-. 0.046±0.006 0.047±0.007
	Serum Leptin [ng/ml]	2.5±0.3 8.5±4.0 11.5±5.8	10.6±3.9 10.5±2.5 13.5±5.6	.-. 11.2±5.7 13.9±7.5	.-. 14.7±3.5 17.1±7.8	.-. 10.3±3.7 10.2±5.3	.-. 12.1±5.5 16.0±6.4	.-. 11.6±6.9 12.1±6.4	.-. 11.9±4.1 17.1±6.1

Data are mean ± standard deviations.

Table 4.4. Trabecular architecture (microCT/histology) and bone marrow fat (histology) of 12 month old animals after 6 months of drug treatment

		AC	OVX	L-ALN	M-ALN	H-ALN	L-PTH	M-PTH	H-PTH
L-4 \Vertebral Body (ex vivo CT)	**BV/TV**	**0.36±0.07** O LP	**0.19±0.04** AC LA MA HA MP HP	**0.36±0.13** O	**0.38±0.08** O	**0.42±0.15** O	**0.19±0.08** AC HP	**0.42±0.13** O HP	**0.52±0.14** AC O LP MP
	Tb.Th. [mm]	**0.11±0.01**	**0.09±0.01** HA MP HP	**0.11±0.02**	**0.11±0.01**	**0.13±0.03** O	**0.09±0.01** HP	**0.12±0.02** O HP	**0.15±0.03** AC O LP MP
	Tb.N.	**3.76±0.50** O LP HP	**2.56±0.40** AC LA MA HA MP HP	**3.89±0.69** O	**4.08±0.58** O	**4.03±0.80** O	**2.74±0.82** AC HP	**3.80±0.84** O HP	**4.23±0.66** AC O LP MP
	Tb.Sp [mm]	**0.25±0.07** O	**0.41±0.08** AC LA MA HA MP HP	**0.26±0.06** O	**0.25±0.05** O	**0.25±0.07** O	**0.40±0.10** AC HP	**0.27±0.09** O HP	**0.22±0.06** O LP MP
	Conn.D [1/mm^3]	**42.8±9.5**	**32.3±7.6** MA	**49.3±16.7**	**57.0±15.4** O	**48.9±18.3**	**33.0±21.6**	**41.1±14.4**	**38.2±17.3**
	App.MD [mg HA/cc]	**357.7±40.7** O LP	**266.9±33.0** AC LA MA HA MP HP	**367.5±66.1** O	**376.0±40.0** O	**397.8±76.3** O	**263.2±57.2** AC HP	**386.9±70.5** O HP	**443.3±71.1** AC O LP MP
	TMD [mg HA/cc]	**685.9±21.4**	**667.9±12.1**	**668.0±14.3**	**661.3±19.7**	**669.4±36.0**	**672.0±16.6**	**673.9±16.9**	**675.5±23.5**
Tibial Metaphysis (Histology)	**Tb.B.Ar. [mm^2]**	**4.12±1.52** O LP	**1.42±0.78** AC MA HA HP	**2.82±1.09** HA	**3.56±1.30** O	**5.39±1.52** O LA	**1.01±0.51** AC MP HP	**3.08±1.87** LP	**5.29±1.00** O LP MP
	Adip.N [#]	**364±181** O	**747±149** AC HA MP HP	**455±141**	**501±168**	**294±171** O	**609±188** HP	**373±59** O	**201±75** O
	Adip. Size [µm]	**195±40**	**181±29**	**170±49**	**171±40**	**138±36**	**201±64**	**188±40**	**203±44**

Data are mean ± standard deviations. Difference in letters denominate significant differences to given groups: AC – age matched controls, O – OVX controls, LA(low)/MA(medium)/HA(high) – Alendronate, LP(low)/MP(medium)/HP(high) – PTH. (ANOVA and Tukey)

Table 4.5. Correlations of fat and bone parameters regressed for all individual animals from 6, 8 and 12 months of age

		B.Vol [mm^3] (*in vivo* µCT)	**App.MD** [mg HA/cc] (*in vivo* µCT)	**BV/TV** (ex *vivo* µCT)	**Tb.Th** [mm] (ex *vivo* µCT)	**Tb.N** [1/mm] (ex *vivo* µCT)	**Tb.B.Ar** [mm^2] (histology)
Quantification of Fat Content	**Visc. Fat Vol** [mm^3]	R^2=0.00 m=3.16 p>0.05	R^2=0.00 m=10.1 p>0.05	R^2=0.03 m=8557 p>0.05	R^2=0.02 m=44477 p>0.05	R^2=0.02 m=1283 p>0.05	R^2=0.00 m=254.8 p>0.05
	Fat Pad Mass [g]	R^2=0.02 m=0.00 p>0.05	R^2=0.07 m=-0.01 p>0.05	R^2=0.06 m=-4.27 p>0.05	R^2=0.04 m=-20.89 p>0.05	R^2=0.03 m=-0.48 p>0.05	R^2=0.02 m=-0.17 p>0.05
	Marrow Fat Cell #	R^2=0.07 m=-0.54 p>0.05	R^2=0.39 m=-2.67 p<0.05	R^2=0.23 m=-0.03 p<0.05	R^2=0.24 m=-4123 p<0.01	R^2=0.15 m=-96 p<0.05	R^2=0.76 m=-103 p<0.001
	Marrow TG [mg/dL]	R^2=0.02 m=0.00 p>0.05	R^2=0.35 m=0.00 p>0.05	R^2=0.18 m=-0.14 p<0.05	R^2=0.12 m=-0.65 p<0.05	R^2=0.12 m=-0.02 p>0.05	R^2=0.33 m=-0.01 p<0.05
	Marrow FFA [mmol/L]	R^2=0.02 m=0.00 p>0.05	R^2=0.03 m=0.00 p>0.05	R^2=0.06 m=-0.22 p>0.05	R^2=0.05 m=-1.09 p>0.05	R^2=0.04 m=-0.03 p>0.05	R^2=0.08 m=-0.02 p<0.05

Table 4.6. Fold change in bone marrow gene expression from AC controls at 8 months of age, after 2 months of drug treatment

		AC	**OVX**	**L-ALN**	**M-ALN**	**H-ALN**	**L-PTH**	**M-PTH**	**H-PTH**
Gene Expressionm (ΔΔCT - β-Actin)	**RUNX2**	1	-17%	-13%	-9%	-4%	-9%	-14%	+11%
	Wnt9b	1	-13%	+109%	+96%	+106%	+50%	+98%	+16%
	TNSF-11	1	-9%	+37%	+14%	+7%	-2%	-13%	-27%
	PPAR-γ	1	-13%	+0.5%	-13%	-24%	+ 5%	+12%	-10%

Chapter 5

CONCLUSIONS

5.1 Summary

Post-menopausal osteoporosis effects 30% of the U.S. population and results in a deterioration of both bone mass and tissue quality and increases fat accumulation and contributes to the development of obesity, type 2 diabetes and metabolic syndrome. In this study, we demonstrated how bone mass and architecture is deteriorated upon the onset of estrogen withdrawal through an ovariectomized rat model and can be dose-dependently preserved with both alendronate and PTH treatments. Preservation of bone mass is critical in preserving overall mechanical capacity, high doses of treatments are detrimental to bone's micro-mechanical properties. High resolution analysis of remodeling sites show drug-specific changes to bone chemistry which correlate to changes in tissue micromechanical properties where alendronate causes reduced bone turnover with bone surfaces that are stiffer and more mineralized than bone surfaces treated with PTH. Alendronate and PTH are effective at mitigating the effects of estrogen-withdrawal related bone loss, but they also have secondary benefits on fat metabolism. Both drugs reduced tissue fat accumulation and prevented an increase in marrow fat that occurred upon the onset of estrogen withdrawal.

In SA 1 we have demonstrating the ability to preserve bone mass and tissue architecture, dose-dependently with both the anti-catabolic drug, alendronate, and the anabolic drug, PTH. In doing so we developed a model with a wide range of both bone mass and overall bone strength. It is clear that bone strength is strongly influenced by bone mass, and coincidentally, parameters of architecture. There were some potential negative effects of long-term, high dose treatments with both ALN and PTH therapy, with a reduction in tissue mineral density which translated to reduced tissue mechanical properties. When this information was applied into a finite element model that measured overall bone stiffness, these changes in tissue mechanics did not

significantly alter the structural properties. In fact, the highest doses of ALN and PTH were the most beneficial in terms of overall bone strength.Yet this is worth monitoring, particularly for patients who have been subjected to long-term treatments of bisphosphonates.

SA2 measured drug-specific changes to bone tissue within areas of active remodeling on bone surfaces compared to older bone through nanoindentation and FTIR. It was critical to closely monitor the site specific changes of tissue properties when measuring the relationship between tissue chemistry and its mechanical properties, and the importance of consistency when collecting correlative data for site specific regions of interest. The significant differences in tissue material properties across treatment groups were localized to bone surfaces. When comparisons were made across treatment groups between their interstitial bone regions, differences were less prevalent or consistent. Alendronate reduced bone remodeling which resulted in more mineralized bone surfaces with higher tissue hardness, while PTH increased bone formation rates which resulted in lower mineralized bone surfaces with lower mechanical properties. In conjunction with microCT data collected from SA1, it is apparent that the relative increases in bone stiffness by ALN treatment was due to maintenance of bone with an overall increase in the mineralization of the already present bone. This led to bone micromechanical properties that varied little across the matrix.

Differentially, PTH increased total bone stiffness by increasing the bone mass through trabecular thickening and new bone formation, and although the tissue material properties of the new bone on bone surfaces after PTH treatments were lower than ALN treatments, but the end result was similar to ALN where PTH was also effective at increasing the total bone stiffness. PTH treated bone at a tissue matrix had chemical makeup and micromechanical properties that varied spatially across the matrix.

In SA3, we expanded our understanding of ALN and PTH by demonstrating their beneficial effects on adiposity, metabolism, and the interrelationship between bone and fat. It is clear that the marrow population is particular sensitive to these pharmaceuticals, and the changes in adiposity were most strongly altered in the bone marrow. Currently, these drugs are classified as either anti-catabolic or anabolic. The bisphosphonate alendronate (ALN) is anti-catabolic and maintains or slightly increases bone mass by blocking bone resorption. The anabolic drug parathyroid hormone (PTH), increases bone mass by increasing bone formation and mineralizing surface rates. Due to their modes of preserving bone mass, there may be differential drug-driven alterations to bone tissue quality, and ultimately bone strength.

Bone strength is derived from an accumulation of factors including, bone mass, structure geometry, microarchitecture, the rate of metabolic activity, tissue mineral density and tissue chemical properties. As these properties are modified by osteoporosis and different drug treatments, it is important to consider their contribution to overall bone strength. Most studies focus on the drug-induced changes to overall bone mass, and architecture. Here, we attempt to elucidate the key elements of bone strength by measuring the relationship after inducing large changes to both structural and tissue material properties. We hypothesize that the OVX rat model for bone loss, treated with PTH and alendronate will differentially and dose-dependently recover bone mass and architecture, but will also alter bone metabolism, tissue level material properties as well as body composition, fat accumulation which will all contribute to overall bone strength.

The overall objective of this dissertation was to determine 1.) drug, dosage and duration-specific changes to bone mass, architecture and chemical composition and to 2.) relate these factors to its structural and tissue level mechanical properties as well as to 3.) determine the interrelationship between bone quality and metabolic health and adiposity in an animal model susceptible to fat accumulation which have been outlined in this PhD thesis.

The results suggest the importance of maintaining bone mass after estrogen withdrawal. The drug induced changes in tissue material properties, although interesting, did not impact overall bone strength, or material properties. Although the accumulation of subtle changes to bone tissue composition and material properties by OVX and drug treatments could ultimately have effects on overall bone strength, particularly when taken for long durations. When studied at higher resolution through nanoindentation and FTIR, it is clear that pharmaceuticals have differential affects on the bone matrix properties. With these findings, the goal for future treatments for osteoporosis medications should focus on minimizing doses, reducing treatment durations but ultimately optimized to ensure preservation of bone architecture, to maintain bone mass while still preserving normal, healthy tissue quality. Additionally, it is clear that these drugs have an influence on marrow adiposity, and potentially metabolic factors that are disturbed during post-menopausal osteoporosis. Future work is needed to determine these potential secondary benefits of ALN and PTH in clinical studies, and perhaps cadaver studies to elucidate the relationship between bone marrow architecture and adipose accumulation, and whether this relationship is altered after osteoporosis drug treatments.

5.2 Limitations of the Study

The drug-induced changes to bone material properties and the rate at which these differences occur are important factors in predicting overall bone strength. It would have been beneficial to make multiple measurements across the cortex of the bone at known tissue age to do a longitudinal study on bone material properties. A series of fluorescent labels could have been used to make various regions of bone at 1 week, 2 weeks, 2 months, etc. This additional information could have been helpful to determine the time course for complete tissue

mineralization through the duration of drug treatment. Additionally, making paired comparisons within a bone from labels created prior to the start of treatment would have strengthened these statistical analyses.

Bone chemical properties varied little across the cortical diaphysis. The chemical composition did not correlate well to tissue mechanical properties or alter the structural mechanical properties. This limits the definitive conclusions that can be drawn about the effects of drug treatment on chemical composition. A larger number of samples, with additional dosages of ALN and PTH may help to strengthen the statistical power of this study in order to evaluate measureable differences in tissue material properties. A model which can have a larger impact on the medication of chemical composition would make correlative analysis more useful.

Bone structure plays an important role in its overall strength. Laboratory mechanical testing provides valuable information regarding response to drug treatment and modulation in bone strength. The rat animal model has small trabecular regions which are not easily accessible for mechanical testing. The sample preparation to accurately mechanically test small bone specimens would introduce such a high amount of variability that the data collected through laboratory testing would be unreliable. Additionally, the rat skeleton does not fracture as humans do because of bone loss, or increased mineralization through suppressed bone turnover, or as a result of falling. This makes the rat model less than ideal to determine fracture mechanics during drug treatment. Unfortunately bone biopsies are not readily available in clinical studies so we must rely on the careful and efficacious use of finite element modeling to predict bone strength during drug use.

The mechanism of action by PTH and alendronate to reduce bone micro-mechanical properties is still unclear. By alendronate administration, we hypothesize that the reduction in

mechanical properties could be due to the accumulation of microcracks and inability of natural self repair. Suppresion of bone turnover can lead to increased tissue crystallinity and mineral content resulting in bone brittleness and microcrack accumulation [152], which may explain micromechanical deficits after high dose treatments of alendronate. No information has been collected on the accumulation of micro-cracks which could potentially be conducted through basic fuchsin staining of histologic bone samples. Additionally, more information is needed on the affects of alendronate treatment on cell survivial. Alendronate-activated osteoclastic apoptosis could change the biochemical environment encompassing bone tissue through osteolysis. Recent studies suggest that alendronate does not kill the osteoclast but only reduces its efficacy through damage of its ruffled cell border making it incapable of active resorption on the bone surface [273].

5.3 Finite Element Modeling to Monitor Drug Efficacy and Bone Quality

Bone quality ultimately should be defined as those factors which contribute to overall bone strength. As measurements of bone quality and strength are standardized, we believe that finite element will become the standard modality. The high resolution imaging analysis of micro-computed tomography of bone provides the tools necessary to predict bone strength in osteoporotic patients through simulated mechanical testing. If we can advance this technology to include information regarding the tissue level mineral density, or other elements of tissue quality we will have a better understanding of the modulation in bone strength by drug treatments. Additionally, further FEM analysis could provide insight into the fracture mechanics of the material, through the creation of a model which emphasizes the important elements of fracture mechanics and its contributing properties. This work could be enhanced by measuring bone's

mechanical response to variable strain rates, crack propagation mechanics, or work energy density or toughness analysis which may provide better insights into drug-induced changes to bone tissue quality. Understanding the dynamic properties of bone such as the effect of variable strain rates may elucidate the effects of changes in mineral content or chemical composition. It has been documented that bone strength increases with increasing strain rate and bone responds to increased strain rate differently depending on mineral content as well as its remodeling activity[274]. Due to the fact that ALN and PTH treatments have differential effects on tissue mineralization and bone remodeling, these bones may have drastically different responses to varying strain rates.

Additionally, fracture mechanics might be a better determinant of drug-induced changes to bone tissue quality. Since we hypothesize that ALN treatments may cause microcrack accumulation through suppression of bone turnover, it is possible that ALN treatment may be considerably detrimental to its fracture propagation mechanics. It has been shown that materials with high mineral content that are uniformly distributed across its matrix allow faster and direct propagation of cracks without the formation of subsidiary cracks at interfaces compared to lower mineralized materials with directional load induced remodeling occurring within the matrix [275]. Although ALN induces changes to the material which is higher in mineral content and stronger in compressive mechanical loading, it might significantly reduce its fracture mechanical properties. We hypothesize that increases in tissue hardness induced by ALN treatment may result in tissue brittleness, brittle materials may have higher elastic moduli in compression, but weak strength in bending or torsion. Further mechanical testing through crack propagation analysis or torsional mechanical testing may better answer the question of why atypical fractures occur during long term alendronate use.

5.4 Osteoporosis Drugs Reduce Bone's Tissue Material Properties

Although only small changes were observed in the tissue level material properties, despite a large range of drug doses, there were some significant changes that are worth paying attention to. High doses of ALN and PTH did affect bone tissue quality, reducing tissue mineral density and altering its bone micro-mechanical properties. Additionally, we saw a reduction in tissue mineralization in both the bone surfaces as well as the interstitial bone with PTH. This indicates that despite their effectiveness at maintaining bone architecture, and improving overall bone strength these drugs do alter bone material quality. As patients are prescribed medications earlier in life and may be on these treatments for long periods of time, it is important to consider the implications of changing bone's matrix properties. Although reductions in overall bone strength were not measured here, there must be some elements of bone strength which are modulated by tissue quality, and therefore if reduced substantially could have significant impacts on bone health.

5.5 Marrow Adiposity Relates to Bone Quality during Osteoporosis Drug Treatment

Understanding the effect of adiposity on bone quality is particularly important in times when diet-induced obesity and type 2 diabetes becomes more prevalent around the world. It is clear that bone is negatively impacted by our bad eating habits and accumulation of body fat. Post menopausal osteoporosis will continue to be a burden as people transition through menopause. Obesity and fat accumulation will only compact the problem. If these drugs can be utilized to combat both bone loss and fat accumulation, the aging population will be healthier. Reversing the obesity epidemic through better eating habits and increased exercise would be a more direct

way of solving this problem, but this provides an alternative mode for, at the very least, reducing the problem.

It is critical to determine how these research findings translate to the clinical studies, particularly the effects of osteoporosis drug treatments on marrow adiposity. Future work could utilize previously obtained biopsies, cadaver bones and data collected during past clinical studies where drug treatments and durations are well documented. It is clear that body mass, or even DXA measured body composition may not be high enough resolution to find the drug-induced effects on the bone-fat connection. Correlative analysis between bone quality in conjunction with marrow adiposity, body weight and fat composition during osteoporosis drug treatments could elucidate whether osteoporosis drug treatments might modulate the bone-fat interaction in post-menopausal women.

5.6 Conclusions

This dissertation demonstrated that ALN and PTH differentially and dose-dependently alter bone architecture which contribute to changes in bone mechanical properties, determined the drug-induced changes to bone surface properties and its modulation of micromechanical properties and finally demonstrated a drug-induced alteration between the relationship between bone and fat through a reduction in fat accumulation. It is clear that despite overall improvements to bone stiffness, there are detrimental effects on tissue mechanical properties which need to be considered, particularly during long term treatment. Additionally, osteoporosis pharmaceuticals may have secondary benefits to metabolic health and fat accumulation, particularly in skeletal compartments.

References

1. Busa, B., et al., *Rapid establishment of chemical and mechanical properties during lamellar bone formation.* Calcif Tissue Int, 2005. **77**(6): p. 386-94.
2. Loveridge, N., *Bone: more than a stick.* J Anim Sci, 1999. **77 Suppl 2**: p. 190-6.
3. Constantz, B.R., et al., *Skeletal repair by in situ formation of the mineral phase of bone.* Science, 1995. **267**(5205): p. 1796-9.
4. Seeman, E., et al., *Microarchitectural deterioration of cortical and trabecular bone: differing effects of denosumab and alendronate.* J Bone Miner Res, 2010. **25**(8): p. 1886-94.
5. Eriksen, E.F., et al., *Cancellous bone remodeling in type I (postmenopausal) osteoporosis: quantitative assessment of rates of formation, resorption, and bone loss at tissue and cellular levels.* J Bone Miner Res, 1990. **5**(4): p. 311-9.
6. Manolagas, S.C., *Role of cytokines in bone resorption.* Bone, 1995. **17**(2 Suppl): p. 63S-67S.
7. Parfitt, A.M., et al., *A new model for the regulation of bone resorption, with particular reference to the effects of bisphosphonates.* J Bone Miner Res, 1996. **11**(2): p. 150-9.
8. Mori, S. and D.B. Burr, *Increased intracortical remodeling following fatigue damage.* Bone, 1993. **14**(2): p. 103-9.
9. Arnett, T., *Regulation of bone cell function by acid–base balance.* Proceedings of the Nutrition Society, 2003. **62**(02): p. 511-520.
10. Malaval, L., et al., *Cellular expression of bone-related proteins during in vitro osteogenesis in rat bone marrow stromal cell cultures.* J Cell Physiol, 1994. **158**(3): p. 555-72.
11. Benhamou, C.L., *Effects of osteoporosis medications on bone quality.* Joint Bone Spine, 2007. **74**(1): p. 39-47.
12. Horowitz, M., *Matrix proteins versus cytokines in the regulation of osteoblast function and bone formation.* Calcif Tissue Int, 2003. **72**(1): p. 5-7.
13. Suda, T., N. Takahashi, and E. Abe, *Role of vitamin D in bone resorption.* J Cell Biochem, 1992. **49**(1): p. 53-8.
14. Parfitt, A.M., *The bone remodeling compartment: a circulatory function for bone lining cells.* J Bone Miner Res, 2001. **16**(9): p. 1583-5.
15. Horowitz, M.C., *Cytokines and Estrogen in Bone: Anti-Osteoporotic Effects.* Science, 1993. **260**(5108): p. 626-627.
16. Allan, R.W., M.A. Ansari-Lari, and S. Jordan, *DRAQ5-based, no-lyse, no-wash bone marrow aspirate evaluation by flow cytometry.* Am J Clin Pathol, 2008. **129**(5): p. 706-13.
17. Nicks, K.M., T.W. Fowler, and D. Gaddy, *Reproductive hormones and bone.* Curr Osteoporos Rep, 2010. **8**(2): p. 60-7.
18. Fowlkes, J.L., et al., *Effects of systemic and local administration of recombinant human IGF-I (rhIGF-I) on de novo bone formation in an aged mouse model.* J Bone Miner Res, 2006. **21**(9): p. 1359-66.
19. Parfitt, A.M., *Interpretation of bone densitometry measurements: disadvantages of a percentage scale and a discussion of some alternatives.* J Bone Miner Res, 1990. **5**(6): p. 537-40.

20. Miller LM, L.W., Schirmer A, Sheik F, Busa B, Judex S, *Accretion of bone quantity and quality in the developing mouse skeleton.* Journal of Bone Mineral Research, 2007. **22**(7): p. 1037-45.
21. Bonewald, L.F. and M.L. Johnson, *Osteocytes, mechanosensing and Wnt signaling.* Bone, 2008. **42**(4): p. 606-15.
22. Duncan, R.L. and C.H. Turner, *Mechanotransduction and the functional response of bone to mechanical strain.* Calcif Tissue Int, 1995. **57**(5): p. 344-58.
23. BURGER, E.H. and J. KLEIN-NULEND, *Mechanotransduction in bone—role of the lacuno-canalicular network.* FASEB J., 1999. **13**(9001): p. 101-112.
24. Nakahama, K.-i., *Cellular communications in bone homeostasis and repair.* Cellular and Molecular Life Sciences, 2010. **67**(23): p. 4001-4009.
25. Rickard, D.J., et al., *Intermittent treatment with parathyroid hormone (PTH) as well as a non-peptide small molecule agonist of the PTH1 receptor inhibits adipocyte differentiation in human bone marrow stromal cells.* Bone, 2006. **39**(6): p. 1361-72.
26. Marshall, D., O. Johnell, and H. Wedel, *Meta-analysis of how well measures of bone mineral density predict occurrence of osteoporotic fractures.* Bmj, 1996. **312**(7041): p. 1254-9.
27. Link, T.M., *Osteoporosis Imaging: State of the Art and Advanced Imaging.* Radiology, 2012. **263**(1): p. 3-17.
28. Jiang, G., H. Matsumoto, and A. Fujii, *Mandible bone loss in osteoporosis rats.* J Bone Miner Metab, 2003. **21**(6): p. 388-95.
29. Laib, A., et al., *The Temporal Changes of Trabecular Architecture in Ovariectomized Rats Assessed by MicroCT.* Osteoporosis International, 2001. **12**(11): p. 936-941.
30. Judex, S., et al., *Adaptations of trabecular bone to low magnitude vibrations result in more uniform stress and strain under load.* Ann Biomed Eng, 2003. **31**(1): p. 12-20.
31. Tommasini, S.M., et al., *The relationship between bone morphology and bone quality in male tibiae: Implications for stress fracture risk.* J Bone Miner Res, 2005. **20**(8): p. 1372-80.
32. Turner, C.H., *Biomechanics of bone: determinants of skeletal fragility and bone quality.* Osteoporos Int, 2002. **13**(2): p. 97-104.
33. Chappard, D., et al., *New laboratory tools in the assessment of bone quality.* Osteoporos Int, 2011. **22**(8): p. 2225-40.
34. Chappard, D., et al., *Bone metastasis: Histological changes and pathophysiological mechanisms in osteolytic or osteosclerotic localizations. A review.* Morphologie, 2011. **95**(309): p. 65-75.
35. Cole, J. and M. van der Meulen, *Whole Bone Mechanics and Bone Quality.* Clinical Orthopaedics and Related Research®, 2011. **469**(8): p. 2139-2149.
36. Cowin, S.C., *Bone Mechanics Handbook*. Second Edition ed2001: CRC Press.
37. Chen, J.S. and P.N. Sambrook, *Antiresorptive therapies for osteoporosis: a clinical overview.* Nat Rev Endocrinol, 2012. **8**(2): p. 81-91.
38. Compston, J.E., *Sex steroids and bone.* Physiol Rev, 2001. **81**(1): p. 419-447.

39. Fox, J., et al., *Daily treatment of aged ovariectomized rats with human parathyroid hormone (1-84) for 12 months reverses bone loss and enhances trabecular and cortical bone strength.* Calcif Tissue Int, 2006. **79**(4): p. 262-72.
40. Recker, R., et al., *Trabecular bone microarchitecture after alendronate treatment of osteoporotic women.* Curr Med Res Opin, 2005. **21**(2): p. 185-94.
41. Neer, R.M., et al., *Effect of parathyroid hormone (1-34) on fractures and bone mineral density in postmenopausal women with osteoporosis.* N Engl J Med, 2001. **344**(19): p. 1434-41.
42. Ogita, M., et al., *Differentiation and Proliferation of Periosteal Osteoblast Progenitors Are Differentially Regulated by Estrogens and Intermittent Parathyroid Hormone Administration.* Endocrinology, 2008. **149**(11): p. 5713-5723.
43. Fonseca, H., et al., *Changes in proximal femur bone properties following ovariectomy and their association with resistance to fracture.* J Bone Miner Metab, 2011.
44. Garthwaite, S.M., et al., *Ageing, exercise and food restriction: effects on body composition.* Mech Ageing Dev, 1986. **36**(2): p. 187-96.
45. Poehlman, E.T., M.J. Toth, and A.W. Gardner, *Changes in energy balance and body composition at menopause: a controlled longitudinal study.* Ann Intern Med, 1995. **123**(9): p. 673-5.
46. Goodpaster, B.H., et al., *Obesity, regional body fat distribution, and the metabolic syndrome in older men and women.* Arch Intern Med, 2005. **165**(7): p. 777-83.
47. Hughes, V.A., et al., *Anthropometric assessment of 10-y changes in body composition in the elderly.* Am J Clin Nutr, 2004. **80**(2): p. 475-82.
48. Tchernof, A., E.T. Poehlman, and J.P. Despres, *Body fat distribution, the menopause transition, and hormone replacement therapy.* Diabetes Metab, 2000. **26**(1): p. 12-20.
49. Sorensen, H.A., et al., *Comparison of quantitative ultrasound and dual X-ray absorptiometry in estrogen-treated early postmenopausal women.* J Clin Densitom, 2001. **4**(2): p. 97-104.
50. Zoth, N., et al., *Physical activity and estrogen treatment reduce visceral body fat and serum levels of leptin in an additive manner in a diet induced animal model of obesity.* J Steroid Biochem Mol Biol, 2010. **122**(1-3): p. 100-5.
51. Ke, H.Z., et al., *Comparative effects of droloxifene, tamoxifen, and estrogen on bone, serum cholesterol, and uterine histology in the ovariectomized rat model.* Bone, 1997. **20**(1): p. 31-9.
52. Petzel, M., *Action of leptin on bone and its relationship to menopause.* Biomed Pap Med Fac Univ Palacky Olomouc Czech Repub, 2007. **151**(2): p. 195-9.
53. Tchernof, A. and E.T. Poehlman, *Weight gain and menopause.* Menopause, 2000. **7**(6): p. 419-21.
54. *National Osteoporosis Foundation Fast Facts on Osteoporosis*.
55. Carmona, R. *Bone Health and Osteoporosis: A Report from the Surgeon General*. [U.S. Department of Health and Human Services Announcement] 2004 10-10-2004; 10-10-2004:[404].
56. Watts, N.B., *Bone: bone density screening leads to reduced fracture risk.* Nat Rev Endocrinol, 2010. **6**(1): p. 17-8.

57. Nancollas, G.H., et al., *Novel insights into actions of bisphosphonates on bone: differences in interactions with hydroxyapatite.* Bone, 2006. **38**(5): p. 617-27.
58. Eckert, R.L., et al., *Regulation of involucrin gene expression.* J Invest Dermatol, 2004. **123**(1): p. 13-22.
59. Black, D.M., et al., *Fracture risk reduction with alendronate in women with osteoporosis: the Fracture Intervention Trial. FIT Research Group.* J Clin Endocrinol Metab, 2000. **85**(11): p. 4118-24.
60. Cummings, S.R. and L.J. Melton, *Epidemiology and outcomes of osteoporotic fractures.* Lancet, 2002. **359**(9319): p. 1761-1767.
61. Pols, H.A., et al., *Multinational, placebo-controlled, randomized trial of the effects of alendronate on bone density and fracture risk in postmenopausal women with low bone mass: results of the FOSIT study. Fosamax International Trial Study Group.* Osteoporos Int, 1999. **9**(5): p. 461-8.
62. Allen, M.R., et al., *Raloxifene enhances material-level mechanical properties of femoral cortical and trabecular bone.* Endocrinology, 2007. **148**(8): p. 3908-13.
63. Allen, M.R., et al., *Alterations in canine vertebral bone turnover, microdamage accumulation, and biomechanical properties following 1-year treatment with clinical treatment doses of risedronate or alendronate.* Bone, 2006. **39**(4): p. 872-9.
64. Allen, M.R., et al., *Raloxifene enhances vertebral mechanical properties independent of bone density.* Bone, 2006. **39**(5): p. 1130-5.
65. Stepan, J.J., et al., *Low bone mineral density is associated with bone microdamage accumulation in postmenopausal women with osteoporosis.* Bone, 2007. **41**(3): p. 378-85.
66. Akerstrom, G., et al., *Parathyroid glands in calcium regulation and human disease.* Ann N Y Acad Sci, 2005. **1040**: p. 53-8.
67. de Paula, F.J. and C.J. Rosen, *Back to the future: revisiting parathyroid hormone and calcitonin control of bone remodeling.* Horm Metab Res, 2010. **42**(5): p. 299-306.
68. Pfeilschifter, J., et al., *Parathyroid hormone increases the concentration of insulin-like growth factor-I and transforming growth factor beta 1 in rat bone.* J Clin Invest, 1995. **96**(2): p. 767-74.
69. Zhou, S., et al., *Effects of age on parathyroid hormone signaling in human marrow stromal cells.* Aging Cell, 2011. **10**(5): p. 780-788.
70. Aslan, D., et al., *Mechanisms for the bone anabolic effect of parathyroid hormone treatment in humans.* Scandinavian Journal of Clinical & Laboratory Investigation, 2012. **72**(1): p. 14-22.
71. Friedl, G., et al., *Intermittent parathyroid hormone (PTH) treatment and age-dependent effects on rat cancellous bone and mineral metabolism.* J Orthop Res, 2007. **25**(11): p. 1454-64.
72. Rosen, V., *Harnessing the parathyroid hormone, Wnt, and bone morphogenetic protein signaling cascades for successful bone tissue engineering.* Tissue Eng Part B Rev, 2011. **17**(6): p. 475-9.
73. Kulkarni, N.H., et al., *Changes in osteoblast, chondrocyte, and adipocyte lineages mediate the bone anabolic actions of PTH and small molecule GSK-3 inhibitor.* J Cell Biochem, 2007. **102**(6): p. 1504-18.

74. Dobnig, H. and R.T. Turner, *Evidence that intermittent treatment with parathyroid hormone increases bone formation in adult rats by activation of bone lining cells.* Endocrinology, 1995. **136**(8): p. 3632-8.
75. Bodenner, D., C. Redman, and A. Riggs, *Teriparatide in the management of osteoporosis.* Clin Interv Aging, 2007. **2**(4): p. 499-507.
76. Vahle, J.L., et al., *Skeletal changes in rats given daily subcutaneous injections of recombinant human parathyroid hormone (1-34) for 2 years and relevance to human safety.* Toxicol Pathol, 2002. **30**(3): p. 312-21.
77. Lindsay, R., et al., *Bone mass among premenopausal women.* Int J Fertil Menopausal Stud, 1993. **38 Suppl 2**: p. 83-7.
78. Lindsay, R. and E. Siris, *Toward optimal health: the experts respond to osteoporosis.. Interview by Jodi Godfrey Meisler.* J Womens Health Gend Based Med, 2000. **9**(2): p. 89-96.
79. Greenspan, S.L., et al., *Effect of recombinant human parathyroid hormone (1-84) on vertebral fracture and bone mineral density in postmenopausal women with osteoporosis: a randomized trial.* Ann Intern Med, 2007. **146**(5): p. 326-39.
80. Hodsman, A.B., et al., *Efficacy and safety of human parathyroid hormone-(1-84) in increasing bone mineral density in postmenopausal osteoporosis.* J Clin Endocrinol Metab, 2003. **88**(11): p. 5212-20.
81. Rubin, C.T., et al., *The use of ultrasound in vivo to determine acute change in the mechanical properties of bone following intense physical activity.* J Biomech, 1987. **20**(7): p. 723-7.
82. Lanyon, L.E., *Using functional loading to influence bone mass and architecture: objectives, mechanisms, and relationship with estrogen of the mechanically adaptive process in bone.* Bone, 1996. **18**(1 Suppl): p. 37S-43S.
83. Gnudi, S., E. Sitta, and N. Fiumi, *Bone density and geometry in assessing hip fracture risk in post-menopausal women.* Br J Radiol, 2007. **80**(959): p. 893-7.
84. Gnudi, S., E. Sitta, and N. Fiumi, *Relationship between body composition and bone mineral density in women with and without osteoporosis: relative contribution of lean and fat mass.* J Bone Miner Metab, 2007. **25**(5): p. 326-32.
85. Bredella, M.A., *Perspective: the bone-fat connection.* Skeletal Radiol, 2010. **39**(8): p. 729-31.
86. Bredella, M.A., et al., *Comparison of DXA and CT in the assessment of body composition in premenopausal women with obesity and anorexia nervosa.* Obesity (Silver Spring), 2010. **18**(11): p. 2227-33.
87. Bredella, M.A., et al., *Determinants of bone mineral density in obese premenopausal women.* Bone, 2011. **48**(4): p. 748-54.
88. Hsu, Y.H., et al., *Relation of body composition, fat mass, and serum lipids to osteoporotic fractures and bone mineral density in Chinese men and women.* Am J Clin Nutr, 2006. **83**(1): p. 146-54.
89. Szulc, P., et al., *Cross-sectional analysis of the association between fragility fractures and bone microarchitecture in older men - the STRAMBO study.* J Bone Miner Res, 2010.
90. Luu, Y.K., et al., *Mechanical Signals As a Non-Invasive Means to Influence Mesenchymal Stem Cell Fate, Promoting Bone and Suppressing the Fat Phenotype.* Bonekey Osteovision, 2009. **6**(4): p. 132-149.

91. Nordin, B.E., et al., *Relative contributions of years since menopause, age, and weight to vertebral density in postmenopausal women.* J Clin Endocrinol Metab, 1992. **74**(1): p. 20-3.
92. Reid, I.R., et al., *Determinants of total body and regional bone mineral density in normal postmenopausal women--a key role for fat mass.* J Clin Endocrinol Metab, 1992. **75**(1): p. 45-51.
93. Cifuentes, M., et al., *Weight loss and calcium intake influence calcium absorption in overweight postmenopausal women.* Am J Clin Nutr, 2004. **80**(1): p. 123-30.
94. Uusi-Rasi, K., et al., *Influence of weight reduction on muscle performance and bone mass, structure and metabolism in obese premenopausal women.* J Musculoskelet Neuronal Interact, 2009. **9**(2): p. 72-80.
95. Ravn, P., et al., *Low body mass index is an important risk factor for low bone mass and increased bone loss in early postmenopausal women. Early Postmenopausal Intervention Cohort (EPIC) study group.* J Bone Miner Res, 1999. **14**(9): p. 1622-7.
96. Seeman, E., et al., *Osteoporosis in anorexia nervosa: the influence of peak bone density, bone loss, oral contraceptive use, and exercise.* J Bone Miner Res, 1992. **7**(12): p. 1467-74.
97. Garnero, P., et al., *Biochemical markers of bone turnover, endogenous hormones and the risk of fractures in postmenopausal women: the OFELY study.* J Bone Miner Res, 2000. **15**(8): p. 1526-36.
98. Shapses, S.A., et al., *Osteopontin facilitates bone resorption, decreasing bone mineral crystallinity and content during calcium deficiency.* Calcif Tissue Int, 2003. **73**(1): p. 86-92.
99. Tuominen, J.T., et al., *Bone mineral density in patients with type 1 and type 2 diabetes.* Diabetes Care, 1999. **22**(7): p. 1196-200.
100. Papakitsou, E.F., et al., *Body mass index (BMI) and parameters of bone formation and resorption in postmenopausal women.* Maturitas, 2004. **47**(3): p. 185-93.
101. Heilbronn, L.K., et al., *Relationship between serum resistin concentrations and insulin resistance in nonobese, obese, and obese diabetic subjects.* J Clin Endocrinol Metab, 2004. **89**(4): p. 1844-8.
102. Sepe, A., et al., *Aging and regional differences in fat cell progenitors - a mini-review.* Gerontology, 2011. **57**(1): p. 66-75.
103. Gastaldelli, A., et al., *Metabolic effects of visceral fat accumulation in type 2 diabetes.* J Clin Endocrinol Metab, 2002. **87**(11): p. 5098-103.
104. Guo, W., et al., *Aging results in paradoxical susceptibility of fat cell progenitors to lipotoxicity.* Am J Physiol Endocrinol Metab, 2007. **292**(4): p. E1041-51.
105. Bowen, D.J., et al., *Effects of dietary fat intervention on mental health in women.* Cancer Epidemiol Biomarkers Prev, 1995. **4**(5): p. 555-9.
106. Wu, C.H., et al., *Truncal fat in relation to total body fat: influences of age, sex, ethnicity and fatness.* Int J Obes (Lond), 2007. **31**(9): p. 1384-91.
107. Wu, S., et al., *The contributions of lean tissue mass and fat mass to bone geometric adaptation at the femoral neck in Chinese overweight adults.* Ann Hum Biol, 2007. **34**(3): p. 344-53.

108. Asiedu, D.K., et al., *Hepatic fatty acid metabolism as a determinant of plasma and liver triacylglycerol levels. Studies on tetradecylthioacetic and tetradecylthiopropionic acids.* Eur J Biochem, 1995. **227**(3): p. 715-22.
109. Zierath, J.R., et al., *Regional difference in insulin inhibition of non-esterified fatty acid release from human adipocytes: relation to insulin receptor phosphorylation and intracellular signalling through the insulin receptor substrate-1 pathway.* Diabetologia, 1998. **41**(11): p. 1343-54.
110. Lewis, J.P. and A.R. Shuldiner, *Genetics of the metabolic complications of obesity.* Prog Mol Biol Transl Sci, 2010. **94**: p. 349-72.
111. Gimble, J.M., et al., *Peroxisome proliferator-activated receptor-gamma activation by thiazolidinediones induces adipogenesis in bone marrow stromal cells.* Mol Pharmacol, 1996. **50**(5): p. 1087-94.
112. Nelson, L.R. and S.E. Bulun, *Estrogen production and action.* J Am Acad Dermatol, 2001. **45**(3 Suppl): p. S116-24.
113. Whitfield, J.F., *Leptin: brains and bones.* Expert Opin Investig Drugs, 2001. **10**(9): p. 1617-22.
114. Sinha, M.K., et al., *Evidence of free and bound leptin in human circulation. Studies in lean and obese subjects and during short-term fasting.* J Clin Invest, 1996. **98**(6): p. 1277-82.
115. Zhao, G., et al., *Targeted overexpression of insulin-like growth factor I to osteoblasts of transgenic mice: increased trabecular bone volume without increased osteoblast proliferation.* Endocrinology, 2000. **141**(7): p. 2674-82.
116. Thomas, T., et al., *Leptin acts on human marrow stromal cells to enhance differentiation to osteoblasts and to inhibit differentiation to adipocytes.* Endocrinology, 1999. **140**(4): p. 1630-8.
117. Holloway, W.R., et al., *Leptin inhibits osteoclast generation.* J Bone Miner Res, 2002. **17**(2): p. 200-9.
118. Considine, R.V. and J.F. Caro, *Leptin: genes, concepts and clinical perspective.* Horm Res, 1996. **46**(6): p. 249-56.
119. Sowers, M.F., et al., *BMI vs. body composition and radiographically defined osteoarthritis of the knee in women: a 4-year follow-up study.* Osteoarthritis Cartilage, 2008. **16**(3): p. 367-72.
120. Rosenbaum, M., et al., *Effects of gender, body composition, and menopause on plasma concentrations of leptin.* J Clin Endocrinol Metab, 1996. **81**(9): p. 3424-7.
121. Yakar, S., et al., *The role of circulating IGF-I: lessons from human and animal models.* Endocrine, 2002. **19**(3): p. 239-48.
122. Poehlman, E.T., C.J. Rosen, and K.C. Copeland, *The influence of endurance training on insulin-like growth factor-1 in older individuals.* Metabolism, 1994. **43**(11): p. 1401-5.
123. Canalis, E., et al., *Insulin-like growth factor I mediates selective anabolic effects of parathyroid hormone in bone cultures.* J Clin Invest, 1989. **83**(1): p. 60-5.
124. Canalis, E., *Insulin like growth factors and the local regulation of bone formation.* Bone, 1993. **14**(3): p. 273-6.
125. Andress, D.L. and R.S. Birnbaum, *A novel human insulin-like growth factor binding protein secreted by osteoblast-like cells.* Biochem Biophys Res Commun, 1991. **176**(1): p. 213-8.

126. Canalis, E., *Update in new anabolic therapies for osteoporosis.* J Clin Endocrinol Metab, 2010. **95**(4): p. 1496-504.
127. Zhang, M., et al., *Osteoblast-specific knockout of the insulin-like growth factor (IGF) receptor gene reveals an essential role of IGF signaling in bone matrix mineralization.* J Biol Chem, 2002. **277**(46): p. 44005-12.
128. Giustina, A., et al., *Guidelines for the treatment of growth hormone excess and growth hormone deficiency in adults.* J Endocrinol Invest, 2008. **31**(9): p. 820-38.
129. BERESFORD, J.N., *Osteogenic Stem Cells and the Stromal System of Bone and Marrow.* Clinical Orthopaedics and Related Research, 1989. **240**: p. 270-280.
130. Pittenger, M.F., *Mesenchymal stem cells from adult bone marrow.* Methods Mol Biol, 2008. **449**: p. 27-44.
131. Marcu, F., et al., *The histopathological study of osteoporosis.* Rom J Morphol Embryol, 2011. **52**(1 Suppl): p. 321-5.
132. Cristancho, A.G. and M.A. Lazar, *Forming functional fat: a growing understanding of adipocyte differentiation.* Nat Rev Mol Cell Biol, 2011. **12**(11): p. 722-34.
133. Akune, T., et al., *PPARgamma insufficiency enhances osteogenesis through osteoblast formation from bone marrow progenitors.* J Clin Invest, 2004. **113**(6): p. 846-55.
134. Wang, Q., et al., *Familial resemblance and diversity in bone mass and strength in the population are established during the first year of postnatal life.* J Bone Miner Res, 2010. **25**(7): p. 1512-20.
135. Taipaleenmäki, H., et al., *Wnt signalling mediates the cross-talk between bone marrow derived pre-adipocytic and pre-osteoblastic cell populations.* Experimental Cell Research, 2011. **317**(6): p. 745-756.
136. Marie, P.J., *Cell and gene therapy for bone repair.* Osteoporos Int, 2011. **22**(6): p. 2023-6.
137. Krause, U., et al., *Pharmaceutical modulation of canonical Wnt signaling in multipotent stromal cells for improved osteoinductive therapy.* Proc Natl Acad Sci U S A, 2010. **107**(9): p. 4147-52.
138. Javed, A., H. Chen, and F.Y. Ghori, *Genetic and transcriptional control of bone formation.* Oral Maxillofac Surg Clin North Am, 2010. **22**(3): p. 283-93, v.
139. Jeong, J.H. and J.Y. Choi, *Interrelationship of Runx2 and estrogen pathway in skeletal tissues.* BMB Rep, 2011. **44**(10): p. 613-8.
140. Krishnan, V., H.U. Bryant, and O.A. Macdougald, *Regulation of bone mass by Wnt signaling.* J Clin Invest, 2006. **116**(5): p. 1202-9.
141. Park, K.H., et al., *Melatonin promotes osteoblastic differentiation through the BMP/ERK/Wnt signaling pathways.* J Pineal Res, 2011. **51**(2): p. 187-94.
142. Maruyama, Z., et al., *Runx2 determines bone maturity and turnover rate in postnatal bone development and is involved in bone loss in estrogen deficiency.* Developmental Dynamics, 2007. **236**(7): p. 1876-1890.
143. Baek, W.Y. and J.E. Kim, *Transcriptional regulation of bone formation.* Front Biosci (Schol Ed), 2011. **3**: p. 126-35.
144. Lippuner, K., *The future of osteoporosis treatment - a research update.* Swiss Medical Weekly, 2012. **142**.

145. Eastell, R., et al., *EVALUATION OF BONE TURNOVER IN TYPE-I OSTEOPOROSIS USING BIOCHEMICAL MARKERS SPECIFIC FOR BOTH BONE-FORMATION AND BONE-RESORPTION.* Osteoporosis International, 1993. **3**(5): p. 255-260.
146. Barger-Lux, M.J. and R.R. Recker, *Bone microstructure in osteoporosis: transilial biopsy and histomorphometry.* Top Magn Reson Imaging, 2002. **13**(5): p. 297-305.
147. Sornay-Rendu, E., et al., *Alterations of cortical and trabecular architecture are associated with fractures in postmenopausal women, partially independent of decreased BMD measured by DXA: the OFELY study.* J Bone Miner Res, 2007. **22**(3): p. 425-33.
148. Fields, A. and T. Keaveny, *Trabecular Architecture and Vertebral Fragility in Osteoporosis.* Current Osteoporosis Reports, 2012. **10**(2): p. 132-140.
149. Misof, B.M., et al., *Effects of 1 Year of Daily Teriparatide Treatment on Iliacal Bone Mineralization Density Distribution (BMDD) in Postmenopausal Osteoporotic Women Previously Treated With Alendronate or Risedronate.* Journal of Bone and Mineral Research, 2010. **25**(11): p. 2297-2303.
150. Tjhia, C.K., et al., *Relating micromechanical properties and mineral densities in severely suppressed bone turnover patients, osteoporotic patients, and normal subjects.* Bone, 2012. **51**(1): p. 114-22.
151. Bala, Y., et al., *Bone micromechanical properties are compromised during long-term alendronate therapy independently of mineralization.* Journal of Bone and Mineral Research, 2012. **27**(4): p. 825-834.
152. Gourion-Arsiquaud, S., et al., *Bisphosphonate treatment modifies canine bone mineral and matrix properties and their heterogeneity.* Bone, 2010. **46**(3): p. 666-672.
153. Kim, B.T., et al., *The structural and hormonal basis of sex differences in peak appendicular bone strength in rats.* J Bone Miner Res, 2003. **18**(1): p. 150-5.
154. Keaveny, T.M., et al., *Effects of Teriparatide and Alendronate on Vertebral Strength as Assessed by Finite Element Modeling of QCT Scans in Women With Osteoporosis.* Journal of Bone and Mineral Research, 2007. **22**(1): p. 149-157.
155. Ozcivici E, F.S., Qin YK, Judex S, *Determination of bone's mechanical matrix properties by nanoindentation.* Methods Molecular Biology, 2008. **455**: p. 323-34.
156. Lublinsky, S., E. Ozcivici, and S. Judex, *An automated algorithm to detect the trabecular-cortical bone interface in micro-computed tomographic images.* Calcif Tissue Int, 2007. **81**(4): p. 285-93.
157. Acerbo, A.S., et al., *Imaging the material properties of bone specimens using reflection-based infrared microspectroscopy.* Anal Chem, 2012. **84**(8): p. 3607-13.
158. Wang, X., et al., *Effect of collagen denaturation on the toughness of bone.* Clin Orthop Relat Res, 2000(371): p. 228-39.
159. Rho, J.-Y., T.Y. Tsui, and G.M. Pharr, *Elastic properties of human cortical and trabecular lamellar bone measured by nanoindentation.* Biomaterials, 1997. **18**(20): p. 1325-1330.

160. Campbell, G.M., et al., *The bone architecture is enhanced with combined PTH and alendronate treatment compared to monotherapy while maintaining the state of surface mineralization in the OVX rat.* Bone, 2011. **49**(2): p. 225-232.
161. Maïmoun, L., et al., *Effects of ovariectomy on the changes in microarchitecture and material level properties in response to hind leg disuse in female rats.* Bone, 2012. **51**(3): p. 586-591.
162. Donnelly, E., et al., *Bone tissue composition varies across anatomic sites in the proximal femur and the iliac crest.* Journal of Orthopaedic Research, 2012. **30**(5): p. 700-706.
163. Guerri-Fernandez, R., et al., *Microindentation for in vivo measurement of bone tissue material properties in atypical femoral fracture patients and controls.* J Bone Miner Res, 2012.
164. Bellingham, C.M., et al., *Bisphosphonate (pamidronate/APD) prevents arthritis-induced loss of fracture toughness in the rabbit femoral diaphysis.* J Orthop Res, 1995. **13**(6): p. 876-80.
165. van der Meulen, M.C. and A.L. Boskey, *Atypical subtrochanteric femoral shaft fractures: role for mechanics and bone quality.* Arthritis Res Ther, 2012. **14**(4): p. 220.
166. Teo, J.C.M., et al., *Correlation of cancellous bone microarchitectural parameters from microCT to CT number and bone mechanical properties.* Materials Science & Engineering C-Biomimetic and Supramolecular Systems, 2007. **27**(2): p. 333-339.
167. Wigderowitz, C.A., et al., *Prediction of bone strength from cancellous structure of the distal radius: Can we improve on DXA?* Osteoporosis International, 2000. **11**(10): p. 840-846.
168. Busa B., M.L.M., Rubin C.T., Qin Y.-X., Judex S., *Rapid Establishment of Chemical and Mechanical Properties during Lamellar Bone Formation.* Calcified Tissue International, 2008(77): p. 386-394.
169. Kalu, D.N., *The ovariectomized rat model of postmenopausal bone loss.* Bone Miner, 1991. **15**(3): p. 175-91.
170. Gadeleta, S.J., et al., *A physical, chemical, and mechanical study of lumbar vertebrae from normal, ovariectomized, and nandrolone decanoate-treated cynomolgus monkeys (Macaca fascicularis).* Bone, 2000. **27**(4): p. 541-50.
171. Cummings, S.R., et al., *Effect of alendronate on risk of fracture in women with low bone density but without vertebral fractures - Results from the fracture intervention trial.* Jama-Journal of the American Medical Association, 1998. **280**(24): p. 2077-2082.
172. Lindsay, R., et al., *Randomised controlled study of effect of parathyroid hormone on vertebral-bone mass and fracture incidence among postmenopausal women on oestrogen with osteoporosis.* The Lancet, 1997. **350**(9077): p. 550-555.
173. Boskey, A.L., *Biomineralization: conflicts, challenges, and opportunities.* J Cell Biochem Suppl, 1998. **31**: p. 83-91.
174. Ruffoni, D., et al., *The bone mineralization density distribution as a fingerprint of the mineralization process.* Bone, 2007. **40**(5): p. 1308-1319.

175. Meng, X.W., et al., *Temporal expression of the anabolic action of PTH in cancellous bone of ovariectomized rats.* Journal of Bone and Mineral Research, 1996. **11**(4): p. 421-429.
176. Roschger, P., et al., *Structural development of the mineralized tissue in the human L4 vertebral body.* J Struct Biol, 2001. **136**(2): p. 126-36.
177. Brennan, T.C., R. Rizzoli, and P. Ammann, *Selective Modification of Bone Quality by PTH, Pamidronate, or Raloxifene.* Journal of Bone and Mineral Research, 2009. **24**(5): p. 800-808.
178. Courtland, H.-W., et al., *Fourier Transform Infrared Imaging Microspectroscopy and Tissue-Level Mechanical Testing Reveal Intraspecies Variation in Mouse Bone Mineral and Matrix Composition.* Calcified Tissue International, 2008. **83**(5): p. 342-353.
179. Boivin, G. and P.J. Meunier, *Effects of bisphosphonates on matrix mineralization.* J Musculoskelet Neuronal Interact, 2002. **2**(6): p. 538-43.
180. Fuchs, R.K., et al., *Bisphosphonates do not alter the rate of secondary mineralization.* Bone, 2011. **49**(4): p. 701-705.
181. Boskey, A.L., et al., *Infrared analysis of the mineral and matrix in bones of osteonectin-null mice and their wildtype controls.* J Bone Miner Res, 2003. **18**(6): p. 1005-11.
182. Guo, X.E. and S.A. Goldstein, *Vertebral trabecular bone microscopic tissue elastic modulus and hardness do not change in ovariectomized rats.* Journal of Orthopaedic Research, 2000. **18**(2): p. 333-336.
183. Wang, X., et al., *Age-related changes in the collagen network and toughness of bone.* Bone, 2002. **31**(1): p. 1-7.
184. Silva, M.J. and S.R. Ulrich, *In vitro sodium fluoride exposure decreases torsional and bending strength and increases ductility of mouse femora.* J Biomech, 2000. **33**(2): p. 231-4.
185. Akkus, O., Y.N. Yeni, and N. Wasserman, *Fracture mechanics of cortical bone tissue: a hierarchical perspective.* Crit Rev Biomed Eng, 2004. **32**(5-6): p. 379-426.
186. Li, M., et al., *[Effects of teriparatide and alendronate on bone mineral density of osteoporotic rats].* Zhonghua Yi Xue Za Zhi, 2005. **85**(5): p. 335-8.
187. Brennan, O., et al., *The effects of estrogen deficiency and bisphosphonate treatment on tissue mineralisation and stiffness in an ovine model of osteoporosis.* Journal of Biomechanics, 2011. **44**(3): p. 386-390.
188. Paschalis, E.P., et al., *Bone mineral and collagen quality in humeri of ovariectomized cynomolgus monkeys given rhPTH(1-34) for 18 months.* J Bone Miner Res, 2003. **18**(4): p. 769-75.
189. Cano-Sanchez, J., et al., *Undecalcified bone samples: a description of the technique and its utility based on the literature.* Med Oral Patol Oral Cir Bucal, 2005. **10 Suppl 1**: p. E74-87.
190. Bouxsein, M.L. and E. Seeman, *Quantifying the material and structural determinants of bone strength.* Best Practice & Research Clinical Rheumatology, 2009. **23**(6): p. 741-753.
191. Parkinson, I.H., et al., *Vertebral body bone strength: the contribution of individual trabecular element morphology.* Osteoporos Int, 2012. **23**(7): p. 1957-65.

192. Lenart, B.A., D.G. Lorich, and J.M. Lane, *Atypical Fractures of the Femoral Diaphysis in Postmenopausal Women Taking Alendronate.* New England Journal of Medicine, 2008. **358**(12): p. 1304-1306.
193. Bala, Y., et al., *Modifications of bone material properties in postmenopausal osteoporotic women long-term treated with alendronate.* European Journal of Endocrinology, 2011. **165**(4): p. 647-655.
194. Fischer, K.J., et al., *Mechanical evaluation of bone samples following alendronate therapy in healthy male dogs.* Journal of Biomedical Materials Research Part B: Applied Biomaterials, 2006. **76B**(1): p. 143-148.
195. Broulik, P.D., et al., *Effect of Alendronate Administration on Bone Mineral Density and Bone Strength in Castrated Rats.* Horm Metab Res, 2005. **37**(07): p. 414-418.
196. Fan, Z., et al., *Anisotropic properties of human tibial cortical bone as measured by nanoindentation.* Journal of Orthopaedic Research, 2002. **20**(4): p. 806-810.
197. Brandi, M.L., *Microarchitecture, the key to bone quality.* Rheumatology, 2009. **48**(suppl 4): p. iv3-iv8.
198. Katsumata, T., et al., *Intermittent cyclical etidronate treatment maintains the mass, structure and the mechanical property of bone in ovariectomized rats.* Journal of Bone and Mineral Research, 1995. **10**(6): p. 921-931.
199. Peng, Z., et al., *Alteration in the Mechanical Competence and Structural Properties in the Femoral Neck and Vertebrae of Ovariectomized Rats.* Journal of Bone and Mineral Research, 1999. **14**(4): p. 616-623.
200. Lemieux, C., et al., *The estrogen antagonist EM-652 and dehydroepiandrosterone prevent diet- and ovariectomy-induced obesity.* Obes Res, 2003. **11**(3): p. 477-90.
201. Kyle, U.G., et al., *Age-related differences in fat-free mass, skeletal muscle, body cell mass and fat mass between 18 and 94 years.* Eur J Clin Nutr, 2001. **55**(8): p. 663-72.
202. de Paula, F.J.A., M.C. Horowitz, and C.J. Rosen, *Novel insights into the relationship between diabetes and osteoporosis.* Diabetes/Metabolism Research and Reviews, 2010. **26**(8): p. 622-630.
203. Zamboni, M., et al., *Effects of age on body fat distribution and cardiovascular risk factors in women.* The American Journal of Clinical Nutrition, 1997. **66**(1): p. 111-5.
204. Loncar, G., et al., *Metabolism and the heart: An overview of muscle, fat, and bone metabolism in heart failure.* International Journal of Cardiology, (0).
205. von Muhlen, D., et al., *Associations between the metabolic syndrome and bone health in older men and women: the Rancho Bernardo Study.* Osteoporosis International, 2007. **18**(10): p. 1337-1344.
206. Iwaniec, U.T., et al., *Body mass influences cortical bone mass independent of leptin signaling.* Bone, 2009. **44**(3): p. 404-412.
207. Reid, I.R., *Relationships among body mass, its components, and bone.* Bone, 2002. **31**(5): p. 547-55.
208. Reid, I.R., *Fat and bone.* Archives of Biochemistry and Biophysics, 2010. **503**(1): p. 20-27.

209. Reid, I.R., *Relationships between fat and bone.* Osteoporosis International, 2008. **19**(5): p. 595-606.
210. Moayyeri, A., et al., *Body fat mass is a predictor of risk of osteoporotic fractures in women but not in men: a prospective population study.* Journal of Internal Medicine, 2011: p. no-no.
211. De Laet, C., et al., *Body mass index as a predictor of fracture risk: a meta-analysis.* Osteoporos Int, 2005. **16**(11): p. 1330-8.
212. Marques, E.A., et al., *Appendicular fat mass is positively associated with femoral neck bone mineral density in older women.* Menopause-the Journal of the North American Menopause Society, 2012. **19**(3): p. 311-318.
213. Gonnelli, S., et al., *The Associations of Body Composition and Fat Distribution With Bone Mineral Density in Elderly Italian Men and Women.* Journal of Clinical Densitometry, (0).
214. Yu, E.W., et al., *Simulated increases in body fat and errors in bone mineral density measurements by DXA and QCT.* J Bone Miner Res, 2011.
215. Trémollieres, F.A., J.-M. Pouilles, and C.A. Ribot, *Relative influence of age and menopause on total and regional body composition changes in postmenopausal women.* American Journal of Obstetrics and Gynecology, 1996. **175**(6): p. 1594-1600.
216. Andreoli, A., et al., *Relationship between body composition, body mass index and bone mineral density in a large population of normal, osteopenic and osteoporotic women.* La Radiologia Medica, 2011. **116**(7): p. 1115-1123.
217. Cui, L.-H., et al., *Association between bone mineral densities and serum lipid profiles of pre- and post-menopausal rural women in South Korea.* Osteoporosis International, 2005. **16**(12): p. 1975-1981.
218. Beresford, J.N., et al., *Evidence for an Inverse Relationship between the Differentiation of Adipocytic and Osteogenic Cells in Rat Marrow Stromal Cell-Cultures.* Journal of Cell Science, 1992. **102**: p. 341-351.
219. Christodoulides, C., et al., *Adipogenesis and WNT signalling.* Trends in endocrinology and metabolism: TEM, 2009. **20**(1): p. 16-24.
220. Halade, G.V., et al., *Obesity-mediated inflammatory microenvironment stimulates osteoclastogenesis and bone loss in mice.* Experimental Gerontology, 2011. **46**(1): p. 43-52.
221. Cao, J.J., *Effects of obesity on bone metabolism.* J Orthop Surg Res, 2011. **6**: p. 30.
222. Cao, J.J., L. Sun, and H. Gao, *Diet-induced obesity alters bone remodeling leading to decreased femoral trabecular bone mass in mice.* Annals of the New York Academy of Sciences, 2010. **1192**(1): p. 292-297.
223. Kyung, T.W., et al., *Osteoclastogenesis by Bone Marrow-Derived Macrophages Is Enhanced in Obese Mice.* Journal of Nutrition, 2009. **139**(3): p. 502-506.
224. Tintut, Y., S. Morony, and L.L. Demer, *Hyperlipidemia promotes osteoclastic potential of bone marrow cells ex vivo.* Arteriosclerosis Thrombosis and Vascular Biology, 2004. **24**(2): p. E6-E10.
225. Oh, S.R., et al., *Saturated fatty acids enhance osteoclast survival.* Journal of Lipid Research, 2010. **51**(5): p. 892-899.

226. Black, D.M., et al., *Randomised trial of effect of alendronate on risk of fracture in women with existing vertebral fractures. Fracture Intervention Trial Research Group.* Lancet, 1996. **348**(9041): p. 1535-41.
227. Duque, G., et al., *Effects of risedronate on bone marrow adipocytes in postmenopausal women.* Osteoporosis International, 2011. **22**(5): p. 1547-1553.
228. Chan, G.K., et al., *PTHrP Inhibits Adipocyte Differentiation by Down-Regulating PPARγ Activity via a MAPK-Dependent Pathway.* Endocrinology, 2001. **142**(11): p. 4900-4909.
229. Chan, G.K., et al., *Parathyroid Hormone-Related Peptide Interacts with Bone Morphogenetic Protein 2 to Increase Osteoblastogenesis and Decrease Adipogenesis in Pluripotent C3H10T½ Mesenchymal Cells.* Endocrinology, 2003. **144**(12): p. 5511-5520.
230. Jin, J., et al., *Risedronate inhibits bone marrow mesenchymal stem cell adipogenesis and switches RANKL/OPG ratio to impair osteoclast differentiation.* Journal of Surgical Research, (0).
231. Fournier, C., et al., *Reduction by strontium of the bone marrow adiposity in mice and repression of the adipogenic commitment of multipotent C3H10T1/2 cells.* Bone, 2012. **50**(2): p. 499-509.
232. Judex, S., et al., *Quantification of adiposity in small rodents using micro-CT.* Methods, 2010. **50**(1): p. 14-19.
233. Lelovas, P.P., et al., *The Laboratory Rat as an Animal Model for Osteoporosis Research.* Comparative Medicine, 2008. **58**(5): p. 424-430.
234. Borba, V.Z.C. and N.C.P. Mañas, *The use of PTH in the treatment of osteoporosis.* Arquivos Brasileiros de Endocrinologia & Metabologia, 2010. **54**: p. 213-219.
235. Laudenslager, M.L., et al., *Energy balance in ovariectomized rats with and without estrogen replacement.* Am J Physiol, 1980. **238**(5): p. R400-5.
236. Landau, I.T. and I. Zucker, *Estrogenic regulation of body weight in the female rat.* Horm Behav, 1976. **7**(1): p. 29-39.
237. Shinoda, M., M.G. Latour, and J.M. Lavoie, *Effects of physical training on body composition and organ weights in ovariectomized and hyperestrogenic rats.* Int J Obes Relat Metab Disord, 2002. **26**(3): p. 335-43.
238. Richard, D., L. Rochon, and Y. Deshaies, *Effects of exercise training on energy balance of ovariectomized rats.* Am J Physiol, 1987. **253**(5 Pt 2): p. R740-5.
239. Wang, Q., et al., *Total and regional body-composition changes in early postmenopausal women: age-related or menopause-related?* The American Journal of Clinical Nutrition, 1994. **60**(6): p. 843-8.
240. Ghezzi, A.C., et al., *Metabolic syndrome markers in wistar rats of different ages.* Diabetol Metab Syndr, 2012. **4**(1): p. 16.
241. Toth, M.J., et al., *Effects of estradiol and progesterone on body composition, protein synthesis, and lipoprotein lipase in rats.* Am J Physiol Endocrinol Metab, 2001. **280**(3): p. E496-501.
242. Mattsson, C. and T. Olsson, *Estrogens and glucocorticoid hormones in adipose tissue metabolism.* Curr Med Chem, 2007. **14**(27): p. 2918-24.

243. Dube, M.C., et al., *Muscle adiposity and body fat distribution in type 1 and type 2 diabetes: varying relationships according to diabetes type.* Int J Obes, 2006. **30**(12): p. 1721-1728.
244. Dube, M.-C., et al., *The Contribution of Visceral Adiposity and Mid-Thigh Fat-Rich Muscle to the Metabolic Profile in Postmenopausal Women.* Obesity, 2011. **19**(5): p. 953-959.
245. Schafer, A.L., et al., *Change in Undercarboxylated Osteocalcin Is Associated with Changes in Body Weight, Fat Mass, and Adiponectin: Parathyroid Hormone (1-84) or Alendronate Therapy in Postmenopausal Women with Osteoporosis (the PaTH Study).* Journal of Clinical Endocrinology & Metabolism, 2011. **96**(12): p. E1982-E1989.
246. Rosen, C.J., et al., *Marrow fat and the bone microenvironment: developmental, functional, and pathological implications.* Crit Rev Eukaryot Gene Expr, 2009. **19**(2): p. 109-24.
247. Benayahu, D., I. Shur, and S. Ben-Eliyahu, *Hormonal changes affect the bone and bone marrow cells in a rat model.* Journal of Cellular Biochemistry, 2000. **79**(3): p. 407-415.
248. Duren, D.L., et al., *Quantitative genetics of cortical bone mass in healthy 10-year-old children from the Fels Longitudinal Study.* Bone, 2007. **40**(2): p. 464-70.
249. Ferron, M., et al., *Osteocalcin differentially regulates β cell and adipocyte gene expression and affects the development of metabolic diseases in wild-type mice.* Proceedings of the National Academy of Sciences, 2008. **105**(13): p. 5266-5270.
250. Pittas, A.G., et al., *Association between serum osteocalcin and markers of metabolic phenotype.* J Clin Endocrinol Metab, 2009. **94**(3): p. 827-32.
251. Pettway, G.J., et al., *Anabolic actions of PTH (1-34): use of a novel tissue engineering model to investigate temporal effects on bone.* Bone, 2005. **36**(6): p. 959-70.
252. Kimura, S., et al., *Parathyroid hormone (1-34) improves bone mineral density and glucose metabolism in Spontaneously Diabetic Torii-Lepr(fa) rats.* J Vet Med Sci, 2012. **74**(1): p. 103-5.
253. Takada, I., et al., *A histone lysine methyltransferase activated by non-canonical Wnt signalling suppresses PPAR-[gamma] transactivation.* Nat Cell Biol, 2007. **9**(11): p. 1273-1285.
254. Gunther, T. and R. Schule, *Fat or bone? A non-canonical decision.* Nat Cell Biol, 2007. **9**(11): p. 1229-1231.
255. Yoo, H., et al., *The differential relationship between fat mass and bone mineral density by gender and menopausal status.* Journal of Bone and Mineral Metabolism, 2012. **30**(1): p. 47-53.
256. Saidak, Z., et al., *Strontium ranelate rebalances bone marrow adipogenesis and osteoblastogenesis in senescent osteopenic mice through NFATc/Maf and Wnt signaling.* Aging Cell, 2012. **11**(3): p. 467-474.
257. Reid, I.R., L.D. Plank, and M.C. Evans, *Fat mass is an important determinant of whole body bone density in premenopausal women but not in men.* J Clin Endocrinol Metab, 1992. **75**(3): p. 779-82.
258. Sheu, Y. and J. Cauley, *The Role of Bone Marrow and Visceral Fat on Bone Metabolism.* Current Osteoporosis Reports, 2011. **9**(2): p. 67-75.

259. Yamaguchi, T., et al., *Associations between components of the metabolic syndrome versus bone mineral density and vertebral fractures in patients with type 2 diabetes.* Bone, 2009. **45**(2): p. 174-179.
260. Toombs, R.J., et al., *The impact of recent technological advances on the trueness and precision of DXA to assess body composition.* Obesity (Silver Spring), 2012. **20**(1): p. 30-9.
261. Bachrach, L.K., *Osteoporosis in children: still a diagnostic challenge.* J Clin Endocrinol Metab, 2007. **92**(6): p. 2030-2.
262. Campos, R.M., et al., *Influence of visceral and subcutaneous fat in bone mineral density of obese adolescents.* Arq Bras Endocrinol Metabol, 2012. **56**(1): p. 12-8.
263. Schellinger, D., et al., *Bone Marrow Fat and Bone Mineral Density on Proton MR Spectroscopy and Dual-Energy X-Ray Absorptiometry: Their Ratio as a New Indicator of Bone Weakening.* American Journal of Roentgenology, 2004. **183**(6): p. 1761-1765.
264. Griffith, J.F., et al., *Vertebral bone mineral density, marrow perfusion, and fat content in healthy men and men with osteoporosis: dynamic contrast-enhanced MR imaging and MR spectroscopy.* Radiology, 2005. **236**(3): p. 945-51.
265. Yeung, D.K.W., et al., *Osteoporosis is associated with increased marrow fat content and decreased marrow fat unsaturation: A proton MR spectroscopy study.* Journal of Magnetic Resonance Imaging, 2005. **22**(2): p. 279-285.
266. Rubin, C.T. and L.E. Lanyon, *Dynamic strain similarity in vertebrates; an alternative to allometric limb bone scaling.* J Theor Biol, 1984. **107**(2): p. 321-7.
267. Crepaldi, G., et al., *Osteoporosis and body composition.* J Endocrinol Invest, 2007. **30**(6 Suppl): p. 42-7.
268. Faje, A. and A. Klibanski, *Body Composition and Skeletal Health: Too Heavy? Too Thin?* Curr Osteoporos Rep, 2012.
269. Prieto-Alhambra, D., et al., *The association between fracture and obesity is site-dependent: A population-based study in postmenopausal women.* Journal of Bone and Mineral Research, 2012. **27**(2): p. 294-300.
270. Compston, J.E., et al., *Obesity Is Not Protective against Fracture in Postmenopausal Women: GLOW.* The American Journal of Medicine, 2011. **124**(11): p. 1043-1050.
271. Zhao, L.-J., et al., *Relationship of Obesity with Osteoporosis.* Journal of Clinical Endocrinology & Metabolism, 2007. **92**(5): p. 1640-1646.
272. Kawai, M., M.J. Devlin, and C.J. Rosen, *Fat targets for skeletal health.* Nature Reviews Rheumatology, 2009. **5**(7): p. 365-372.
273. Sato, M., et al., *Bisphosphonate action. Alendronate localization in rat bone and effects on osteoclast ultrastructure.* J Clin Invest, 1991. **88**(6): p. 2095-105.
274. Currey, J.D., *The effects of strain rate, reconstruction and mineral content on some mechanical properties of bovine bone.* Journal of Biomechanics, 1975. **8**(1): p. 81-86.
275. Currey, J.D., *Mechanical properties of bone tissues with greatly differing functions.* J Biomech, 1979. **12**(4): p. 313-9.